N° d'ordre :

REPUBLIQUE ALGERIENNE DEMOCRATIQUE & POPULAIRE

MINISTERE DE L'ENSEIGNEMENT SUPERIEUR & DE LA RECHERCHE SCIENTIFIQUE

UNIVERSITE DJILLALI LIABES
FACULTE DES SCIENCES EXACTES
SIDI BEL ABBES

THESE DE DOCTORAT

Présentée par

DJAAFRI Tayeb

Spécialité : PHYSIQUE
Option : PHYSIQUE DES MATÉRIAUX

Intitulé

Full potential calculations of the elastic, magnetic and thermodynamic properties of some metal Heusler Alloys

Soutenue le 08/06/2015

Devant le jury composé de :

Président:	**M^{r}. BENKHETTOU Nour-Eddine**	**Pr.**	UDL de Sidi Bel-Abbès
Examinateurs:	**M^{r}. MERADJI Hocine**	**Pr.**	Université de Annaba
	M^{r}. GHEMID Sebti	**Pr.**	Université de Annaba
	M^{r}. KHACHAI Houari	**MCA**	UDL de Sidi Bel-Abbès.
Co-Encadreur:	**M^{r}. RACHED Djamel**	**Pr.**	UDL de Sidi Bel-Abbès.
Encadreur:	**M^{r}. KHENATA Rabah**	**Pr.**	Université de Mascara.

Année universitaire 2014-2015

Dedication

I thank "Allah" who gave me the power to
accomplish this modest work.
I would like to express my deep gratitude and
sincere thanks to my parents.
First of all; to my beloved mother,
who helped me by her love
and support. To the memory of my father
who has paved the path of my future.
To my supervisor: Rabah Khenata
To my brothers: Abdelkader, Mohamed, Oussama, Issam, Hicham, Zakaria,
Ahmed, youcef, Ramzi, and Abdeldjabar
To my dear sisters and their husbands
Ahmed and Abdellah
To my respectful wife
To my sons
To the person who was very sympathic with me and I will never forget him
Saadaoui, Abada, Alkeurti, Zamouli and Boudali.
To my best friend Sahraoui
And all who love me.

Acknowledgement

Praise and great thanks to Allah who granted me health, will and patience to achieve this work.

Deepest thanks go to my supervisor Pr. Rabah Khenata, who guided me during my research.

I wish to express great thanks to Pr. Djamel Rached and the jury Pr. Nour-Eddine BENKHETTOU, Pr. Hocine MERADJI, Pr. Sebti GHEMID, Dr. KHACHAI Houari who agreed to judge this modest work. My gratitude to my teachers from primary school till university. Special thanks to all who gave me help and advice .

Thanks

Abstract

First-principles spin polarized density functional theory (DFT) investigations of the structural, electronic, magnetic and thermodynamics characteristics of the half-Heusler, CoMnTe and RuMnTe, compounds are carried out. Calculations are accomplished within the state of the art full-potential (FP) linearized (L) augmented plane wave (APW) computational approach framed within DFT. Generalized gradient approximation (GGA) parameterized by Perdew, Burke and Ernzerhof (PBE) is implemented as an exchange correlation functional as a part of total energy calculation. From the analysis of calculated electronic band structure as well as density of states for both compounds, a strong hybridization between d states of the higher valent transition metal (TM) atoms (Co, Ru) and lower valent TM atoms of (Mn) is observed. Furthermore total and partial density of states (PDOS) of ground state and the results of spin magnetic moments reveal that these compounds are both stable and ideal half-metallic ferromagnetic. The effects of the unit cell volume on magnetic properties and half-metallicity are crucial. It is worth noting that our computed results of total spin magnetic moments, for CoMnTe equal to $4\,\mu_B$ and $3\,\mu_B$ per unit cell for RuMnTe, nicely follow the rule $\mu_{tot} = Z_t\text{-}18$. Using the quasi-harmonic Debye model which considers the phononic effects, the effects of pressure P and temperature T on lattice parameter, bulk modulus, thermal expansion coefficient, Debye temperature, and heat capacity for these compounds are investigated for the first time.

Résumé

La théorie de la fonctionnelle de la densité DFT est utilisée pour étudier les caractéristiques structurelles, électroniques, magnétiques et thermodynamiques des composés half-Heusler CoMnTe et RuMnTe. Les calcules sont réalisés via FP-LAPW computationnelle approches dans le cadre de l'approximation des gradients généralisée GGA paramétrée par Perdew, Burke and Ernzerhof (PBE) et implémenté comme une corrélation et échange fonctionnelle autant qu'une partie de calcul de l'énergie total. A partir de l'analyse de la structure des bandes d'énergies et des densités d'états calculées pour les deux composés, une forte hybridisation entre les états d des atomes des métaux de transition de forte valence (Co,Ru) et les états d des atomes du métal de transition de faible valence (Mn) est observée. De plus, les densités d'états totales et partielles (PDOS) et les résultats des moments magnétiques de spin révèlent que ces composés sont à la fois stable et half-métallique ferromagnétique idéaux. Les effets du volume de la maille élémentaire sur les propriétés half-metalliques et magnétiques sont cruciaux. Il est intéressant de noter que nos résultats du moment magnétique total pour CoMnTe égale à $4\mu_B$ et $3\mu_B$ par maille élémentaire pour RuMnTe, obéit à la règle $\mu_{tot} = Z_t$-18. On utilisant le modèle quasi-harmonique de Debye qui considère les effets phononiques, les effets de la pression P et de la température T, le paramètre de maille, le module de masse, le coefficient de dilatation thermique, la température de Debye et la capacité calorifique de ces composés sont étudies pour la première fois.

ملخص

باستعمال نظرية الكثافة الوظيفية DFT تمت دراسة الخواص البنيوية، الالكتروبية، المغناطيسية و الديناميكية الحرارية للمركبين النصف-هاسلر RuMnTe وCoMnTe. أجريت الحسابات على أساس مقاربة الكمون التام للموجات الخطية المتزايدة (FP-LAPW) بتقريب معمم التدرج (GGA) في إطار نظرية باري، بارك و ارنزرهف (PBE) باعتبارها بالأ□ص علاقة تبادل وظيفية أكثر من كونها جزء من حساب الطاقة الكلية. من □لال التحليل البنيوي للأشرطة الطاقوية و كثافة المستويات المحسوبة من اجل المركبين لوحظ تهجين قوي بين الحالات (د) للذرات ذات التكافؤ العالي (Co,Ru) و الحالات (د) للذرات ذات التكافؤ المنخفض (Mn) للمعادن الانتقالية TM. من □لال دراسة كثافة المستويات العامة و الجزئية (PDOs) و العزم المغناطيسي تبين أن هذان المركبان هما نصف-معادن ممغنطة مستقرة. كما أن تأثير حجم الخلية الأساسية على الخواص نصف-معدنية و المغناطيسية كبير. انه لمن المهم الإشارة إلى أن نتائجنا في ما يخص العزم المغناطيسي الكلي ل CoMnTe يساوي4 μ_B و3 μ_B من اجل RuMnTe تخضع للقاعدة $\mu_{tot} = Z_T$-18. باستعمال نموذج ديباي شبه التوافقي الذي يأ□ذ بعين الاعتبار التأثيرات الفونونية, تمت دراسة لأول مرة تأثيرات الضغط و درجة الحرارة على معامل الخلية، معامل الحجم، معامل التمدد الحراري، درجة حرارة ديباي و السعة الحرارية لهذين المركبين.

Table of content

Table of Figures

List of tables

1. General introduction

Ferromagnetic Heusler alloys exhibited magnetic shape memory effect, magnetic field induced superelasticity and large strain-induced changes in the magnetization are recently very attractive subject of current researches.[1–14] The ferromagnetic martensites are experimentally found in different Heusler alloys such as Ni–Mn–Ga, Ni–Fe–Ga, Co–Ni–Ga and other alloys. The magnetic shape memory effect is related to martensite transformations that are sensitive to pronounced magnetoelastic interaction. A high efficiency of the magneto-mechanical properties makes these materials very attractive for applications as different kind of actuators, sensors, magnetic micro-electro-mechanical systems, for the recording and storage of information, etc. The current advantages in new materials are promising for engineering of new spintronic devices. In this context the problem of local magnetic properties can be one of the most important in the physics of these materials.

It is known that magnetic properties of Heusler alloys are strongly dependent on both the conduction electron concentration and chemical bonding. For example Mn-based compounds demonstrate rather localized magnetism due to configuration of Mn d-orbitals [9,13,14] whereas Co-based compounds show more itinerant behavior.[15] So-called full-Heusler alloys with a general formula unit of X_2YZ, here X and Y denote the transition metals and Z is s-p element such as Al, Ga, Sn, Sb, etc., are studied also with respect to the transition from the ferromagnetic phase to an antiferromagntic one with changing of the concentration of the carriers. Half-metallic Heusler ferromagnets (XYZ) have an energy gap for minority spin bands and the conduction electrons at the Fermi level (E_F) show 100% spin polarization and can be used as spin-polarized electron sources along with metal oxides and III–V group semiconductors. It is known that the full-Heusler alloys such as Co_2MnZ with Z is Si, Ge demonstrate half-metallic behavior also.

The magnetic properties of the Heusler alloys are very sensitive to the local geometry and chemical composition. In order to understand the dependence of magnetic properties on the atomic composition and crystal structure the ab-initio investigation of the electronic structure can be very useful.

The Ni_2MnGa remains most investigated Heusler alloy by both experimental and theoretical approaches. It is known from the literature that the physical properties of this alloy very sensitive to structural disorder and deviations from stoichiometric composition. At present exist several band structure calculations of Ni_2MnGa which were performed using different ab-initio techniques, in particular augmented spherical-wave method [9] full-potential linearized augmented-plane-wave method [12,15] pseudo potential plane-wave approach [16] etc. Less attention was paid to other alloys but a number of the theoretical investigations of the full-Heusler alloys are sharply increased.[17] The similar tendency is observed for half-metallic Heusler alloys.[18,19] The calculations were mainly performed using the local spin density approximation (LSDA), which are known to be underestimated lattice constants and provide smaller magnetic moments.

In present thesis we report the results of ab-initio calculations of the electronic structure and structural and magnetic properties in different series of full and half-Heusler alloys based on Mn, focusing on the effects of their composition and s-p Z atom and extend our study on the half-Heusler CoMnTe and RuMnTe alloys also using the full-potential approach within the generalized gradient approximation (GGA) for exchange correlation potential.

In the chapter II, we will deal with the general properties of the full and the half-Heusler alloys, from a theoretical and experimental point of view. A review of what has been already published will be presented.

Before starting our discussion about these systems, it is appropriate to point out the differences between full-Heusler and half-Heusler and explain shortly their properties, in order to approach the argument in a systematic way. In order to show the importance of these materials we mentioned in this part briefly their different fields of application.

In the chapter III, we recall the principle of the Density Functional Theory, The Local Density Approximation LDA, The Generalised Gradient Approximation GGA and the FP-LAPW computational approximation

In the chapter IV, the First-principles spin polarized density functional theory (DFT) investigations of the structural, electronic, magnetic and thermodynamics characteristics of the half-Heusler, CoMnTe and RuMnTe, compounds are carried out. The calculations are accomplished within the state of the art full-potential (FP) linearized (L) augmented plane wave (APW) computational approximation. The generalized gradient approximation (GGA) parametrized by Perdew, Burke and Ernzerhof (PBE) is implemented as an exchange correlation functional as a part of total energy calculation.

Finally, in the last part, we summarized the main results and we shall conclude that this work opens interesting perspectives, including the study of a several properties in order to use this type of materials in the technological applications.

References

[1] Heusler F, Verh. Dtsch. Phys. Ges. **5**, (1903) 219

[2] R. A. de Groot, F. M. Mueller, P. G. van Engen and K. H. J. Buschow Appl. Phys. **55**, (1984) 2151

[3] I. Galanaki and P. H. Dederich,J. Phys.: Condens. Matter **676,** (2005) 1

[4] K. Endo, T. Phayama and R. Kitamura, J. Phys. Soc. Jpn. **19,** (1964) 1494

[5] J. Kubler, Physica B **127,** (1984) 257

[6] R. Dunlap, G. Stroink and K. Dini, J. Phys. F: Met. Phys. **16,** (1986) 1083

[7] W. Zukovski, A. Andrejezuk, L. Dobrzyeski, M. J. Cooper, M. A. G. Dixon, S. Gardelis, P. K. Lawson, T. Buslaps, S. Kaprzyk, K. U. Neumann and K. R. Ziebeck, J. Phys.: Condens. Matter **9**, (1997) 10993

[8] J. Worgull, E. Petti and J. Trivisonno, Phys. Rev. B **54**, (1996) 15695

[9] S. Plogmann, T. Schlatholter, J. Braun and M. Neumann, Phys. Rev. B **60,** (1999) 6428

[10] S, Ishada, J, Ishada, S. Asano and J. Yamashita, J. Phys. Soc. Jpn. **45**, (1978) 1239

[11] J. Kubler, A. R. Williams and C. B. Sommers, Phys. Rev. B **28**, (1983)1745

[12] S. Fujii, S. Ishida and S. Asano, J. Phys. Soc. Jpn. **58**, (1989) 3657

[13] P. J. Webster and K. R. A. Ziebeck, J. Phys. Chem. Solids **34,** (1973) 1647

[14] A. A. Aquela, J. Enkovaara, K. Uliakko and R. E. Nieminen, J. Phys.: Condens. Matter **11,** (1999) 2017

[15] V. A. Chernenko, V. A. L'vov, R. Mullner, G. Kostorz and T. Takagi, Phys. Rev. B **69,** (2004) 134410

[16] S. E. Kulkova, S. V. Eremeev, T. Kakeshita, S. S. Kulkov and G. E. Rudenski, Mater. Trans. **47**, (2006) 599

[17] R. A. de Groot, A. M. van der Kraan and K. H. J. Buschow, J. Magn. Magn. Mater. **61,** (1986) 330

[18] A. Bouhemadou, R. Khenata and B. Amrani, Physica B **404,** (2009) 3534

[19] M. J. Otto, R. A. M. van Woerden, P. J. van der Valk, J. Wijngaard, C. F. van Bruggen, C. Haas and K. H. J. Buschow, J. Phys.: Condens. Matter **1**, (1989)2341

2 Full and half-Heusler alloys

2.1 Areas of technological application

Since the discovery of giant magnetoresistance (GMR) spintronics has become a field of intense commercial and research interest. A magnetoresistive sensor can be found in the read head of every hard disk drive sold every year. The field of spintronics continues to grow with renewed interest and vigour as second generation magnetic random access memory (MRAM) becomes commercially viable. All spintronic devices need a source of spins. This is usually in the form of a ferromagnet. However, these typical transition metal ferromagnets have low spin polarisation or low spin injection efficiency, typically less than 50%. Half-metallic ferromagnets are a leading candidate to replace current materials and offer much greater spin polarisation, possibly up to 100%. However there are a number of key issues that must be overcome before these films can be used in commercial devices.

2.1.1 Spintronics

Today the integrated circuit and semiconductors are the backbone of modern technology. Complementary metal-oxide-semiconductor (CMOS) and metal-oxide-semiconductor field effect transistor (MOSFET) technologies form the building blocks of this backbone [1]. In recent years there have been a number of astonishing advances in this technology, driven by advances in the scalability of these devices. The drive towards the current state of technology is due to Moore's law [2] which states that the number of transistors on a single chip doubles every 18 months. This has held true for over 30 years to the point where today's most advanced home computer components have 7.1bn transistors per chip [3].

However, this trend cannot continue. We are approaching the physical limit where these devices can function, either due to high leakage currents [4] or simply the limitations of lithography to pattern them. This technological advancement is mirrored in the magnetic storage industry where the same trend is seen for areal density, information stored per unit area. However this is beginning to plateau due to material limitations in both the hard disk and the read head sensor. New technologies are required to overcome these difficulties and continue the technological advance.

Spin-electronics is a promising candidate to allow further development of current semiconductor technologies as it is widely used in the hard disk industry for read head sensors. This means that the processes for commercialising spintronics are already in-place. To improve spintronic devices beyond their current limitations new materials and device technologies must be implemented. Spintronics is a field comprising many sub disciplines although these can be broadly divided up into semiconductor spintronics [5] and magnetoelectronics [6,7]. The latter is concerned with all metallic systems such as magnetoresistive devices.

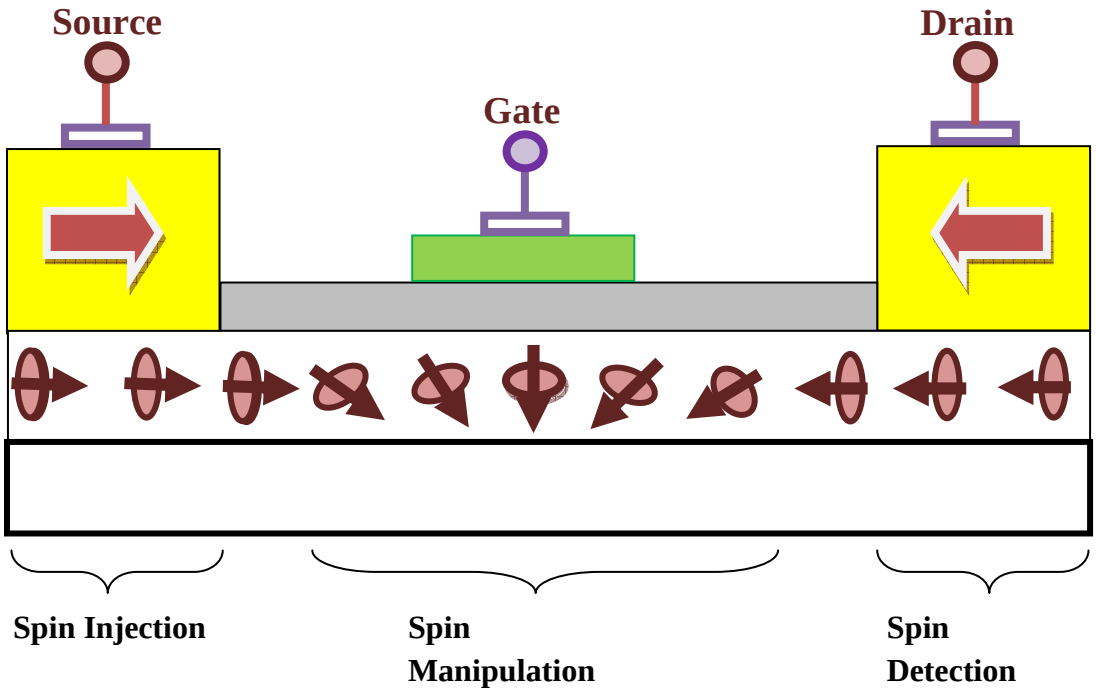

Fig. 2.1: Schematic diagram of Datta-Das Spin FET. **[8]**

Spintronics is based around the concept of using quantised angular momentum, spin, of an electron instead of or as well as its charge. Although the effects of the spin of the electron had been observed experimentally in the late 19th century it was not defined until the early 20th century by *Dirac*. In 1857 *Lord Kelvin* (formally W. Thomson) observed anisotropic magnetoresistance (AMR) [9]. AMR is the directional dependence of the resistivity of a material relative to a magnetic field. AMR is one of many forms of magnetoresistance. Since these early observations of spin dependent electron transport many different devices have been designed and fabricated all using slightly different spin dependent phenomena. The most basic and best example of the requirements of a spintronic device is the spin field effect transistor (SpinFET) as designed by *Datta* and *Das* [8], shown in Figure 2.1.

This work is primarily concerned with the spin source where a high spin polarisation is required. The simplest spin source is a typical ferromagnet interfaced with non-magnetic metal or semiconductor. The Heusler alloys used in this work are intended for use in such a spin source. However spin generation has also been achieved through the manipulation of magnetisation dynamics, resulting in a phenomenon known as spin pumping [10].

2.1.2 Magnetoresistance

Although AMR was discovered in 1857 it was mainly of academic importance due to it only having a small effect (a few per cent). It was used for a number of early hard disk designs until superseded by the discovery of other magnetoresistive effects such as giant magnetoresistance (GMR).

GMR was discovered in 1988 through electrical magnetotransport measurements of ferromagnetic/non-magnetic/ferromagnetic multi-layered systems. This was an attempt to further understand the dependence of interlayer exchange coupling on the spacer thickness in thin film multilayers [11].

Grünberg [12] and *Fert* [13] discovered the effect simultaneously while measuring Fe/Cr/Fe superlattices spaced sufficiently to induce antiferromagnetic coupling between the two Fe layers. The pair received the Nobel prize in Physics for their discovery in 2007. In their initial publications both observed a large change in resistance for the structures when the spaced magnetic layers were changed from anti-parallel to parallel alignment.

This was explained using the two current model initially proposed by *Mott* in 1936 [14,15]. Simply that the current through a transition metal can be separated into two spin channels. This model has since been extended by *Campbell* [16] and *Fert* [17] to include a large number of different electron scattering terms that provide better agreement with the experimental data. This effect in a GMR multilayer is often best explained pictorially as shown in Figure 2.2.

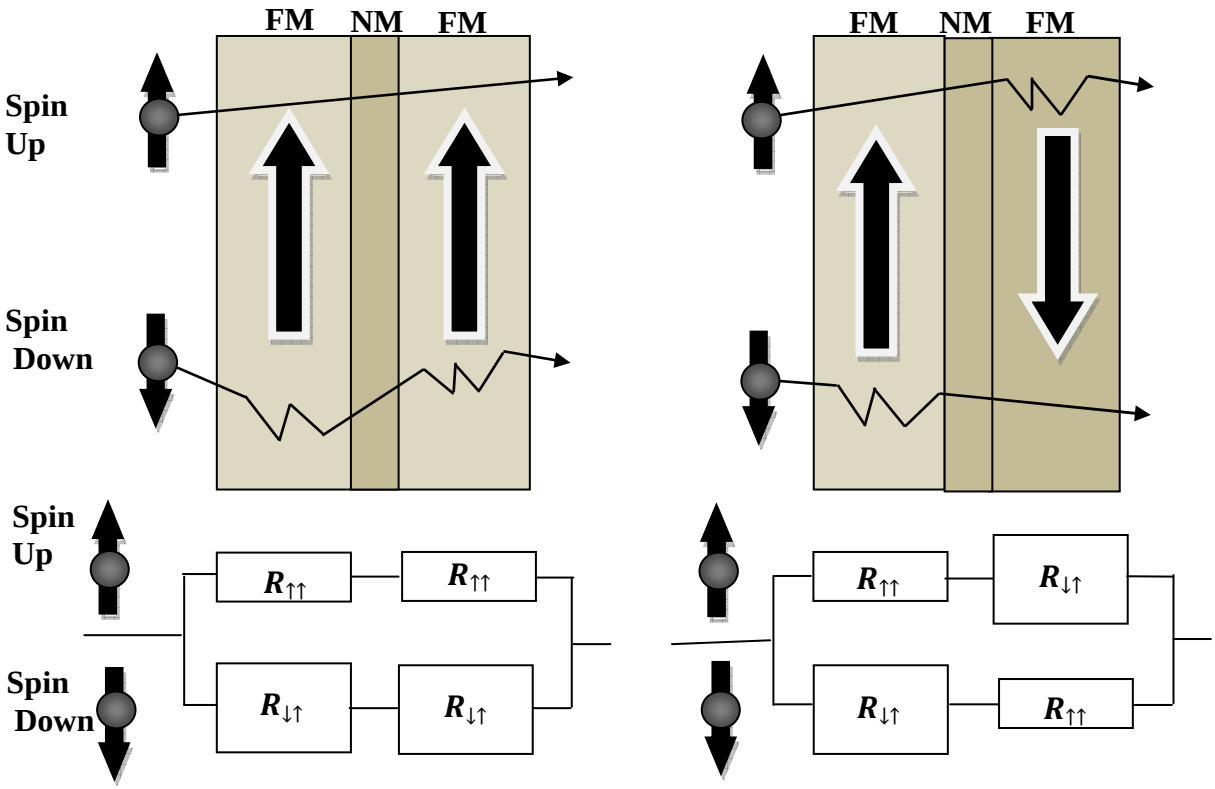

FiG. 2.2 : Schematic of the GMR effect [18].

For the parallel aligned case, one spin channel experiences small or no spin scattering through both ferromagnetic layers. This leads to a low resistance state. In the anti-parallel aligned case, both spin channels experience spin scattering in one of the ferromagnetic layers leading to a high resistance state. Initially this effect was small (1.5% at room temperature) [12]. Since its discovery, large developments have seen the magnitude of the GMR effect increase to 34% at room temperature [19]. There have also been demonstrations of the effect in two different orientations, known as current-in-plane (CIP) and current-perpendicular-to-plane (CPP) [18]. These two orientations have a number of different properties, however CPP-GMR is the current focus of much research interest due to its applicability to current generation MRAM.

If the non-magnetic spacer is replaced by a non-metallic spacer then another phenomenon known as tunnelling magnetoresistance (TMR) can occur. This was first observed by *Julliere* in 1975 [20] with a resistance change of 14% between parallel and anti-parallel states at 4.2K. It was not until the early 1990s that this effect was observed at room temperature, initially by *Miyazaki* (18%) [21] and then by *Moodera* (11.8%) [22]. These experiments used amorphous insulating spacers such as AlOx however, since the pioneering theoretical work of *Butler* in 2001 [23], there has been much greater interest in using crystalline MgO barriers. These were predicted to allow TMR ratios of over 1000%. Experimentally, values of 600% at room temperature have been achieved by *Ikeda et al.* using CoFeB/MgO/CoFeB multilayer films [24]. Although similar in many ways to GMR, TMR is fundamentally quite different.

TMR depends on the conduction states available to tunnel into across the barrier, not just the spin dependent scattering within the electrodes. This is shown schematically in figure 2.3. For the parallel orientation there are a large number of majority conduction states and majority valance states resulting in a large electron flow and thus low resistance. For the anti-parallel orientation there are fewer majority and minority states resulting in a high resistance.

This makes TMR dependent upon the number of available states for each spin direction at the Fermi energy or the spin polarisation, equation 2.1.

$$TMP = \frac{\Delta R}{R} = \frac{2P_1P_2}{1-P_1P_2} \quad (2.1)$$

where P_1 and P_2 are the spin polarisations of ferromagnetic layers in the junction. This means that for the most of the Heusler alloys the achievable TMR should be extremely high due to large values of spin polarisation from these materials.

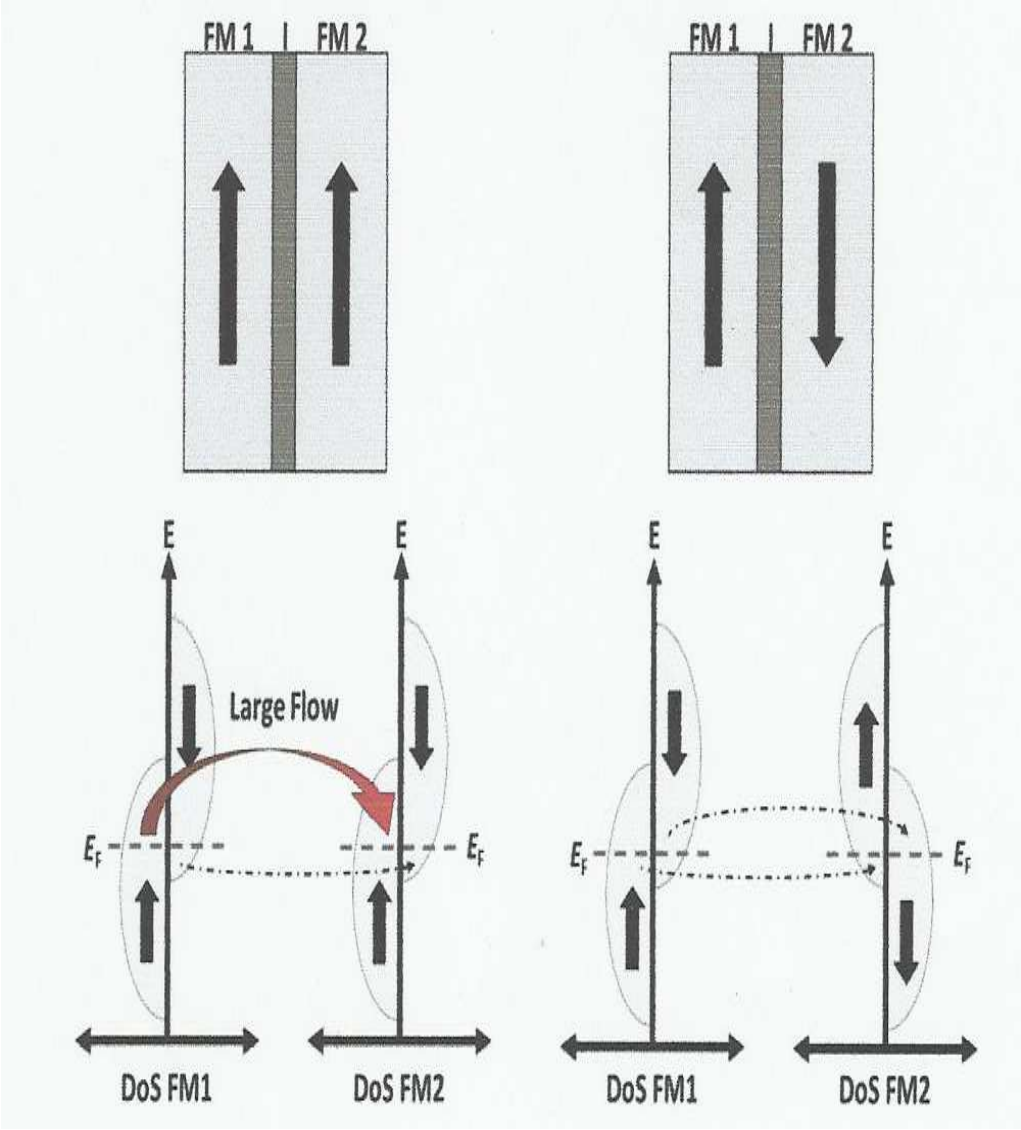

Fig. 2.3 : Schematic of the TMR effect.

2.1.3 Spin Transfer Torques

The most promising new spintronic technology is MRAM. This will potentially replace current semiconductor based dynamic random access memory (DRAM). MRAM has a large number of advantages, most importantly it is non-volatile. This means that when the power is turned off the information is retained. 1st generation MRAM used the Oersted field generated by a current carrying wire to write information to an array of magnetic spin valves. The 2nd generation of MRAM will use a phenomenon known as spin-transfer-torque (STT) as a much more efficient way to write data.

STT was first considered as a way to reverse the magnetisation in a magnetic multilayer by *Slonczewski* [25]. However the effect of spin transfer had been introduced by *Berger* 12 years earlier [26]. STT is easiest to consider in the case of a ferromagnetic/non-magnetic/ferromagnetic junction like those used for GMR. The two ferromagnetic layers have their magnetisations aligned at an angle to one another. When electrons flow into the junction they are initially aligned or polarised to the direction of the magnetisation in the first ferromagnetic layer. When the electrons then travel to the second ferromagnetic layer their spins align with the magnetisation of that layer. However as the spins align to the new direction of magnetisation they exert a torque on that magnetisation. This is the spin transfer torque. Figure 2.4 shows this effect schematically.

If a sufficient number of electrons are injected into the second ferromagnetic layer the torque can be large enough to overcome the torque due to the magnetisation of the material and as a result align the magnetisation of the second ferromagnetic layer M_2 with that of the first M_1. It is also possible to reverse the direction of M_2 back to its original state by injecting the electrons in the opposite direction. In this situation the spins align with M_2 and are then injected into M_1. However, those spins aligned antiparallel to M_1 are reflected back at the interface and injected back into the second ferromagnetic layer where they once again exert a torque on M_2.

Thus the magnetisation in one ferromagnetic layer can be switched by changing the polarity of the applied voltage. The form of the spin transfer torque is given by equation 2.2 [10]:

$$\tau_{STT} = M_1 \times (M_1 \times M_2) P \frac{\gamma_{gm}}{M_s V e} I \qquad (2.2)$$

Here the cross products of the magnetisations M_1 and M_2 give the direction of the torque. The magnitude of the torque is then dictated by the spin polarisation of the ferromagnets P, the saturation magnetisation M_s, the volume of the magnetic layer on which the torque is acting V and the current applied to the junction I. γ_{gm} is the gyromagnetic ratio. The dependence of STT on the spin polarisation of the electrodes makes Heusler alloys a promising candidate for use in these devices due to their high spin polarisation. A detailed examination of spin transfer torques in a large number of systems can be found in *Maekawa* [27].

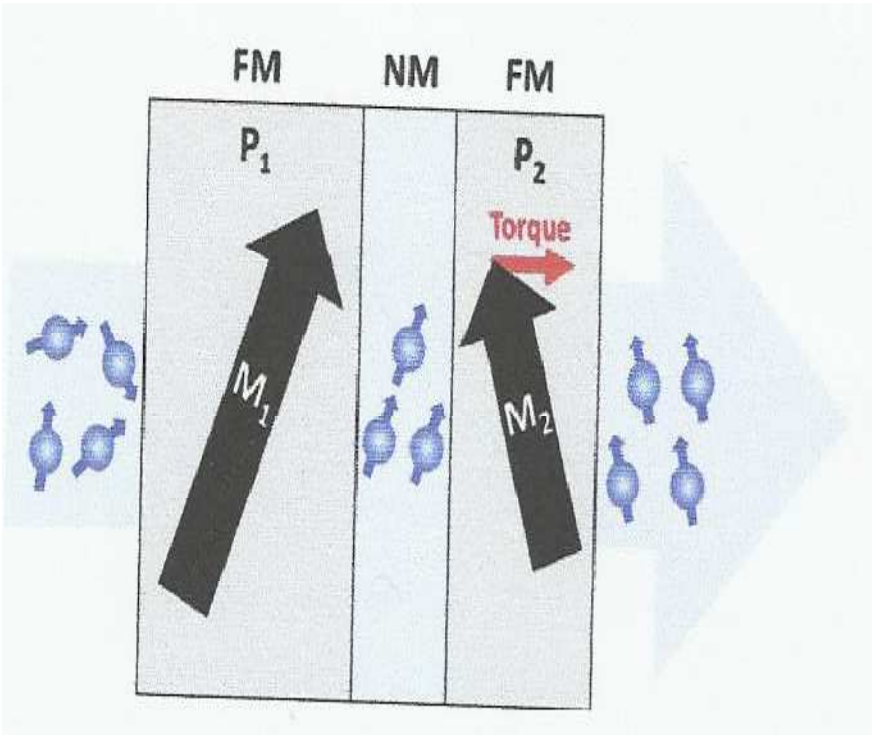

Fig.2.4 : Schematic diagram of the spin transfer torque effect on magnetisation in a FM/NM/FM junction.

2.1.4 Half Metallic Ferromagnets

Half metallic ferromagnets (HMF) are a possible route to highly spin polarised materials. This class of materials was initially proposed by *de Groot et al.* [28] in the early 1980s. In conventional ferromagnets, the spin polarisation arises from an imbalance in the density of states for up (majority) and down (minority) spin electrons. In HMFs the conduction properties for the minority channel are completely different to that of the majority spin channel. The majority band has filled electron states up to the Fermi energy giving metallic conduction while the minority states have a band gap resembling a semiconductor. This is shown schematically in Figure 2.5.

Since the original studies of half-metallic ferromagnetism on NiMnSb [28] a large number of compounds have been found to be half metallic. Many of these are complex alloys, predominantly Heusler alloys [29-31] although half-metallic ferromagnetism has been shown in CrO_2 [32] and even predicted in graphene [33]. Because of these unusual conduction properties HMFs could potentially provide a material with 100% spin polarisation. This would provide extremely high values of TMR and GMR (TMR 832% [34] and GMR of 80% [19]) as well as large spin transfer torques for future spintronic devices. A more detailed discussion of the origin of this half metallicity in Mn-based Heusler alloys can be found in chapter 4.

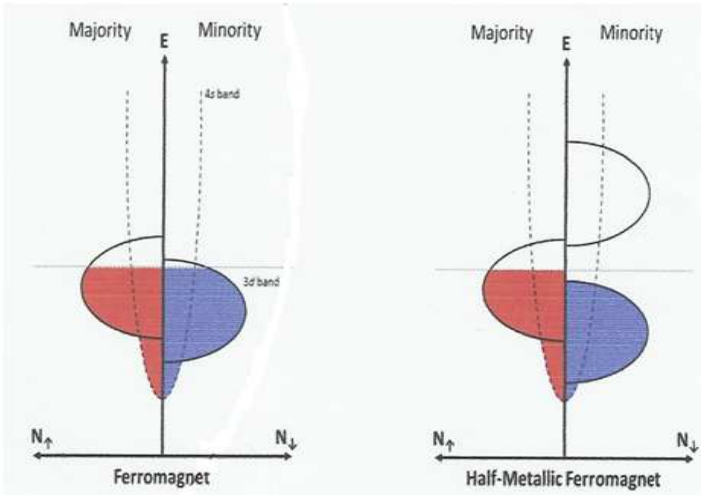

Fig. 2.5: Schematic diagrams of the band structures for a ferromagnet and a half metallic ferromagnet.

2.1.5 Heusler Alloys in Magnetoresistive Devices

Since the discovery of half metallic ferromagnetism in a number of Heusler alloys they have been a field of great research interest for spintronic devices. Co-based Heusler alloys are of particular interest due to their high magnetic moment and Curie temperature, as well as their predicted 100% spin polarisation. Alloys of $Co_2(Mn_{1-x}Fe_x)Si$ [35], $Co_2Fe(Al_{1-x},Si_x)$[34] and Co_2MnGe [36] have found application in many different devices.

The properties of Heusler alloy devices are extremely dependent upon their structure. This includes the Heusler film itself as well as any effects from those films around it. As such, many different structures and growth methods have been used to optimise these properties. Initially, Co_2FeSi films deposited on V buffered Si substrates resulted in reasonable values of TMR of up to 52% at 16K (28% at room temperature) [37]. However this has been improved using Co_2FeSi/Co_2MnSi multi-layered electrodes [37]. Improved values from single layer Co_2FeSi electrodes have been achieved using MgO substrates and crystalline MgO tunnel barriers (TMR = 42% at RT) [38]. The real improvements to these values have occurred since the optimisation of the alloy composition to $Co_2FeAl_{0.5}Si_{0.5}$.

$Co_2FeAl_{0.5}Si_{0.5}$ is optimised so that the Fermi energy lies in the middle of the minority band gap resulting in much improved spin polarisation (90%) [39,40]. Optimisation of both the alloy and the deposition conditions has led to the highest reported value of TMR in a Heusler alloy system, 832% at 9K and 386% at 300K [34].

GMR structures have also been created using $Co_2FeAl_{0.5}Si_{0.5}$ electrodes with both Ag [41,42] and Cr [43] spacers. Extremely high values of GMR, 80% at 14K (34% at room temperature), have been achieved in these systems [41]. Magnetisation switching through spin transfer torque has also been observed in these structures with critical current densities for switching as low as 106 A/cm^2 [42]. However, all these devices have a number of flaws for commercial applications.

The main problems are the high temperatures required to crystallise the Heusler alloy electrodes as well as the UHV deposition conditions. Recently, polycrystalline films have been used in device structures resulting in GMR values of up to 10% at room temperature. These films have significant advantages of reduced fabrication temperatures as well as much lower resistance values ($30 m\Omega\mu m^2$) [44].

2.2 Theoretical and experimental background

In this chapter we will deal with the general properties of the full and the half-Heusler alloys, from a theoretical and experimental point of view. A review of what has been already published will be presented. Before starting our discussion about these systems, it is appropriate to point out the differences between semimetals and half-metals and explain shortly their properties, in order to approach the argument in a systematic way.

2.2.1 Semimetals and half-metals

A semimetal is defined as a material which presents a small overlap in the energy of the conduction band and valence bands. One band is almost filled whereas the other band is nearly empty at zero temperature. Each atom is positioned closer to three of its neighbor atoms than to the rest. As an example, the structure of antimony and arsenic is composed of spheres that intersect along at circular areas. The covalent character of the bonds joining the four closest atoms is linked to the electronegative nature of the semimetals, reflected by their position in the periodic table. They lie between metals and non metals. Members of this group are fairly brittle, and do not conduct heat and current as well as the native metals. The bond type suggested by these properties is intermediate between metallic and covalent; it is consequently stronger and more directional than pure metallic bonding, resulting in crystals of lower symmetry. The classic semimetallic elements are arsenic, antimony and bismuth.

These are also considered metalloids but the concepts are not synonymous. Semimetals, in contrast to metalloids, can also build compounds such as HgTe; tin and graphite are typically not considered metalloids. The electronegativities and ionization energies of the metalloids are between those of the metals and nonmetals, so the metalloids exhibit characteristics of both classes. Silicon, for example, possesses a metallic luster, though it is an inefficient conductor and is brittle. The reactivity of the semimetals depends on the element with which they react. For example, boron acts as a nonmetal when reacting with sodium and as a metal when reacting with fluorine. The boiling points, melting points, and densities of the semimetals vary widely. The intermediate conductivity of semimetals means that they tend to make good semiconductors.

A half-metal is defined as a ferromagnetic metal showing a band gap at the Fermi energy for one spin direction. Consequently, only charge carriers of one spin direction contribute to the conduction. Since the band gap is the essential ingredient in half-metals, it is important to consider its origin. Dozens of half-metals are known by now.

Three categories can be distinguished on the basis of the nature of the band gap: (1) half-metals with covalent band gaps; (2) Charge transfer band gaps, and (3) d - d band gaps. This distinction is important because the origin of the half-metallicity is different in each category. Hence the influence of external perturbations (e.g., pressure) is different as well as the sensitivity to disorder, behavior at surfaces and interfaces, etc. A description of the three different categories follows below.

2.2.1.1 Covalent band gaps

The origin of the band gap in these materials is strongly related with the well known semiconductors of group III-V type, like GaAs. A well known example is NiMnSb. It crystallizes in the half-Heusler structure "$C1_b$", which is closely related with the zincblend structure: one of the empty positions is occupied by the third constituent, Ni in this case, and both Mn and Sb have to occupy sites with tetrahedral

coordination. The presence of occupied d minority states is essential in these materials: half-metals of this category are weak magnets.

2.2.1.2 Charge-transfer band gaps

This category is found in strongly magnetic compounds, where the d bands of the transition metals are empty for the minority spin direction and the itinerant s,p electrons of the transition metals have been localized on the anions. Examples of half-metals in this category are CrO_2, the colossal magnetoresistance (CMR) materials and double perovskites such as $La_{0.7}Sr_{0.3}MnO_3$. The presence of band gaps in these materials is not very dependent on the crystal structure. Compounds in this category are strong magnets.

2.2.1.3 d-d band gap

Half metals in this category show rather narrow bands, so that gaps occur between crystal- field split bands. The exchange splitting can be such that the Fermi level is positioned in a gap for one spin direction only. These materials are weak magnets by definition. Examples in this category are Fe_3O_4, $Fe_xCo_{1-x}S_2$ and Mn_2VAl.

As a comparison, in figure 2.1 we show the band structures of three half metals, each of them belonging to one of the different categories described above. The images were taken from refs [45], [46], respectively. In figure 2.1.a the band structure for NiMnSb is shown. This system crystallizes in the structure $C1_b$. As we will see later on, also another Heusler structure exists (called $L2_1$), where the fourth position is filled. If this is the case, compounds like Ni_2MnSb, which is a normal ferromagnet, can result. According to what has been studied by Weht et al. [45], the half metallic properties of NiMnSb should be attributed to the lower density with respect to Ni_2MnSb.

In figure 2.1.b the structure of CrO_2 is presented. As already stated, this system is a strong ferromagnet and shows for the minority channel a clear gap between the empty and nonempty states at the Fermi level. CrO_2 crystallizes in the rutile structure. This structure allows for stoichiometric (001) surface, which is unlikely to reconstruct or to show surface segregation. Calculations show two oxygen-derived surface states in the band gap for the minority spin direction, but these states are located well below the Fermi energy and do not corrupt the half-metallic properties at the surface.

Experimentally CrO_2 shows the highest degree of spin polarization of all materials studied by Andreev reection. As a third example we show the band structure calculations for Mn_2VAl [46]. We notice that the majority and minority bands, within 1 eV of the Fermi level are very different.

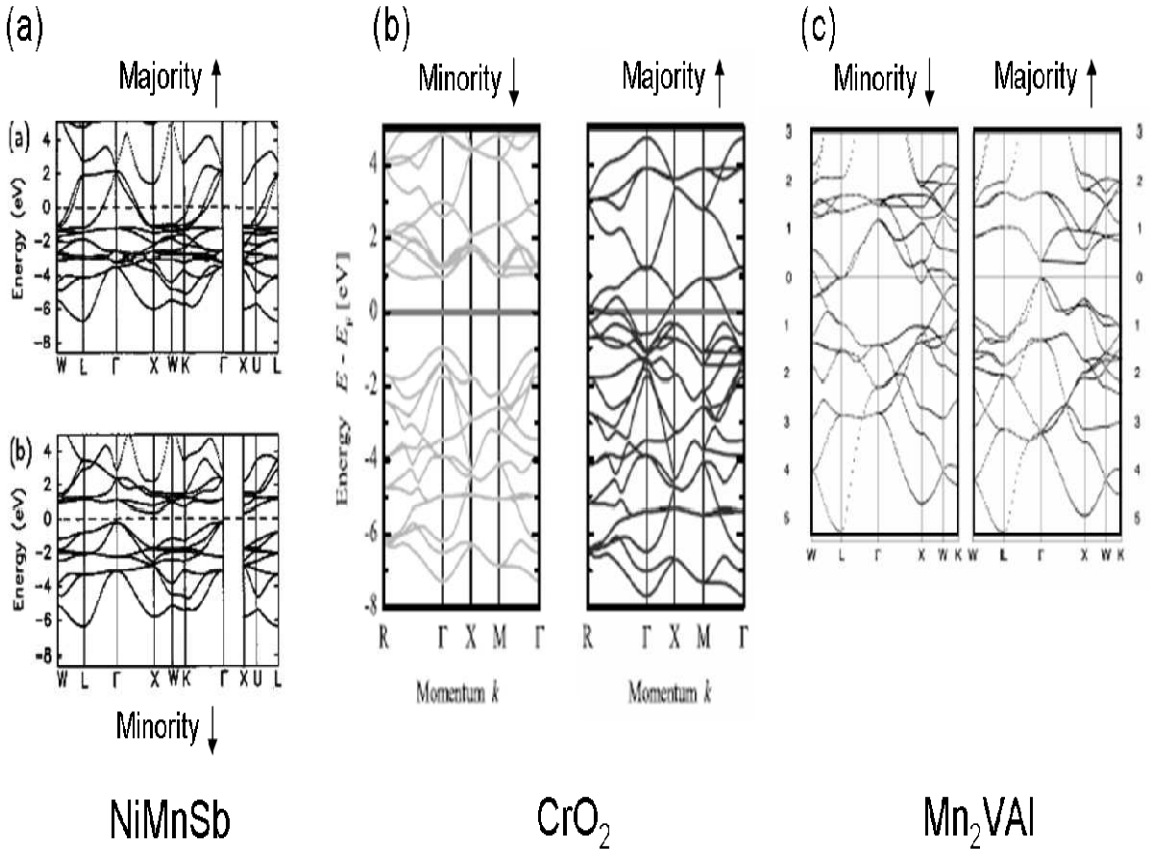

FiG. 2.6 : Band structures of (a) NiMnSb, (b) CrO_2, (c) Mn_2VAl.

In figure 2.2 we observe the different materials which are commonly classified as half-metals. They can assume different structures known as rutile, zincblend, spinel, perovskite and Heusler. We will focus our attention on the Heusler alloys, since most of this thesis work has been devoted to them.

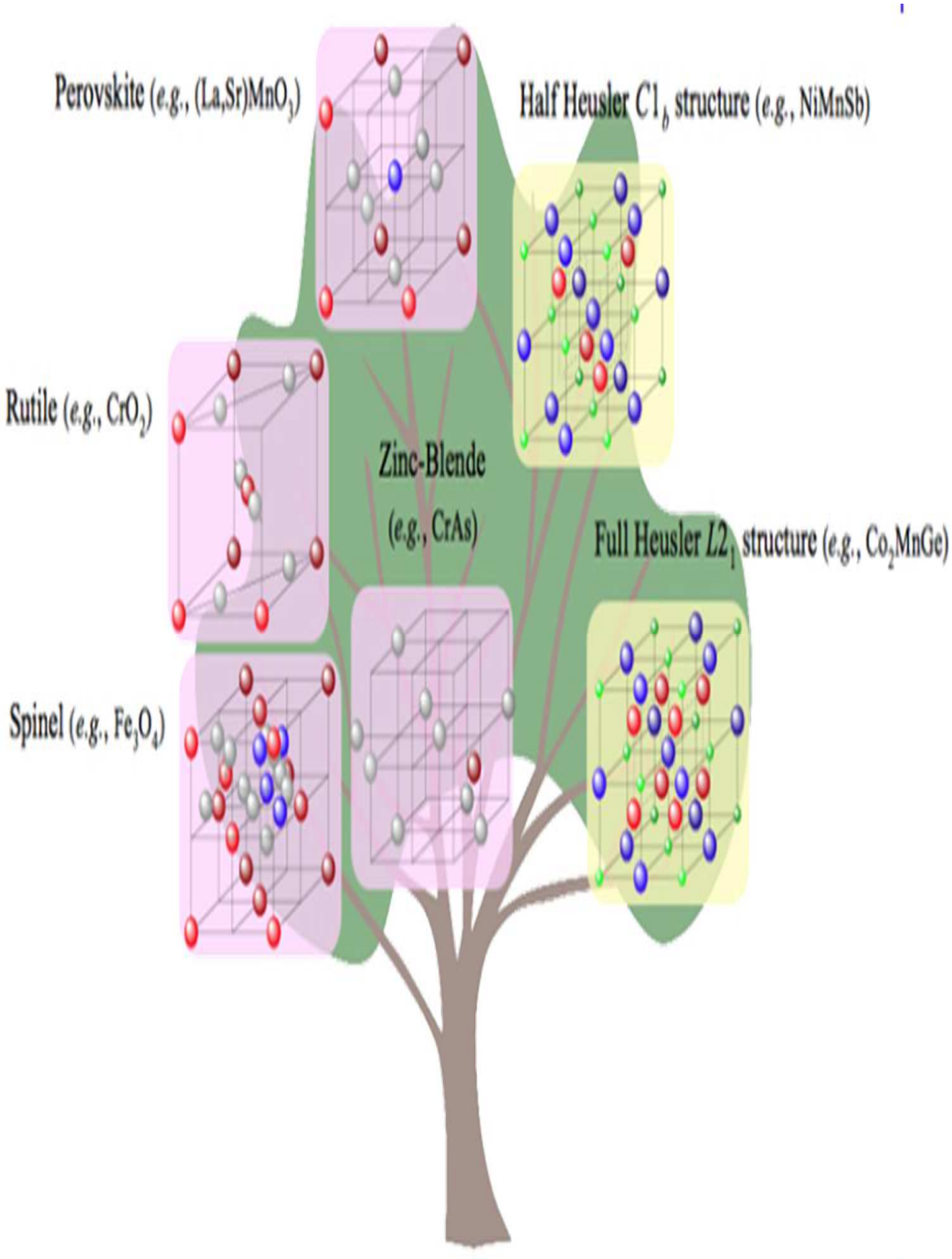

Fig. 2.7: The tree of half metallic ferromagnets.

2.3 Stuctural properties of full and half-Heusler alloys

The discovery of Heusler alloys dates back to 1903 when A. Heusler reported that the addition of sp elements (Al, In, Sn, Sb or Bi) in a Cu-Mn alloy turn it into a ferromagnetic material, even though no ferromagnetic element was contained [47]. The basic understanding of crystal structure and composition of these alloys remained unknown for a long time. In 1929 X-ray measurements of Potter [48] on a Cu-Mn-Al alloy revealed that all constituents of this system were ordered in a fcc lattice. Bradley and Rodgers [49] investigated the Cu-Mn-Al system in detail using X-ray and anomalous X-ray scattering.

They established a relationship between composition, chemical order and magnetic properties. After a successful interpretation of the crystal structure numerous investigations were made on these systems. It was found that the Heusler structure is formed essentially from the ordered combination of two binary B2 compounds XY and XZ. Both compounds may have the CsCl type crystal structure, for instance CoMn and CoAl yield Co_2MnAl. Thus the ability of compounds to form B2 structure indicates the possibility of forming new Heusler compounds. It was also discovered that it is possible to leave one of the four sublattices unoccupied ($C1_b$ structure). The latter compounds are often called half- or semi-Heusler alloys, while the $L2_1$ compounds, where all four sublattices are occupied are referred to as full-Heusler alloys. Extensive experimental studies showed that the majority of Heusler compounds order ferromagnetically in stoichiometric composition. Crystal structure, composition and heat treatment were found to be important parameters for determining magnetic properties.

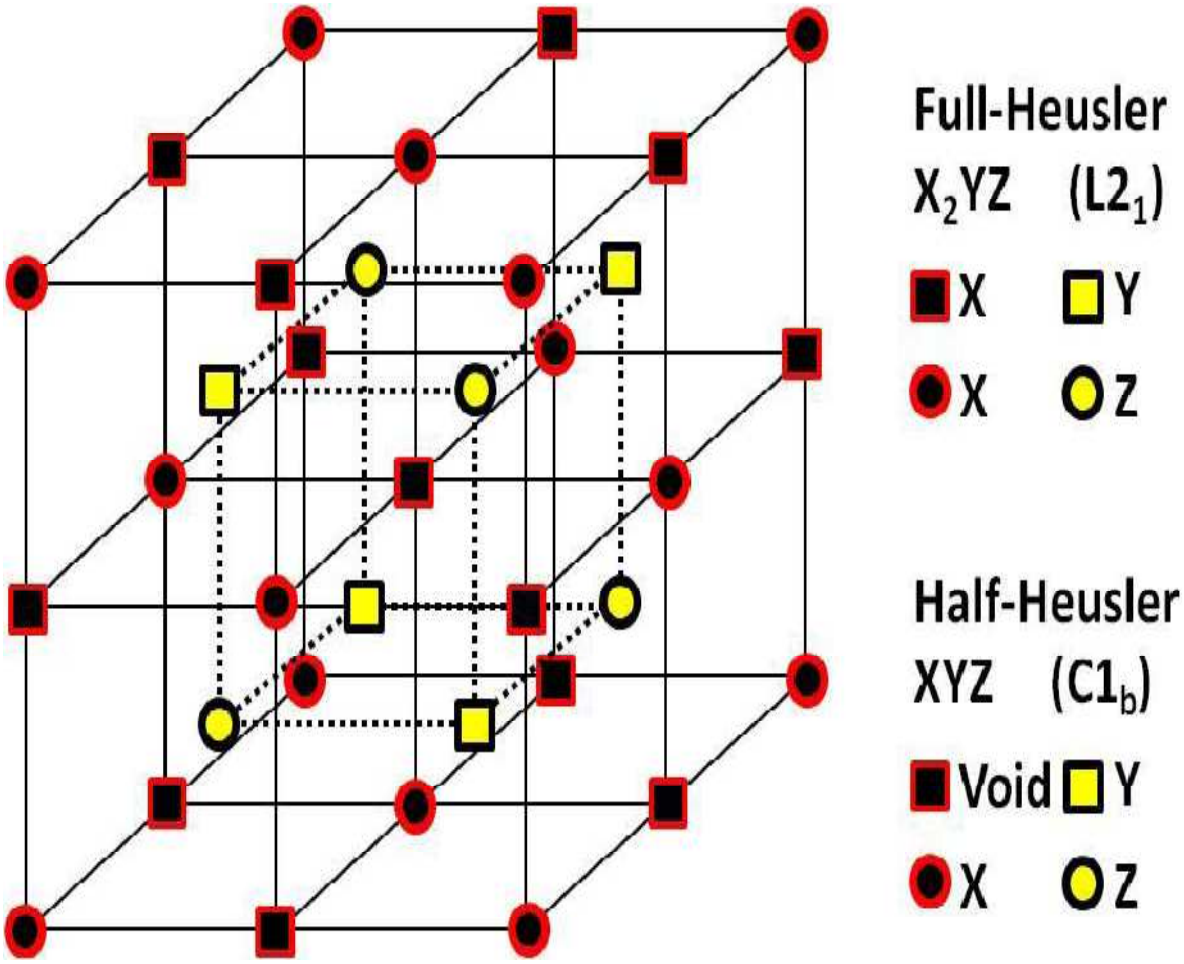

Fig. 2.8 : Structure of full and half-Heusler

With the discovery of half-metallic ferromagnetism in NiMnSb and the observation of shape memory effect in Ni_2MnGa compound, Heusler alloys received tremendous experimental and theoretical interest. In the following we will briefly present the previous experimental and theoretical studies on structural and magnetic properties of Heusler alloys. Also, an overview of the experimental and theoretical studies in literature will be given.

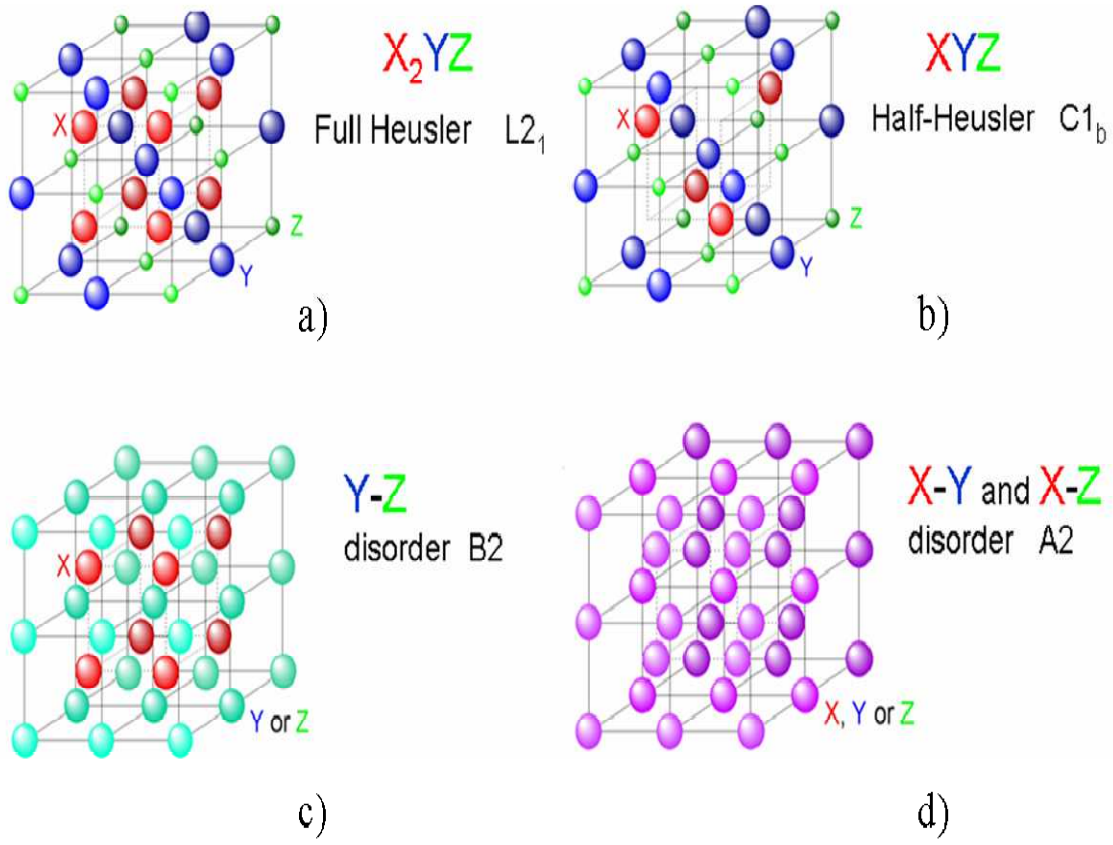

Fig. 2.9 : (a) $L2_1$ full-Heusler and (b) $C1_b$ half-Heusler ordered structures. The structure consists of 4 interpenetrating fcc lattices. In the case of the half-Heusler alloys one of the four sublattices is empty. One notices that if all atoms are identical, the lattice is simply bcc.

Heusler alloys are ternary intermetallic compounds. At the stoichiometric composition, the full Heusler alloys X_2Y Z and the half-Heusler XYZ crystallize in the $L2_1$ and $C1_b$ structures, respectively. The elements associated with X and Y are transition metal elements; the atom which sits in position Z is non-magnetic. The unit cell consists of four interpenetrating fcc sublattices with the positions (000) and $(\frac{1}{2},\frac{1}{2},\frac{1}{2})$ for X, $(\frac{1}{4},\frac{1}{4},\frac{1}{4})$ for Y and $(\frac{3}{4},\frac{3}{4},\frac{3}{4})$ for Z atom. The site $(\frac{1}{2},\frac{1}{2},\frac{1}{2})$ is empty in half-Heusler compounds as shown in the figures 2.8 and 2.9. The two structures are closely related with vacant site.

The $C1_b$ structure can be obtained from the $L2_1$ one by replacing the half of the X sites in an ordered manner. In most of the Heusler alloys Mn enters as the Y element. The compounds where Mn occupies the X positions are very rare: Mn_2VAl [50] and Mn_2VGa [51, 46] are two examples.

2.4 Magnetic properties of Heusler alloys

Heusler alloys are very interesting materials which possess attractive magnetic properties. One can study in the same family of alloys a series of interesting diverse magnetic phenomena like itinerant and localized magnetism, antiferromagnetism, helimagnetism, Pauli paramagnetism or heavy-fermionic behavior [52], [53], [54], [55].

2.4.1 Ferromagnets

The majority of the full and the half-Heusler alloys order ferromagnetically and saturate in weak applied magnetic fields. If the magnetic moment is carried by Mn atoms, as it often happens in the alloys X_2MnZ, a value close to $4\mu B$ is usually observed. Although they are metals, these compounds have localized magnetic properties and are ideal model systems for studying the effects of both atomic disorder and changes in the electron concentration on magnetic properties. In order to reveal the role played by the 3d (X) and sp (Z) atoms on the magnetic properties of Heusler alloys, extensive magnetic measurements have been performed on quaternary Heusler alloys [57]. It has been shown that sp electron concentration has a primary importance in establishing magnetic properties, inuencing both the magnetic moment formation and the type of the magnetic order.

2.4.2 Antiferromagnets and ferrimagnets

Although the majority of Heusler alloys are ferromagnetic, some of them order antiferromagnetically, in particular those compounds containing 3d element in which the magnetic moment is only carried by Mn atoms at the Y site.

Experimentally, antiferromagnetic order is measured both in half-Heusler ($C1_b$ structure) and in full-Heusler alloys ($L2_1$ and B2 structure). Antiferromagnetism is more favorable in full Heusler alloys presenting B2-type crystal structure due to smaller interatomic Mn-Mn distances. Antiferromagnetic behaviour has been reported in several B2-type disordered X_2MnZ (X=Ni, Pd; Z=Al,In) Heusler alloys [57]. The situation is different in half-Heusler alloys. Due to large Mn-Mn distances in $C1_b$ structure the antiferromagnetic interaction between Mn atoms is assumed to be mediated by intermediate atoms (X or Z). Ferrimagnetic ordering (antiferromagnetic coupling of X and Y atoms) is very rare in Heusler alloys compared to ferromagnetic or antiferromagnetic order, though ferrimagnetism has been detected in CoMnSb, Mn_2VAl and Mn_2VGa compounds. Mn_2VAl received much experimental attention, because it is among the few Heusler alloys where Mn sits in the X position. This compound is somewhat peculiar regardless of its detailed electronic structure: while there are many Heusler compounds of the form X_2YZ where Y is Mn, in this compound the X site is occupied by Mn. When Mn sits on the Y site, it has a spin around $4\mu B$, while when sitting on the X site (which is the case for Mn_2VAl) it has a lower spin moment, in agreement with LDA calculation. Although V and Al atoms may substitute on each others sublattice, in the system $Mn_2V_{1-x}Al_{1-x}$ the lattice constant and x-ray intensities show a kink at x = 0, clearly identifying the stoichiometric composition. The structure remains the Heusler one from x between -0.3 and +0.2, with linearly varying saturation moment. At stoichiometry the saturation moment is reported to be $1.9\mu B$, close to the integral value characteristic of the spin moment of half-metallic magnets and the Curie temperature is $T_C = 760K$.

2.5 band structure calculations

The band structure calculations of Heusler alloys has been initiated by Ishida et al., in the early eighties. The authors used non-self-consistent spherical augmented plane wave method (SAPW) to study electronic structure of Ni_2MnSn, Pd_2MnSn [62] and Cu_2MnAl [63].

In 1983 Kübler et al., gave a detailed study on the formation and coupling of the magnetic moments in several Heusler alloys using self-consistent augmented spherical wave method (ASW) [64]. In the same year de Groot et al., [65] discovered the half-metallic ferromagnetism in semi Heusler compounds NiMnSb and PtMnSb. Since then many efforts have been devoted to the study of electronic and magnetic properties of these systems on the basis of band structure calculations. Here we would like to present the theoretical explanations given in literature, which should help us to clarify the behaviour of these systems, starting from a theoretical background.

The origin of ferromagnetic behaviour in Heusler alloys is rather complicated and the mechanisms of magnetic moment localization in transition metals (and their alloys) is one of the most interesting problems in modern magnetism. The picture that emerged from the systematic calculations of Kübler et al. of the microscopic mechanism responsible for the formation of magnetic moments in these systems is that the magnetization is very much confined to the Mn atoms. The localized character of the magnetic moment results from the fact that the large exchange splitting of the Mn d states implies that Mn atoms support d states of only one spin direction. In the ferromagnetic state the spin-up d electrons of the Mn atom hybridize with those of the X atoms in forming a common d band, but spin-down d electrons are almost completely excluded from the Mn sites. Thus we are left with the completely localized magnetic moments composed of completely itinerant electrons. Using the calculated total energies, it was possible to compare the relative stability of various magnetic phases (one ferromagnetic phase and two different antiferromagnetic ones) for a number of Heusler compounds [64] and study the coupling of magnetic moments. Based on these results, it was found that there is no significant direct interaction between the d states on different Mn atoms.

2.5.1 Half-metallic ferromagnetism

The concept of half-metallic ferromagnetism was introduced by de Groot et al., on the basis of band structure calculations in NiMnSb and PtMnSb semi Heusler compounds [64]. In these materials one of the spin sub-bands (usually majority spin band) is metallic, whereas the Fermi level falls into a gap of the other sub-band. Ishida et al. have proposed that also the full-Heusler alloys of the type Co_2MnZ, (Z=Si,Ge) are half-metals. Since then a number of further systems were predicted to be half-metallic. Among them the binary magnetic oxides (CrO_2 and Fe_3O_4), colossal magnetoresistance materials (Sr_2FeMoO_6, CrO_2 and $La_{0,7}Sr_{0,3}MnO_3$), diluted magnetic semiconductors (GaAs, $Ga_{1-x}Mn_xAs$) and zinc-blende compounds MnAs and CrAs.

2.5.2 Origin of the half-metallic gap

The half-metallic ferromagnetism of Heusler alloys is intimately connected to their $C1_b$ crystal structure and consequently to the symmetry of the system. Due to a vacant site at the position (1/2,1/2,1/2) in the $C1_b$ crystal structure the symmetry of the systems is reduced to tetrahedral from the cubic in the case of $L2_1$ type full Heusler alloys. As described by Galanakis et al. [66] the gap arises from the covalent hybridization between the lower-energy d states of the high-valent transition metal atom (like Ni or Co) and the higher-energy d states of the lower-valent atom, leading to the formation of bonding and anti-bonding bands with a gap in between. The bonding hybrids are localized mainly at the high-valent transition metal atom site while the unoccupied anti-bonding states are mainly at the lower-valent transition metal atom site. This is shown schematically in figure 2.10. All Mn atoms are surrounded by six Z nearest neighbors - for the Mn atom at the (0,0,0) these neighbors are at (1/2,0,0), (0,1/2,0); (0,0,1/2), (-1/2,0,0),(0, -1/2,0) and (0,0,-1/2). As a result the interaction of Mn with the Z sp states splits the Mn 3d states into a low-lying triplet of t_{2g} states (dxy; dxz and a higher lying doublet of eg states dx^2-y^2 , $d3z^2-r^2$). The splitting is partly due to the different electrostatic repulsion, which is strongest for the eg states which directly point at the Z atoms.

In the majority band the Mn 3d states are shifted to lower energies and form a common 3d band with X (X=Ni, Co) 3d states, while in the minority band the Mn 3d states are shifted to higher energies and are unoccupied. A band gap at E_F is formed, which separates the occupied d bonding states from the unoccupied d antibonding states as shown in the figure 2.10.

For instance, in the compound NiMnSb the minority occupied bonding d states are mainly of Ni character while the unoccupied anti-bonding states are mainly of Mn character. These structures are particularly stable when only the bonding states are occupied. The p states strongly hybridize with the transition metal d states and the charge in these bands is delocalized. What counts is that the s and p bands accommodate eight electrons per unit cell, effectively reducing the d charge of the transition metals atoms. The sp-elements like Sb play an important role for the existence of the Heusler alloys with a gap at the E_F. Thus NiMnSb is a half-metal with a gap at E_F in minority band and a metallic DOS at the Fermi level in majority band. Also for systems with more (or less) than 18 electrons, the gap can still exist.

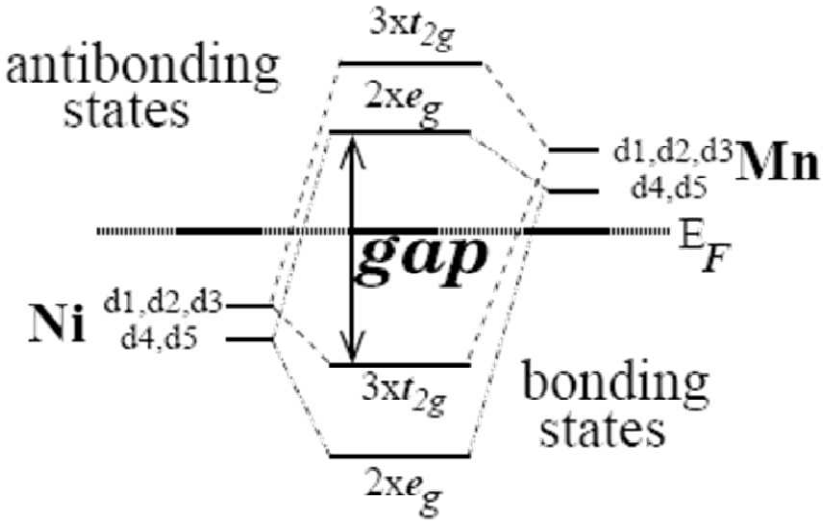

Fig. 2.10: Illustration of the origin of the gap in the minority band in half-Heusler alloys, as described in ref. [66].

The explanation of the valence and conduction bands given in ref.[66] is internally consistent. It explains the existence of exactly nine minority valence bands and simultaneously describes the magnetic properties of these compounds. With small modifications it can be also extended to explain the properties of the half-ferromagnetic full-Heusler alloys like Co_2MnGe. Nevertheless the Sb atoms or in general the sp atoms are important for the properties of the Heusler alloys. The calculated total magnetic moment is $4\mu B$ per unit cell and mostly located in Mn atom. NiMnSb has 22 valence electrons per unit cell, 10 from Ni, 7 from Mn and 5 from Sb. Because of the gap at E_F , in the minority band exactly 9 bands are fully occupied (1 Sb-like s band, 3 Sb-like p bands and 5 Ni-like d bands) and the remaining 13 electrons are accommodated in majority band, resulting in a magnetic moment of 13-9=4μB per unit cell. Note that half-Heusler alloys like CoTiSb with 18 valence electrons show semiconducting behavior. It should be noted that the halfmetallic character of half-Heusler compounds is highly sensitive to the crystal structure and symmetry e.g., the cubic point symmetry at Mn sites in ordinary X_2MnZ Heusler alloys gives rise to a symmetry of Mn-3d-t2g, states that is different from the symmetry of the Sb p states. Hence, these states do not hybridize, so that no gap is opened in the minority spin band.

2.5.3 Slater-Pauling behavior

The total moment of the half- and full-Heusler alloys follows the rule: $M_t = Z_t - 18$ (half) and $M_t = Z_t - 24$ (full) where Z_t is the total number of valence electrons [23]. Z_t is given by the sum of the number of spin-up and spin-down electrons $Z_t = N\uparrow + N\downarrow$, while the total moment M_t is given by the difference $M_t = N\uparrow - N\downarrow$. Since 9 (12) minority bands of half (full) Heusler alloys are fully occupied, a simple rule of 18 (24) is obtained for half-metallicity in $C1_b$-type ($L2_1$) Heusler alloys. This is analogous to the well-known Slater-Pauling behavior of the binary transition metal alloys.

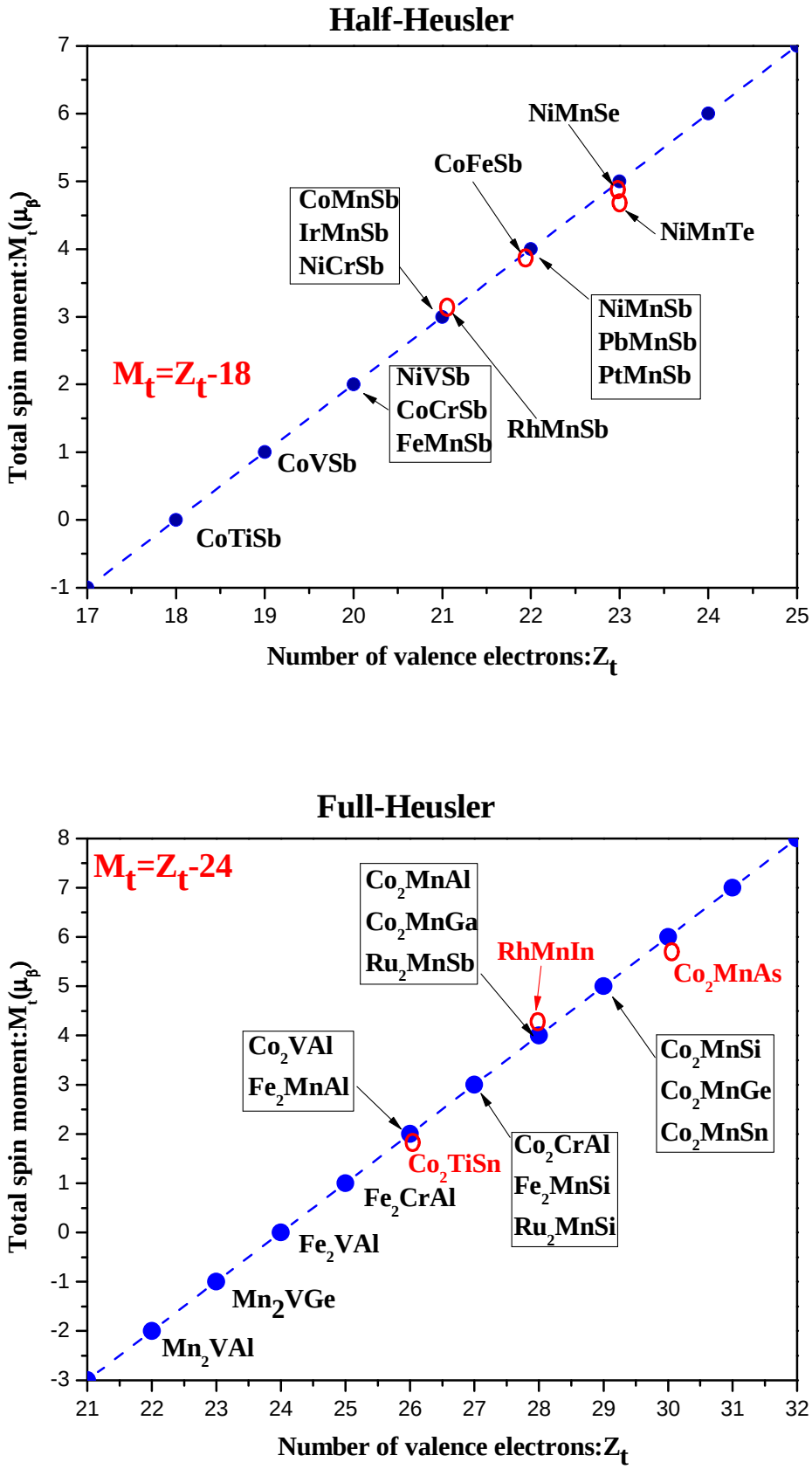

Fig 2.11: Total spin moments for half- Heusler alloys and full- Heusler

The dashed line represents the Slater Pauling behavior. The open circles indicate the compounds deviating from SP behavior. The difference with respect to these alloys is that in the half-Heusler alloys the minority population is fixed to 9 and 12, so that the screening is achieved by filling the majority band, while in the transition metal alloys the majority band is filled with 5d states or completely empty and charge neutrality is achieved by filling the minority or majority states. Therefore in the transition metals alloys the total moment is given by $M_t = 10 - Z_t$ for the systems on the left side and $M_t = Z_t$ for the systems on the right side of the Slater-Pauling curve. For the half-metallic zinc-blende compounds like CrAs the rule is: $M_t = Z_t - 8$, since the minority As-like valence bands accommodate 4 electrons. In all cases the moments are integer. In Figure 2.11 the calculated total spin magnetic moments for both Heusler alloys, plotted as a function of the total number of valence electrons, are gathered. The dashed line represents the rule $M_t = Z_t - 18$ ($M_t = Z_t - 24$) fulfilled by these compounds. The total moment Mt is an integer quantity, assuming the values 0, 1, 2, 3, 4 and 5 if $Z_t > 18$. In the case of full Heusler alloys ($Z_t = 24$) M_t can also take -2, -1 and 6. The value 0 corresponds to the semiconducting phase [67].

References

[1] S. M. Sze and K. K. Ng, Physics of Semiconductor Devices. Wiley, (2006)

[2] G. E. Moore, Proceedings of the IEEE **86**, (1998) 82-85

[3] B. D. Rizzo, NVIDIA Introduces Ge Force GTX TITAN: DNA Of The World's Fastest Supercomputer, Powered By World's Fastest GPU, <http://nvidianews.nvidia.com/Releases/NVIDIA-Introduces-GeForce -GTX-TITAN-DNA-of-the-World-s-Fastest-Supercomputer-Powered-by-World-s-Fa-925.aspx> (2013)

[4] N. S. Kim, T.Austin, D. Baauw, T. Mudge, K. Flautner, J. S. Hu, M. J. Irwin, M. Kandemir and V. Narayanan, Computer **36**, (2003) 68-75

[5] D. D. Awschalom and M. E. Flatte, Nature Physics **3**, (2007) 153-159,

[6] G. A. Prinz, Science **282**, (1998)1660-1663

[7] G. A. Prinz Journal of Magnetism and Magnetic Materials **200**, (1999) 57-68

[8] S. Datta and B. Das Applied Physics Letters **56**, (1990) 665-667

[9] W. Thomson, Proceedings of the Royal Society of London **8**, (1856) 546-550

[10] A. Brataas, A. D. Kent and H. Ohno, Nature Materials **11**, (2012) 372-381

[11] S. S. P. Parkin, Physical Review Letters **67**, (1991) 3598-3601

[12] G. Binasch, P. Grünberg, F. Saurenbach and W. Zinn, Physical Review B **39**, (1989) 4828-4830

[13] M. N. Baibich, J. M. Broto, A. Fert, F. N. Van Dau, F. Petroff, P. Etienne, G. Creuzet, A. Friederich, and J. Chazelas, Physical Review Letters **61**, (1988) 2472-2475

[14] N. F. Mott, Proceedings of the Royal Society of London. Series A, Mathematical and Physical Sciences **153**, (1936) 699-717

[15] N. F. Mott, Proceedings of the Royal Society of London. Series A, Mathematical and Physical Sciences **156**, (1936) 368-382

[16] I. A. Campbell, A. Fert, and R. Pomeroy, Philosophical Magazine **15**, (1967) 977-983

[17] A. Fert, and I. A. Campbell, Physical Review Letters **21**, (1968) 1190-1192

[18] S. M. Thompson, Journal of Physics D: Applied Physics **41**, (2008) 093001

[19] T. M. Nakatani, , T. Furubayashi, and K. Hono, Journal of Applied Physics **109**, (2011) 724-723

[20] M. Julliere, Physics Letters A 54, (1975) 225-226

[21] T. Miyazaki, and N. Tezuka, Journal of Magnetism and Magnetic Materials 139, (1995) 231-234

[22] J. S. Moodera, L. R. Kinder, T. M. Wong, and R. Meservey, Physical Review Letters 74, (1995) 3273-3276

[23] W. H. Butler, X. G. Zhang, T. C. Schulthess, and J. M. MacLaren, Physical Review B **63**, (2001) 054416

[24] S. Ikeda, J. Hayakawa, Y. Ashizawa, Y. M. Lee, K. Miura, H. Hasegawa, M. Tsunoda, F. Matsukura, and H. Ohno, Applied Physics Letters **93**, (2008) 082508-082503

[25] Slonczewski, J. C. Journal of Magnetism and Magnetic Materials 159, (1996) 1-7

[26] L. Berger, Journal of Applied Physics **55**, (1984) 1954-1956

[27] S. Maekawa, S. O. Valenzuela, E. Saitoh and T. Kimura, Spin Current. OUP Oxford, (2012)

[28] R. A. de Groot, F. M. Mueller, P. G. v. Engen and K. H. J. Buschow, Physical Review Letters 50, (1983) 2024-2027

[29] C. Felser, and B. Hilllebrands, Journal of Physics D: Applied Physics (2007) 40

[30] H. C. Kandpal, G. H. Fecher and C. Felser, Journal of Physics D: Applied Physics **40**, (2007) 1507

[31] C. G. F. Blum, C. A. Jenkins, J. Barth, C. Felser, S. Wurmehl, G. Friemel, C. Hess, G. Behr, B. Buchner, A. Reller, S. Riegg, S. G. Ebbinghaus, T. Ellis, P. J. Jacobs, J. T. Kohlhepp and H. J. Swagten, M. Applied Physics Letters **95**, (2009) 161903-161903

[32] R. S. Keizer, S. T. B. Goennenwein, T. M. Klapwijk, G. Miao, G. Xiao and A. Gupta, Nature **439**, (2006) 825-827

[33] Y. W. Son, M. L. Cohen and S. G. Louie, Nature **444**, (2006) 347-349

[34] N. Tezuka, N. Ikeda, F. Mitsuhashi and S. Sugimoto, Applied Physics Letters **94**, (2009) 162504-162503,.

[35] V. K. Lazarov, K. Yoshida, J. Sato, P. J. Hasnip, M. Oogane, A. Hirohata and Y. Ando, Applied Physics Letters **98**, (2011) 242508-242503,.

[36] T. Ambrose, J. J. Krebs and G. A. Prinz, Applied Physics Letters **76**, (2000) 3280-3282

[37] D. Ebke, J. Schmalhorst, N. N. Liu, A. Thomas, G. Reiss and A. Hutten, Applied Physics Letters **89**, (2006) 162506-162503

[38] K. Inomata, S. Okamura, A. Miyazaki, M. Kikuchi, N. Tezuka, M. Wojcik and E. Jedryka, Journal of Physics D: Applied Physics **39**, (2006) 816

[39] T. M. Nakatani, A. Rajanikanth, Z. Gercsi, Y. K. Takahashi, K. Inomata and K. Hono, Journal of Applied Physics 102, (2007) 033916-033918

[40] R. Shan, H. Sukegawa, W. H. Wang, M. Kodzuka, T. Furubayashi, T. Ohkubo, S. Mitani, K. Inomata and K. Hono, Physical Review Letters **102**, (2009) 246601

[41] T. M. Nakatani, T. Furubayashi, S. Kasai, H. Sukegawa, Y. K. Takahashi, S. Mitani and K. Hono, Applied Physics Letters **96**, (2010) 212501-212503

[42] H. Sukegawa, S. Kasai, T. Furubayashi, S. Mitani and K. Inomata, Applied Physics Letters **96**, (2010) 042508-042503

[43] T. Furubayashi, K. Kodama, H. S. Goripati, Y. K. Takahashi, K. Inomata and K. Hono, Journal of Applied Physics **105**, (2009) 305-303,.

[44] T. M. Nakatani, Y. Du, Y. K. Takahashi, T. Furubayashi and K. Hono, Acta Materialia **61**, (2013) 3695-3702

[45] C. M. Fang, G. A. de Wijs, and R. A. de Groot, J. of Appl. Phys., vol. **91**, (2002)8340-8344

[46] R. Weht and W. E. Pickett, Phys. Rev. B, vol. **60**, (1999) 006-010

[47] F. Heusler, Verh. Dtsch. Phys. Ges., vol. **5**, (1903) 219

[48] H. H. Potter, Proc. Phys. Soc., vol. **41**, (1929) 135

[49] A. J. Bradley and J. W. Rodgers, Proc. R. Soc. London Ser. A, vol. **144**, (1934) 340

[50] H. Itoh, T. Nakamichi, Y. Yamaguchi, and N. Kazama, Trans. Jpn. Inst. Met., vol. **24**, (1983) 265

[51] K. H. J. Buschow and P. G. van Engen, J. Mag. Magn. Mater., vol. **25**, (1981) 90

[52] P. J. Webster and K. R. A. Ziebeck, Alloys and Compounds of d-Elements with Main Group Elements - Part 2. H. P. J. Wijn, Landolt-Bornstein, New Series, Group III, Vol. 19/c (Springer, Berlin), (1988).

[53] P. J. Webster, K. R. A. Ziebeck, and K.-U. Neumann, Magnetic Properties of Metals. Landolt-B ornstein, New Series, Group III, Vol. 32/c (Springer, Berlin), (2001).

[54] J. Pierre, R. V. Skolozdra, J. Alloys Comp., vol. **101**, (1997) 262-263

[55] J. Tobola, J. Pierre, S. Kaprzyk, R. Skolozdra, and M. Kouacou, J. Phys.: Condens. Matter, vol. **10**, (1998) 1013

[56] S. Ishida, Y. Kubo, J. Ishida, and S. Asano, J. Phys. Soc. Jpn., vol. **48**, (1980) 814

[57] S. Ishida, J. Ishida, S. Asano, and J. Yamashita, J. Phys. Soc. Jpn., vol. **45**, (1978) 1239

[58] J. Kuebler, A. R. Williams, and C. B. Sommers, Phys. Rev. B, vol. **28**, (1983) 4

[59] R. A. de Groot, F. M. Mueller, P. G. van Engen, and K. H. J. Buschow, Phys. Rev. Lett, vol. **50**, (1983) 2024

[60] I. Galanakis, P. H. Dederichs, and N. Papanikolaou, Phys. Rev. B, vol. **66**, (2002) 134428

[61] I. Galanakis, P. H. Dederichs, and N. Papanikolaou, Phys. Rev. B, vol. **66**, (2002) 174429

[62] S. Ishida, S. Akazawa, Y. Kubo, and J. Ishida, J. Phys. F: Met. Phys., vol. **12**, (1982) 1111

[63] S. Kaemmerer, S. Heitmann, D. Meyners, D. Sudfeld, A.Thomas, A. Huetten, and G. Reiss, Journ. Appl. Phys., vol. **93**, (2003) 10

[64] T. Saito, T. Katayama, T. Ishikawa, M. Yamamoto, D. Asakura, and T. Koide, Appl. Phys. Lett., vol. **91**, (2007) 262502

[65] A. Bergmann, PhD thesis, Ruhr-University, Bochum, (2006)

[66] J. Sagar, PhD thesis, Department of Physics, University of York, (2013)

[67] M. Vadala, PhD thesis, faculty of physics and astronomy, Ruhr-University, Bochum, (2008)

3 Density Functional Theory

Physics and chemistry use a theory called Density functional theory (DFT), which is a quantum mechanical theory, to examine the electronic structure of many body systems, especially, atoms, molecules and the condensed phases. DFT is one of the most common and flexible technique obtainable in condensed matter physics, computational physics, and computational chemistry [1], due to its capability to deal with large numbers of electrons with complete precision [2].

Time-dependent density-functional theory (TDDFT) is the generalization of ground-state DFT to include time-dependent external potentials on electrons, and its formal validity was set up with the Runge- Gross theorem [3]. The analogous connection between time-dependent densities and time-dependent potentials for a given preliminary state guides to the time-dependent Kohn-Sham system, which is a set of no interacting presumptive electrons moving in a time-dependent Kohn-Sham potentials.

TDDFT has been applied to many problems in atomic, molecular and solid state systems, including optical response, dynamic polarizabilities and hyper-polarizabilities, excitation energies, species in intense laser fields and highly energetic collisions [4].

The principle of DFT is to illustrate an interconnecting system of fermions by means of its density and not by its many-body wave function [5]. While DFT chiefly gives a good explanation and portrayal of ground state qualities. Practical applications of DFT rely on rough calculations for the so-called exchange-correlation probability. The exchange-correlation probability portrays the influences of the Pauli principle and the Coulomb possibility beyond a pure electrostatic interaction of the electrons. The precise exchange-correlation probability gives a solution of the many-body problem precisely, which is obviously not possible in solids [6].

In spite of the fact that density functional theory has its theoretical roots in the Thomas-Fermi model, it was put on a solid hypothetical foundation by the two Hohenberg-Kohn theorems (H-K) [7]. The original H-K theorems held only for non-degenerate ground states in the absence of a magnetic field, although they have since been generalized to include them [8].

The ground state properties of a many-electron system are exclusively decided by an electron density that depends only on 3 spatial coordinates, this is shown in the first H-K theorem. It puts down the base work for reducing the many-body problem of N electrons with 3N spatial coordinates to only 3 spatial coordinates, by the use of functional of the electron density. This theorem can be expanded to the time-dependent sphere to build up time-dependent density functional theory, which can be applied to portray stimulated conditions. The second H-K theorem defines an energy functional for the system and gives evidences to prove that the proper ground state electron density reduces this energy functional [1].

The intractable many-body problem of interacting electrons in a static external potential, within the framework of Kohn-Sham DFT(KSDFT), is reduced to a tractable problem of non-interacting electrons moving in an effectual potential. The effective potential contains the external potential and the effects of the Coulomb interactions between the electrons, e.g., the exchange and correlation interactions. Modeling the latter two interactions becomes the difficulty within KS DFT. The simplest rough calculation is the local-density approximation (LDA), which depends on precise exchange energy for a uniform electron gas, which can be obtained from the Thomas-Fermi model, and from fits to the correlation energy for a uniform electron gas.

3.1 The Hohenburg-Kohn Theorems

Hohenberg and Kohn [6] were the first to formulate the special place of DFT in 1964 which becomes directly clear from the fundaments, Here a derivation of DFT and its formula.

The nuclei of the treated molecules or clusters, as usual in many body electronic structure calculations, are seen as fixed (the Born-Oppenheimer approximation), generating a static external potential *V* in which the electrons are moving. A stationary electronic state is then portrayed by a wave function $\Psi(\vec{r}_1, \ldots, \vec{r}_N)$ satisfying the many-electron Schrodinger equation:

$$\begin{aligned}\hat{H}\Psi &= \left[\hat{T} + \hat{V} + \hat{U}\right]\Psi \\ &= \left[\sum_i^N -\frac{\hbar^2}{2m}\nabla_i^2 + \sum_i^N V(\vec{r}_i) + \sum_{i<j}^N U\left(\vec{r}_i, \vec{r}_j\right)\right]\Psi \\ &= E\,\Psi \end{aligned} \tag{3.1}$$

Where $\hat{H}$ is the electronic molecular Hamiltonian, N is the number of electrons, $\hat{T}$ is the N-electron kinetic energy, $\hat{V}$ is the N–electron potential energy from the external field, and $\hat{U}$ is the electron-electron interaction energy for the N-electron system. The operators $\hat{T}$ and $\hat{U}$ are so-called universal operators as they are alike for any system, while $\hat{V}$ is system dependent, i.e. non-universal. The differentiation between having separate single-particle problems and the much more complex many-particle problem stems from the interaction term $\hat{U}$.

The many-body Schrodinger equations solved by many complicated technique based on the extension of the wave function in Slater determinants. While the easiest one is the Hartree-Fock technique, more sophisticated techniques are usually classified as post-Hartree-Fock techniques. However, the problem with these techniques is the vast computational effort, which makes it almost unfeasible to apply them competently to larger, more complicated systems.

Here DFT offers an attractive substitute, being much more adaptable as it provides a way to systematically map the many-body problem, with $\hat{U}$, onto a single-body problem without $\hat{U}$. In DFT the key changeable is the particle density $n(\vec{r})$, which for a normalized is given by:

$$n(\vec{r}) = N \int d^3r_1 \int d^3r_2 \dots \int d^3r_N \Psi^*(\vec{r}_1\vec{r}_2, \dots, \vec{r}_N)\Psi(\vec{r}_1\vec{r}_2, \dots, \vec{r}_N) \quad (3.2)$$

This relation can be reversed, that is to say, for a given ground-state density $n_0(\vec{r})$ it is principally potential, to work out the equivalent ground-state wave function $\Psi_0(\vec{r}_1,\dots, \vec{r}_N)$. That is to say, $\Psi_0$is a sole functional of n_0, $\Psi_0 = \Psi[n_0]$ and as a result the ground-state expectation value of an observable $\hat{O}$ is also a functional of n_0

$$O[n_0] = \langle \Psi[n_0] | \hat{O} | \Psi[n_0] \rangle \quad (3.3)$$

In particular, the ground-state energy is a functional of n_0

$$\begin{aligned} E_0 = E[n_0] &= \langle \Psi[n_0] | \hat{T} + \hat{V} + \hat{U} | \Psi[n_0] \rangle \\ &= \langle \Psi[n_0] | \hat{T} | \Psi[n_0] \rangle + \langle \Psi[n_0] | \hat{V} | \Psi[n_0] \rangle + \langle \Psi[n_0] | \hat{U} | \Psi[n_0] \rangle \\ &= \hat{T}[n_0] + \hat{V}[n_0] + \hat{U}[n_0] \end{aligned} \quad (3.4)$$

Where the contribution of the external $\langle \Psi[n_0] | \hat{V} | \Psi[n_0] \rangle$

The potential can be written clearly in terms of the ground-state density n_0

$$V[n_0] = \int V(\vec{r}) n_0(\vec{r}) d^3r \quad (3.5)$$

More commonly, the contribution of the external potential $\langle \Psi | \hat{V} | \Psi \rangle$ can be written clearly in terms of the density n,

$$V[n] = \int V(\vec{r})n(\vec{r})d^3r \tag{3.6}$$

As mentioned above, the functional $T[n]$ and $U[n]$ are called universal functional, whereas $V[n]$ is called a non-universal functional, as it relies on the system under study. Having a definite system, i.e., having specified $\hat{V}$, one then has to reduce the functional

$$E(n) = T[n] + U[n] + \int V(\vec{r})n(\vec{r})d^3r \tag{3.7}$$

In regards to n ($\vec{r}$), taking for granted one has got dependable terms for $T(n)$ and $U(n)$. A successful reduction of the energy functional will produce the ground-state density n_0 and thus all other ground-state observables.

The Lagrangian technique of undetermined multipliers [7] can be applied to solve the variation problems of minimizing the energy functional $E(n)$. First, one takes into accounts an energy functional that doesn't clearly have an electron-electron interaction energy term,

$$E_s[n] = \langle \Psi_s[n] | \hat{T}_s + \hat{V}_s | \Psi_s[n] \rangle \tag{3.8}$$

where $\hat{T}_s$ indicates the non-interacting kinetic energy and $\hat{V}_s$ is an external effectual potential in which the particles are moving. Clearly, if $\hat{V}_s$ is $n_s(\vec{r}) = n(\vec{r})$ selected to be

$$\hat{V}_s = \hat{V} + \hat{U} + (\hat{T} - \hat{T}_s) \tag{3.9}$$

Consequently, one can solve the so-called Kohn-Sham equations of this assisting non-interacting system,

$$\left[-\frac{\hbar^2}{2m}\nabla^2 + V_s(\vec{r})\right]\Phi_i(\vec{r}) = \epsilon_i\Phi_i(\vec{r}) \tag{3.10}$$

which produces the Φ_i orbital that reproduce the density $n(\vec{r})$ of the authentic many-body system.

$$n(\vec{r}) = n_s(\vec{r}) = \sum_i^N |\Phi_i(\vec{r})|^2 \tag{3.11}$$

The effective single-particle potential can be written in more detail as

$$V_s(\vec{r}) = V(\vec{r}) + \int \frac{e^2 n_s(\vec{r}')}{|\vec{r}-\vec{r}'|} d^3r' + V_{XC}[n_s(\vec{r})] \tag{3.12}$$

where the second term stands for the so-called Hartree expression portraying the electron-electron Coulomb repulsion, while the last expression V_{XC} is called the exchange-correlation possibility. Here, V_{XC} has all the many-particle interactions. Since the Hartree expression and V_{XC} rely on $n(\vec{r})$, which relies on the Φ_i , which in turn relies on $\hat{V}_s$, the problem of solving the Kohn-Sham equation has to be done in a selfconsistent way. One typically begins with an first guess for $n(\vec{r})$, then works out the equivalent $\hat{V}_s$ and solves the Kohn-Sham equations for the Φ_i [1].

To conclude, techniques in DFT are complex and different, but can roughly be partitioned into three categories [8]:

- Techniques that apply a local density rough calculation (LDA). The LDA is decided exclusively and based on the qualities of the electron density. The significant supposition of this approximation is that, for a molecule with many electrons in a gaseous state, the density is consistent throughout the molecule.

This is not the case for molecules, where the electron density is decidedly not consistent.

This approximation does, however, work well with electronic band structures of solids, which illustrates the scope of energies in which electrons are allowed or not allowed . Outside of these applications, however, LDA's are not very acceptable.

- Techniques that unite the electron density calculations with a gradient correction factor. A gradient in mathematics is a function that measures the rate of change of some property. In this case, the gradient seems to explain the non-uniformity of the electron density, and as such is known as gradient-corrected. Another expression for this is non-local.

- Techniques that are a mixture of a HF approximation to the exchange energy and a DFT approximation to the exchange energy, all united with a functional that has electron correlation. These Techniques are known as hybrid techniques, and are now the most common and popular DFT techniques used in practically.

3.2 Kohn-Sham Equations

A set of eigen value equations within density functional theory (DFT) are called Kohn Sham equations. As mentioned above , DFT tries to minimize a many-body problem for the N particle wave function $\Psi_0(\vec{r}_1, \dots, \vec{r}_N)$ to one in terms of the charge density $n(\vec{r})$ which relies on 3 variables, using the Hohenberg-Kohn theorems[9]. The total energy E of the system as a functional of the charge density can be written as:

$$E(n) = T(n) + \int V_{ext}(r)n(r)dr + V_H[n] + E_{xc}[n] \qquad (3.13)$$

where T is the kinetic energy of the system, V_{ext} is an external potential acting on the system, and

$$V_H = \frac{e^2}{2}\int \frac{n(r)n(r')}{|r-r'|}drdr' \tag{3.14}$$

Is the Hartree energy and Ex*c* is the exchange-correlation energy.

The straight forward application of this formula has two barriers:

First, the exchange-correlation energy Ex*c* is not known precisely, and second, the kinetic term must be created in terms of the charge density. As was first suggested by Kohn and Sham, the charge density n(r) can be written as the sum of the squares of a set of orthonormal wave functions $\Phi_i(r)$:

$$n(r) = \sum_{i}^{N} |\Phi_i(r)|^2 \tag{3.15}$$

The unit of charge density n(r) is (c/m^3).

Equation (3-15) represents the solution to the Schrodinger equation for *N* non-interacting electrons moving in an effectual potential $V_{eff}(r)$

$$-\frac{\hbar^2}{2m}\nabla^2\Phi_i(r) + V_{eff}(\vec{r})\Phi_i(r) = \varepsilon_i\Phi_i(r) \tag{3.16}$$

where the effectual potential is defined to be

$$V_{eff}(r) = V_{ext}(r) + e^2\int \frac{n(r')}{|r-r'|}dr' + \frac{\delta E_{xc}[n]}{\delta_n} \tag{3.17}$$

These three equations form the Kohn-Sham orbital equations in their standard form. This system is then solved iteratively, until self-consistency is approached. Note that the eigen values ε_i have no physical meaning, only the total sum, which matches the energy of the entire system *E* through the equation [10]:

$$E = \sum_{i}^{N} \varepsilon_i - V_H[n] + E_{xc}[n] - \int \frac{\delta E_{xc}[n]}{\delta n(r)} n(r) dr \qquad (3.18)$$

Schematic representation of the self-consistent loop for solution of the Kohn-Sham equations. Generally speaking one must repeat two such circles at once for the two spins, with the potential for each spin relying upon the density of both spins [11].

Practically, there are several distinct ways in which Kohn-Sham theory can be applied depending on what is being examined. In solid state calculations, the local density approximations are still commonly used along with plane wave basis sets, as an electron gas approach is more suitable for electrons delocalized through an infinite solid. In molecular calculations, however, more complicated functional are needed, and a huge variety of exchange-correlation functional have been developed for chemical applications. Some of these are incompatible with the uniform electron gas approximation, however, they must reduce to LDA in the electron gas limit. For molecular applications, in particular for hybrid functional, Kohn-Sham DFT techniques are usually applied just like Hartree-Fock itself [12].

The main difficulty with DFT is that the precise functional for exchange and correlation are not identified except for the free electron gas. However, rough calculations exist which allow the calculation of certain physical amounts rather precisely. In physics the most widely used approximation is the local-density approximation (LDA).

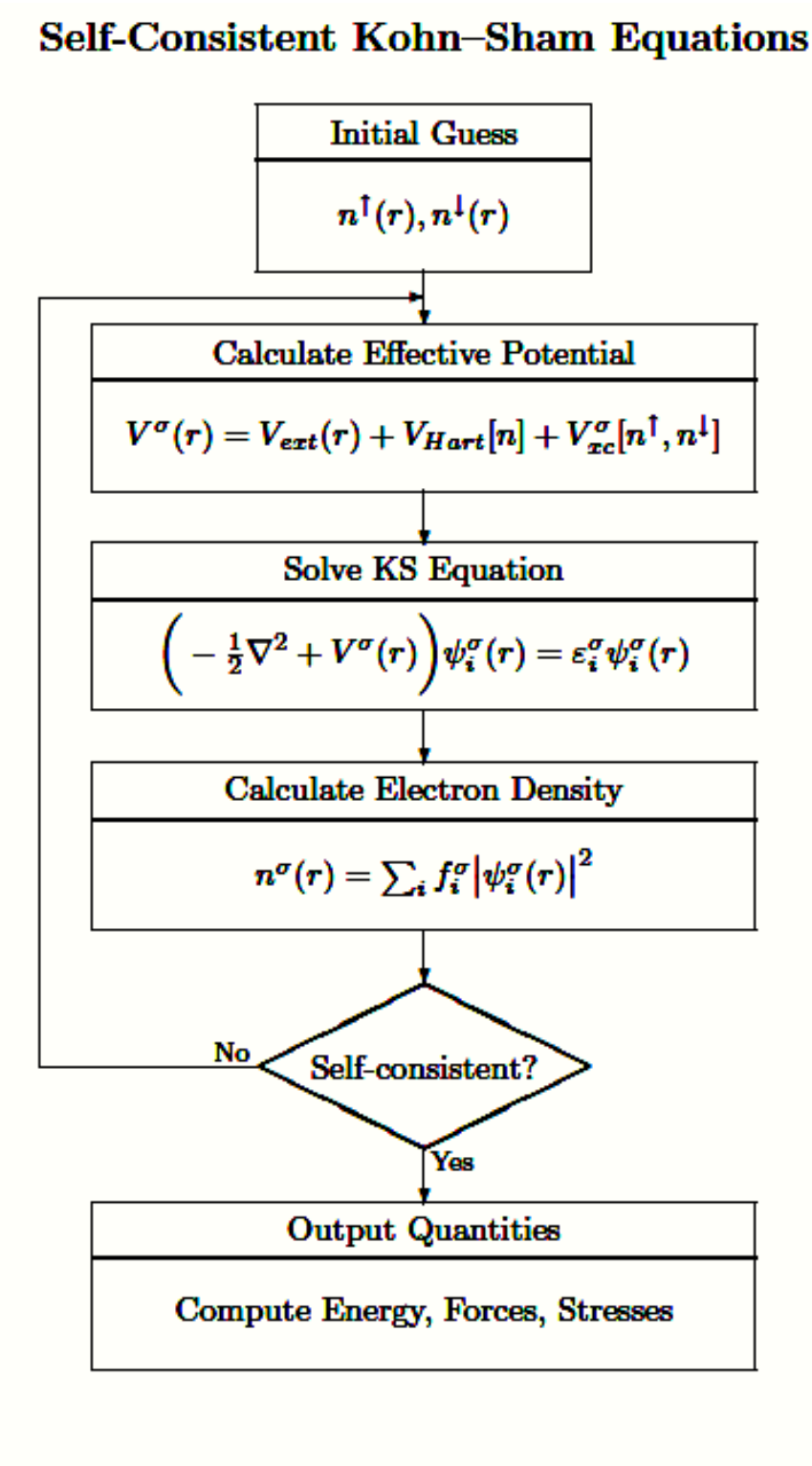

Fig. 3.1: flow chart of solving the self-consistent Kohn-Sham equation

3.3 Local Density Approximation

One of the efficient rough calculation techniques for working out the exchange-correlation term in the density functional theory (DFT) is the local density approximation (LDA). LDA has widely been applied to portray a variety of close-ranged exchange-correlation interactions of, for instance, covalent bonding systems. However, LDA has serious limitation that this approximation cannot provide estimation to the long-ranged exchange-correlation interaction, as typified by the Van der Waals (VdW) interaction. The VdW interaction is one of the long-ranged electronic interactions which mainly add to the first stage of the material reactions such as the chemical reaction, crystal growth and physical absorption. To assess the VdW interaction, many efforts have been devoted to develop useful calculating recipes for the non-local exchange-correlation term [13].

Kohn and Sham applied LDA approximation to DFT [9]. The Hohenberg-Kohn theorem states that the energy of the ground state of a system of electrons is a functional of the electronic density, especially, the exchange and correlation (XC) energy is also a functional of the density (this energy can be seen as the quantum part of the electron-electron interaction). This XC functional is not identified accurately and must be approximated [6]. LDA is the simplest approximation for this functional, it is local in the sense that the electron exchange and correlation energy at any point in space is a function of the electron density at that point only.

The XC functional is the total of a correlation functional and an exchange functional:

$$E_{xc} = E_x + E_c \tag{3.19}$$

LDA uses the exchange for the uniform electron gas of a density equal to the density at the point where the exchange is to be assessed:

$$E_{xc} = \int d^3 r n(\vec{r}) \left(\frac{-3e^2}{4\pi}\right) (3\pi^2 n(\vec{r}))^{1/3} \quad (3.20)$$

In SI units, $n(\vec{r})$ is the electron density per unit volume at the point $\vec{r}$; and e is the charge of an electron [14].

While looking for the ways out to the system of Schrodinger equation:

$$E\Psi(x) = -\frac{1}{2m}\nabla^2\Psi(x) + V(x)\Psi(x) \quad (3.21)$$

It is found that all amounts are represented as functional of the electronic $\varepsilon_{xc}(r)$ charge density. The significant point that makes this system easier to solve (or more accurately, needs less computation) than, for instance the Hartree-Fock equations, is that the efficient possibility is local. Therefore there is no more complication added in solving Schrodinger equation than there is in the Hartree approximation. Of course, this is only true if the exchange-correlation energy can be portrayed as a function of the local charge density. A technique of doing so is known as the local density approximation (LDA) [9]. As mentioned above in LDA, the exchange-correlation energy of an electronic system is built by taking for granted that the exchange-correlation energy for each electron at a point $\vec{r}$ in the electron gas is equal to the exchange-correlation energy for each electron in a identical electron gas that has the same electron density at the point $\vec{r}$. It follows that:

$$E_{xc}[n(\vec{r})] = \int \varepsilon_{xc}(n(\vec{r})n(\vec{r})dr \quad (3.22)$$

So that

$$\mu_{xc}(\vec{r}) = \frac{\delta[n(\vec{r})\varepsilon_{xc}(n(\vec{r}))]}{\delta n(\vec{r})} \quad (3.23)$$

With

$$\varepsilon_{xc}\left(n(\vec{r})\right) = \varepsilon_{xc}^{hom}(n(\vec{r})) \tag{3.24}$$

Where $\varepsilon_{xc}^{hom}(n(\vec{r}))$ is exchange-correlation energy in identical electron gas. Equation (3-24) is the supposition that the exchange correlation energy is purely local. Several parameterizations for $\varepsilon_{xc}^{hom}(n(\vec{r}))$exist, but the most commonly used is that of Perdew and Zunger [15]. This parameterisation is based on the quantum Monte Carlo calculations of Ceperley and Alder [16] on homogeneous electron gases at various densities. The parameterization uses interpolation formulas to link these precise outcomes for the exchange and correlation energy at many dissimilar densities.

Adjustment to the exchange-correlation energy because of the inhomogeneities in the electronic charge density about $\vec{r}$ are overlooked, in LDA,. Therefore, it may at first seem somewhat surprising that such calculations are so successful, when taking into account this inexact nature of the approximation. This can be to some extent ascribed to the fact that LDA gives the accurate sum rule to the exchange-correlation hole. That is, there is a total electronic charge of one electron excluded from the vicinity of the electron at $\vec{r}$. Endeavors to improve on LDA, such as gradient extensions to correct for in-homogeneities do not seem to show any enhancement in results got by the simple LDA. One of the reasons for this failure is that the sum rule is not obeyed by the exchange-correlation hole.

The contributions of electron-electron interactions in N-electron systems are shown briefly in Figure (3.2). It demonstrates the conditional electron probability distributions *n* (*r*) of *N*-1 electrons around an electron with given spin located at r = 0.

All electrons are dealt with as independent, in the Hartree approximation [19], Figure (3-2a), therefore is structureless. Figure (3-2b) stands for the Hartree-Fock approximation where the N-electron wave function reflects the Pauli exclusion principle.

Around the electron at r = 0. The exchange hole can be seen where the density of spins equal to that of the central electron is reduced. Electrons with opposite spins are unchanged. In the LDA (Figure (3-2c)), where spin states are degenerate, each sort of electron sees the same exchange-correlation hole (the sum rule being demonstrated where the size of the hole is one electron).

Figure (3-2d) shows electron-electron interaction for non-degenerate spin systems (the local spin density approximation (LSDA). It can be seen that the spin degenerate LDA is basically the average of the LSDA.

GGA's approximation has minimized the LDA errors of atomization energies of standard set of small molecules. This enhanced precision has made DFT an important element of quantum chemistry.

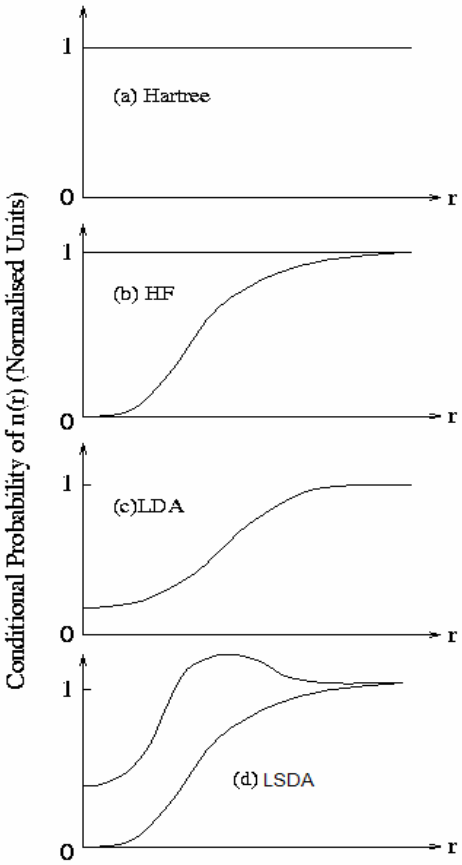

Fig. 3.2: Summary of the electron-electron interaction (excluding coulomb effects) in (a) the Hartree approximation, (b) the Hartree-Fock approximation, (c) the local density approximation and (d) the local spin density approximation which allows for different interactions for like-unlike spins.

3.4 Generalized Gradient Approximation (GGA)

The local spin density (LSD) approximation has been the basis of electronic structure calculations in solid-state physics for many years [9]. This rough calculation may be written as:

$$E_{xc}^{LSD}(n_{\uparrow}, n_{\downarrow}) = \int d^3 r n(\vec{r}) \varepsilon_{xc}^{unif}[n_{\uparrow}(\vec{r}), n_{\downarrow}(\vec{r})] \tag{3.25}$$

$\varepsilon_{xc}^{unif}(n_{\uparrow}, n_{\downarrow})$ exchange-correlation energy for each particle of a uniform electron gas [50]. The LSD exchange-correlation energies are inadequately negative (by about 10%) for almost all atoms, molecules, and solids. The LSD is a dependable, moderate-accuracy approximation. For many solid state objectives , the LSD level of precision is adequate, but LSD is not precise enough of most chemical applications, which need the determination of energy diversities with substantial accuracy. Hence the disinterest of the quantum chemistry community toward density functional techniques until recently [19]. New gradient-corrected functional of the form:

$$E_{xc}^{GGA}[n_{\uparrow}, n_{\downarrow}] = \int d^3 r \, f(n_{\uparrow}(\vec{r}), n_{\downarrow}(\vec{r}), \nabla n_{\uparrow}, \nabla n_{\downarrow}) \tag{3.26}$$

where f are functionals for different energies of the same system. These functionals may be partitioned into two wide categories : locally based functional, whose construction starts from the uniform electron gas, and "semi empirical" functional, which has one or more parameters fitted to a particular finite system, which have minimized LSD atomization energy errors by about a factor of 5 [20]. The generalized gradient approximation (GGA) has attracted much attention for its abstract simplicity and moderate computational workloads. At present, two GGA functional, one suggested by Becke and Perdew (BP)] and one suggested more recently by Perdew and Wang (PW), are the most popular ones in the literature [21].

Many calculations assessing the accuracy of the GGA have been reported and commonly demonstrate that the GGA substantially corrects the LDA error in the cohesive energies of molecules and solids [22]. Generalized gradient approximations (GGA s) to the exchange-correlation **(**XC**)** energy in density-functional theory, are at present receiving increasing attention as a straightforward substitute to improve over the local-density approximation (LDA) in ab initio total-energy calculations [18]. In a variety of fields, the GGA provided evidence to be more suitable than the LDA:

1. Binding energies of molecules and solids became more precise, correcting the trend of the LDA to over binding [24].
2. Activation energy obstacles, e.g., for the dissociate adsorption of H_2 on metal and semiconductor surfaces, are in distinctly better accordance with experiment. Reaction and activation energies for a variety of chemical reactions give the same enhancement [25].
3. The relative constancy of structural phases seems to be anticipated more realistically for magnetic and for nonmagnetic materials, too [26].

Bulk structural qualities are often not developed within the GGA. While the lattice parameters always rise in comparison with the LDA, a closer agreement with experimental data is reported for alkali metals, 3*d* metals, and some *4d* metals. However, an overestimation of up to several percent is found for *5d* metals and common semiconductors, their bulk moduli accordingly turning out to be too small (typically by $\leq$ 25%) [27].

3.5 The full-potential linearized augmented-plane wave technique

The full-potential linearized augmented-plane wave (FP-LAPW) technique is well known to allow most precise calculation of the electronic structure and magnetic qualities of crystals and surfaces.

The application of atomic forces has greatly maximized its applicability, but it is still commonly supposed that FP-LAPW computations need considerable higher computational effort in comparison with the pseudopotential plane wave (PPW) based techniques [28].

FP-LAPW has recently showed important progress. For example, researchers habitually work out magnetism and nuclear quantities (for example, isomer shifts, hyperfine fields, electric field gradients, and core level shifts) [29]. Also, forces and molecular dynamics have been applied, and recent optimizations have decreased the CPU time of FP-LAPW calculations significantly [28]. Nevertheless, because the computational expense and memory requirements are still fairly high, FP-LAPW implementations are suitable only to fairly complicated systems.

One successful implementation of the FP-LAPW technique is the program package WIEN2K, a code enhanced by Blaha, Schwarz and coworkers [30]. It has been successfully implemented to a various scope of difficulties such as electric field gradients [31] and systems such as high-temperature superconductors, minerals [32], surfaces of transition metals [33], or antiferromagnetic oxides [34] and even molecules [35]. Reducing the total energy of a system by comforting the atomic counterparts for complicated systems became potential by the application of atomic forces, and even molecular dynamics became possible. So far the main disadvantage of the FP-LAPW-technique in comparison with the pseudopotential plane-wave (PPW) [36] method has been its higher computational expense. This may be largely because of an inconsistency in optimization efforts spent on both techniques, and so we have investigated the FP-LAPW technique from a computational arithmetical viewpoint.

Lately, the development of the Augmented Plane Wave (APW) techniques from Slater's APW, to LAPW and the new APW+lo was portrayed by Schwarz et al. [37]. One of the most precise techniques for performing electronic structure calculations for crystals is the full potential linearized augmented plane wave FP-LAPW technique.

It is based on the density functional theory for the handling of exchange and correlation and uses (for example, the local spin density approximation) (LSDA).

Effects, for valence states relativistic, can be incorporated either in a scalar relativistic handling or with the second dissimilarity technique including spin-orbit coupling. Core states are treated fully relativistically.

The FP-LAPW technique ,which is Like most ``energy-band techniques ,is a process for solving the Kohn-Sham equations for the ground state density, total energy, and (Kohn-Sham) eigen values (energy bands) of a many-electron system by presenting a basis set which is particularly modified to the problem.

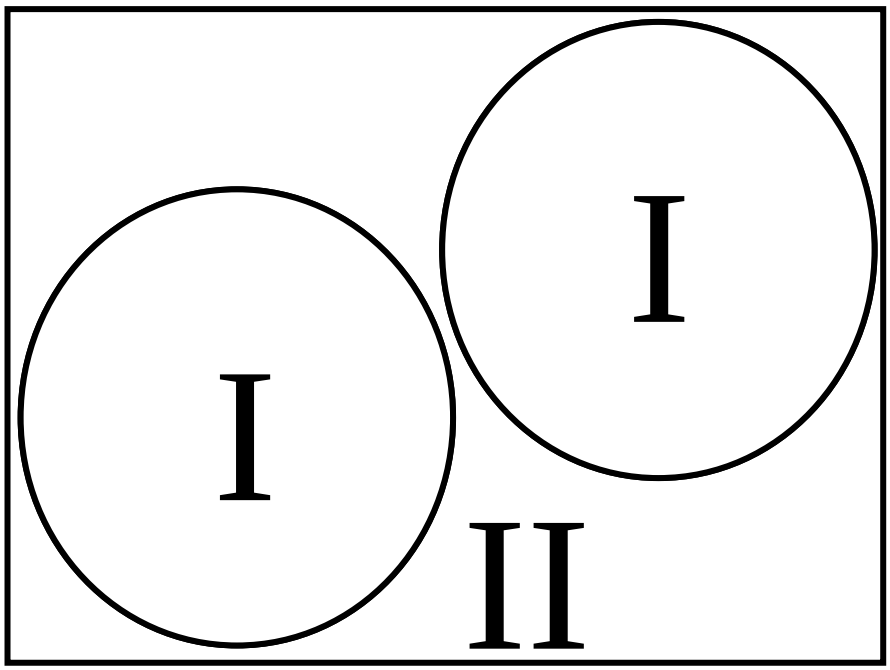

Fig. 3.3: Partitioning of the unit cell into atomic spheres (I) and an interstitial region (II).

This alteration is achieved by partitioning the unit cell into (I) nonoverlapping atomic circles (centered at the atomic sites) and (II) an interstitial region, that is to say, a region between two spaces. In the two sorts of regions diverse basis sets are used:

- Inside atomic sphere I of radius R_I a linear combination of radial functions times spherical harmonics $Y_{lm}(r)$ is used

$$\Phi_{kn} = \sum_{lm}[A_{lm}u_1(\vec{r}, E_l) + B_{lm}\dot{u}_1(\vec{r}, E_l)]\, Y_{lm}(\vec{r}) \tag{3.27}$$

where $u_1(r, E_1)$ is the (at the origin) normal way out of the radial Schrodinger equation for energy E_1 and the spherical part of the potential inside sphere, $\dot{u}_l(r, E_l)$is the energy derived of u_1 taken at the similar energy. A linear mixture of these two functions comprise the linearization of the radial function; the coefficients A_{lm} and B_{lm} are functions of k_n decided by requiring that this root function $\dot{u}_l$ goes with the equivalent basis function of the interstitial region; u_l and are achieved by numerical integration of the radial Schrodinger equation on a radial mesh inside the sphere.

- (II) in the interstitial zone a plane wave extension is applied

$$\Phi_{kn} = \frac{1}{\sqrt{w}} e^{iK_n r} \tag{3.28}$$

where $K_n = k + k_n$, k_n are the mutual lattice vectors and k is the wave vector inside the first Brillouin zone . Each plane wave is increased by an atomic-like function in every atomic sphere.

The solutions to the Kohn-Sham equations are extended in this joint basis set of LAPW's according to the linear dissimilarity technique

$$\Psi_k = \sum_n C_n \Phi k_n \tag{3.29}$$

and the coefficients C_n are decided by the Rayleigh-Ritz variation rule. The union of this basis set is controlled by a disconnected parameter $R_{mt}K_{max}$, where R_{mt} is the smallest atomic sphere radius in the unit cell and K_{max} is the magnitude of the largest K vector.

Additional (K_n independent) basis functions can be added to improve upon the linearization and to make possible a reliable treatment of semi core and valence states in one energy window. They are called "local orbitals" and consist of a linear combination of 2 radial functions at 2 dissimilar energies and one energy derivative:

$$\Phi_{lm}^{LO} = \left[A_{lm}u_l(\vec{r}, E_{1,l}) + B_{lm}\dot{u}_l(\vec{r}, E_{1,l}) + C_{lm}u_l(\vec{r}, E_{2,l})\right]Y_{lm}(\hat{r}) \quad (3.30)$$

The coefficients A_{lm}, B_{lm}, and C_{lm}, are decided by the necessities that Φ^{LO} should be regularized and has zero value and slope at the sphere border.

The FP- LAPW technique, in its general form, extends the potential in the following form

$$V(\vec{r}) = \begin{cases} \sum_{lm} V_{lm}(\vec{r})Y_{lm}(\hat{r}) & insidesphere \\ \sum_K V_K e^{ikr} & outsidesphere \end{cases} \quad (3.31)$$

And the charge densities analogously. Thus no form of rough calculations are made, a process often called the "full- potential" technique.

The "muffin-tin" rough calculation applied in early band calculations matches to keeping only the $L= 0$ and $M=0$ component in the initial idiom of final equation. and only the $K=0$ constituent in the second. This process matches to take the spherical rate inside the spheres and the volume rate in the interstitial region. The entire energy is calculated according to Weinert *et al* [38]. The forces at the atoms are worked out according to Yu *et al* [39].

The Fermi energy and the weights of each band state can be worked out using an adapted tetrahedron (having four surfaces) technique [40].

References

[1] http://en.wikipedia.org/wiki/DFT

[2] P. Hessler, N. T. Maitra, K. Burke , Journal of Chemical Physics. **117**, (2002) 72-81

[3] E. Runge, E. K. U. Gross, Physical. Review. Lett. **52**, (1984) 997

[4] O. J. Wacker, R. Kummel, E. K. U. Gross, Physical. Review. Lett. **73**, (1994) 2915

[5] http://www.physics.ohio-state.edu/~aulbur/dft.html

[6] P. Hohenberg, W. Kohn, Physical. Review. **136**, (1964) 864-871

[7] G. Vignale, Rasolt, Mark, Physical. Review. Lett. **59**, (1987) 2360-2363

[8] http:// chemistry.ncssm.edu/book/Chap9DFT

[9] W. Kohn and L. J. Sham, Physical. Review. **140**, (1965) 1133

[10] R. G. Parr and W. Yang, Density-Functional Theory of Atoms and Molecules. Oxford Science Publications, (1989) 145-147

[11] Richard M. Martin, Electronic Structure Basic Theory and Practical Methods. Cambridge University Press, (2004) 173

[12] http:// en.wikipedia.org/wiki/Density_functional_theory

[13] J. Dobson et al, Physical. Review. Lett **96**, (2006) 073201

[14] J. Tao and John P. Perdew, Physical. Review. Lett. **95**, (2005) 196403

[15] J. P. Perdew and A. Zunger, Physical. Review. B **23**, (1981) 5048

[16] D. M. Ceperley and B. J. Alder, Physical. Review. Lett. **45**, (1980) 566

[17] http:// cmt.dur.ac.uk/sjc/thesis/thesis/node13.html

[18] R. O. Jones and O. Gunnarsson, Rev. Mod. Phys. **61**, (1989) 689

[19] S. H. Vosko, L. Wilk, and M. Nusair, Can. J. Phys. **58**, (1980) 1200

[20] K. Burke, J. P. Perdew, and M. Levy, in Modern Density Functional Theory, J. M. Seminario and P. Politzer, Eds , Elsevier, Amsterdam (1995)

[21] A. D. Becke, Physical. Review. A **38**, (1988) 3098

[22] P. Bagno, O. Jepsen and O. Gunnarsson, Physical. Review. B **40**, (1989) 1997

[23] A. D. Becke, J. Chem. Phys. **97**, (1992) 9173

[24] D. Porezag and M. R. Pederson, J. Chem. Phys. **102**, (1995) 9345

[25] D. R. Hamann, Physical. Review. Lett. **76**, (1996) 660

[26] G. Ortiz, Physical. Review. B **45**, (1992) 328

[27] M. Petersen, F. Wagner, L. Hufnagel, M. Schffler, P. Blaha, and K. Schwarz. Computer Physics communications . **126**, (2000) 294-309

[28] D. J. Singh, Physical Review. B. **60**, (1999) 16359-16363

[29] P. Blaha, K. Schwarz, P. Sorantin, S.B. Trickey, Comput. Phys. Commun. **59**, (1990) 399

[30] P. Blaha, K. Schwarz, P. Herzig, Physical. Review. Lett. **54**, (1985) 1192

[31] B. Winkler, P. Blaha, K. Schwarz, Am. Mineralogist **81**, (1996) 545.

[32] B. Kohler, P. Ruggerone, S. Wilke, M. Scheffler, Physical. Review. Lett. **74**, (1995) 1387.

[33] X. G.Wang, W. Weiss, Sh.K. Shaikhutdinov, M. Ritter, M. Petersen, F. Wagner, R. Schlgl, M. Scheffler, Physical. Review. Lett. **81**, (1998) 1038

[34] M. Bockstedte, A. Kley, J. Neugebauer, M. Scheffler, Comp. Phys. Commun. **107**, (1997) 187

[35] K .Schwarz, P.Blaha and Madsen, G. K. H, Comp.Phys.Commun (2001)

[36] Weinert M., Wimmer E., and Freeman A. J, Physical. Review. B **26**, (1982) 4571

[37] Yu R., Singh D. and Krakauer H., Physical. Review. B **43**, (1991) 6411

[38] Bl chl P.E., Jepsen O. and Andersen O.K., Physical. Review. B **49**, (1994) 16223

[39] Omar Mahmood PhD thesis, An-Najah National University, Nablus, Palestine, (2008)

[40] Haneen Yousef, PhD thesis, An-Najah- National University, Nablus, Palestine, (2009)

4 Study of the half-metallic behavior and the magnetic and thermodynamic properties of half-Heusler CoMnTe and RuMnTe compounds: A first-principles study

The magnetic materials particularly of the crystallographic phase $C1_b$ of the half-Heusler compounds have been an active field of research, as a consequence of their frequently emerging novel properties and field of applications since their first discovery by Fritz Heusler.[1] In 1983, Groot et al.[2] discovered the half-metallic ferromagnetism in half- Heusler NiMnSb and PtMnSb compounds, and further revealed their potentials for promising technological applications. Moreover the importance of these materials has been uncovered by viewing the novel features of the electronic band structure and magnetic behavior of half Heusler NiMnSb compounds.[3]

The target of recent research related to half Heusler materials is to investigate ferromagnetic half-Heusler compounds exhibiting magnetic shape memory effect, magnetic field induced super-elasticity and large strain-induced changes in the magnetization. [4–20] In this regard several efforts have been devoted and a lot of them are on the way to the study of their electronic, magnetic and thermodynamic properties of these systems on the basis of band structure calculations,[21] however some aspects are still vague. To contribute to this active area of research, which is expected to soon undergo a revolution in technological applications because of the multi functional properties that can be offered by a single half-Heusler ternary compound, we study the structural, electronic, magnetic and thermodynamic properties of CoMnTe and RuMnTe by one of the most accurate approaches to electronic band structure, i.e. first-principles. The main difference between NiMnSb and, CoMnTe and RuMnTe compounds is that the magnetic moments of Co and Ni are higher than Ru moment.[3,19] Surprisingly the properties of a large number of Heusler compounds can be predicted by the direct counting of valence electrons.

Based on their $C1_b$ structure and the total number of valence electrons, the compounds CoMnTe and RuMnTe are expected to exhibit their half-metallic ferromagnetic natures. Electronic band structures of CoMnTe and RuMnTe compounds exhibit their metallic natures for spin up, and show their semiconductor behaviors for spin down. The effects of the unit cell volume on the magnetic properties and the half-metallicity are crucial. It is interesting to note that the scale of total spin moment is exactly consistent with total number of valence electrons. Moreover by applying quasi-harmonic Debye model to CoMnTe and RuMnTe compounds, calculations of heat capacity at constant volume (C_V), heat capacity at constant pressure (C_P), Debye temperature (θ), thermal expansion (α), and the Grüneisen parameter (γ) in a temperature range of 0 K–1200 K in steps of 100 K and in a pressure range of 0 GPa–45 GPa in steps of 5 GPa are performed, and the obtained results are in nice agreement with those from the Debye theory which is extensively applied to a wide range of materials.

4.1 Crystal structure

Heusler compounds (X_2YZ) are defined as the ternary intermetallic compounds. [1] At the stoichiometric composition, the half-Heusler compounds (XYZ) each crystallize into a $C1_b$ structure. The elements associated with the X, Y, and Z are (Co, Ru), Mn, and Te, respectively. The unit cell consists of four interpenetrating face-centered cubic sublattices with the positions (0, 0, 0) for Co and Ru, (1/4, 1/4, 1/4) for Mn, and (3/4, 3/4, 3/4) for Te. The site (1/2, 1/2, 1/2) is vacant in the half-Heusler compound. The crystal structure of half Heusler CoMnTe compound is shown in figure 4.1 as prototype.

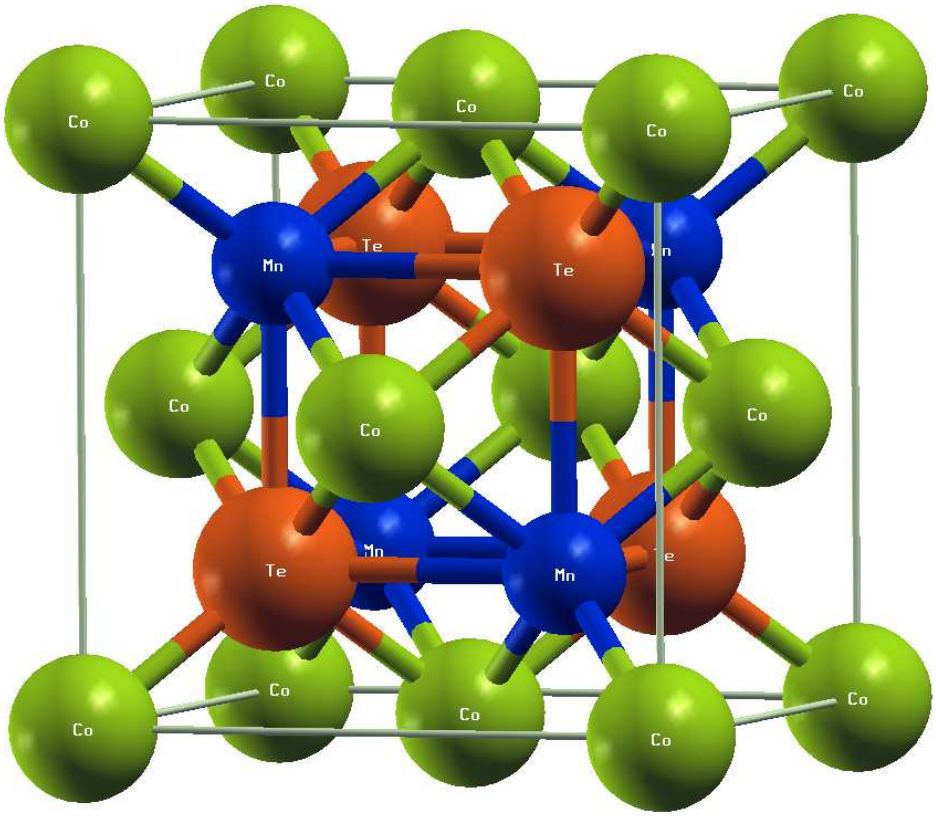

Fig. 4.1: Crystal structure of the CoMnTe.

4.2 Computational details

Computations regarding geometry optimization, electronic structure calculations and magnetic properties are performed within FP-LAPW computational approach is realized in WIEN2k package. [22] To incorporate exchange correlation functional part into total energy functional calculations, GGA-PBE [23] is used whereas to include the relativistic effects the scalar approximation suggested by Koelling and Harmon is adopted. To control the size of basis set for reasonable convergence, the value of cutoff parameter $R_{MT}K_{max}$ = 8.0 as shown in the figures 4.2 and 4.3, and the value of l = 10 is used to control the expansion of the partial waves inside the Muffin tins spheres. The values of radius RMT are chosen to be proportional to their ionic radii such that the spheres do not overlap.

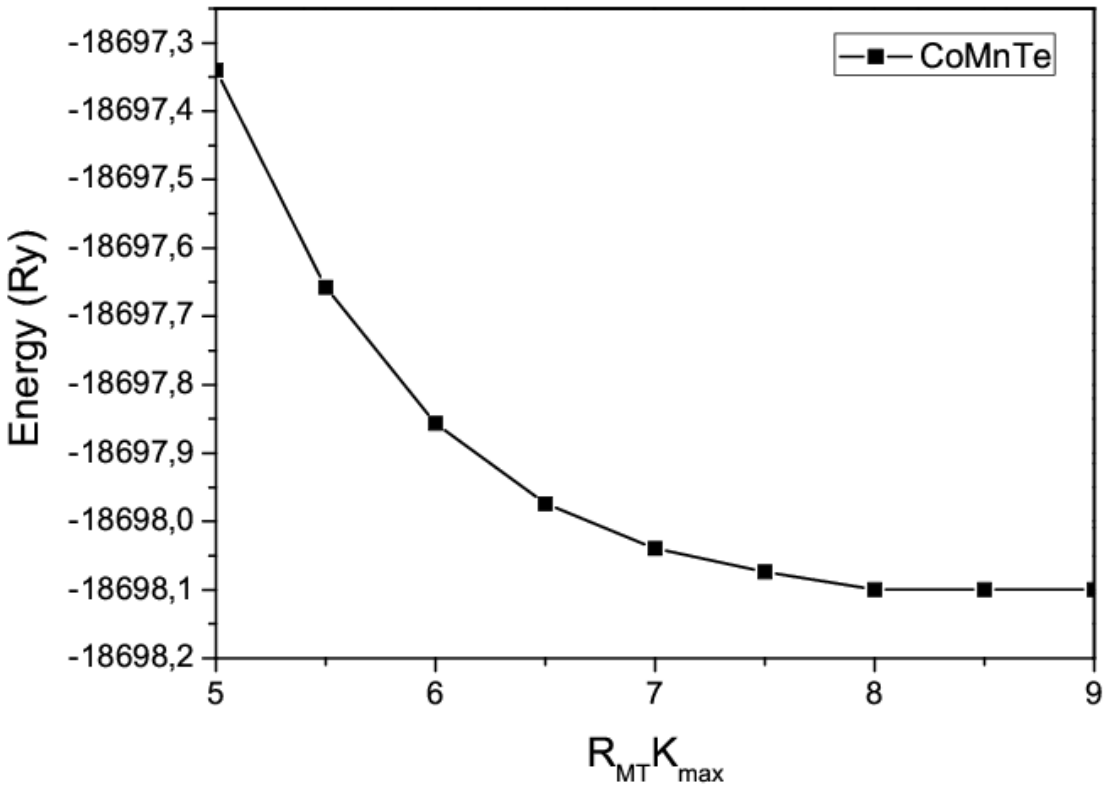

Fig. 4.2: Energy as function of the cutoff parameter $R_{MT}K_{max}$ for CoMnTe.

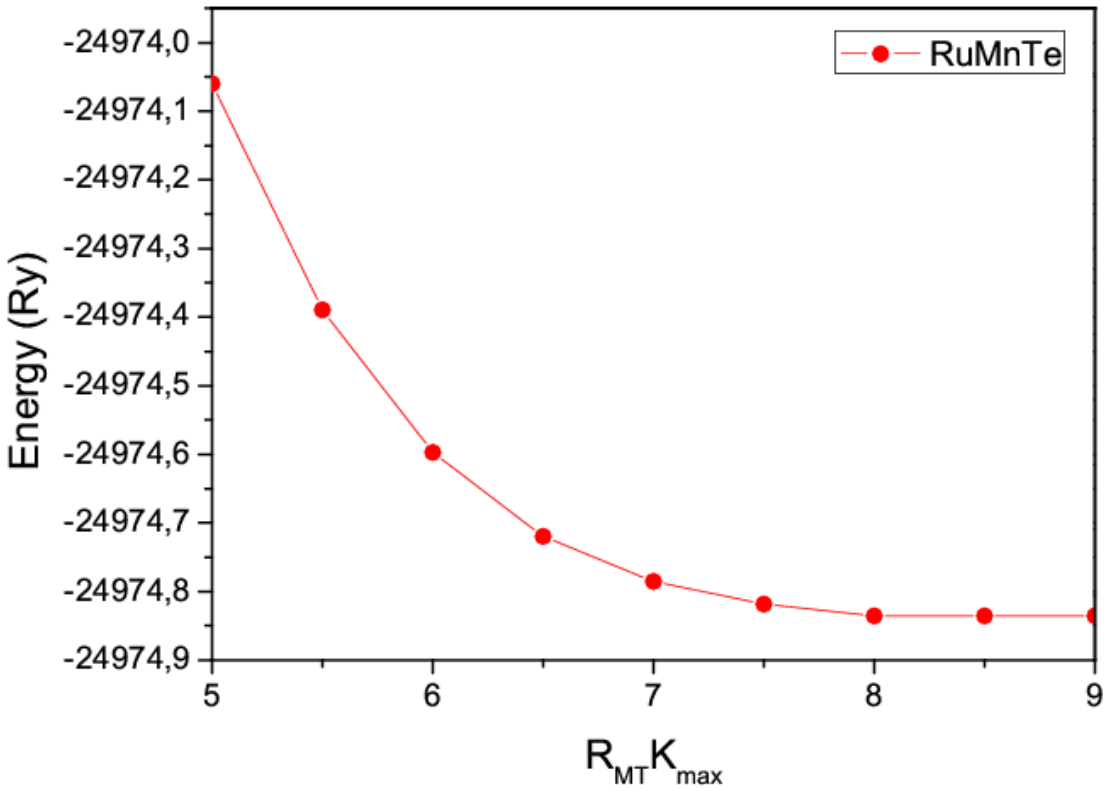

Fig. 4.3: Energy as function of the cutoff parameter $R_{MT}K_{max}$ for RuMnTe.

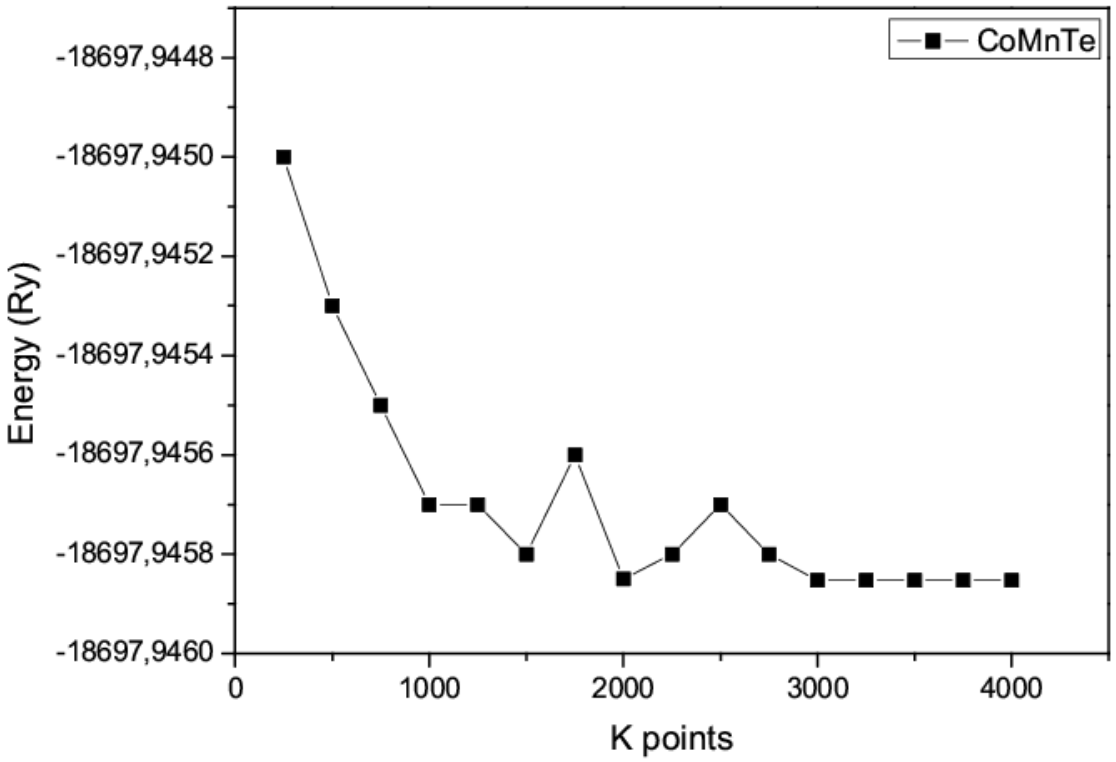

Fig. 4.4: Energy as function of K points for CoMnTe.

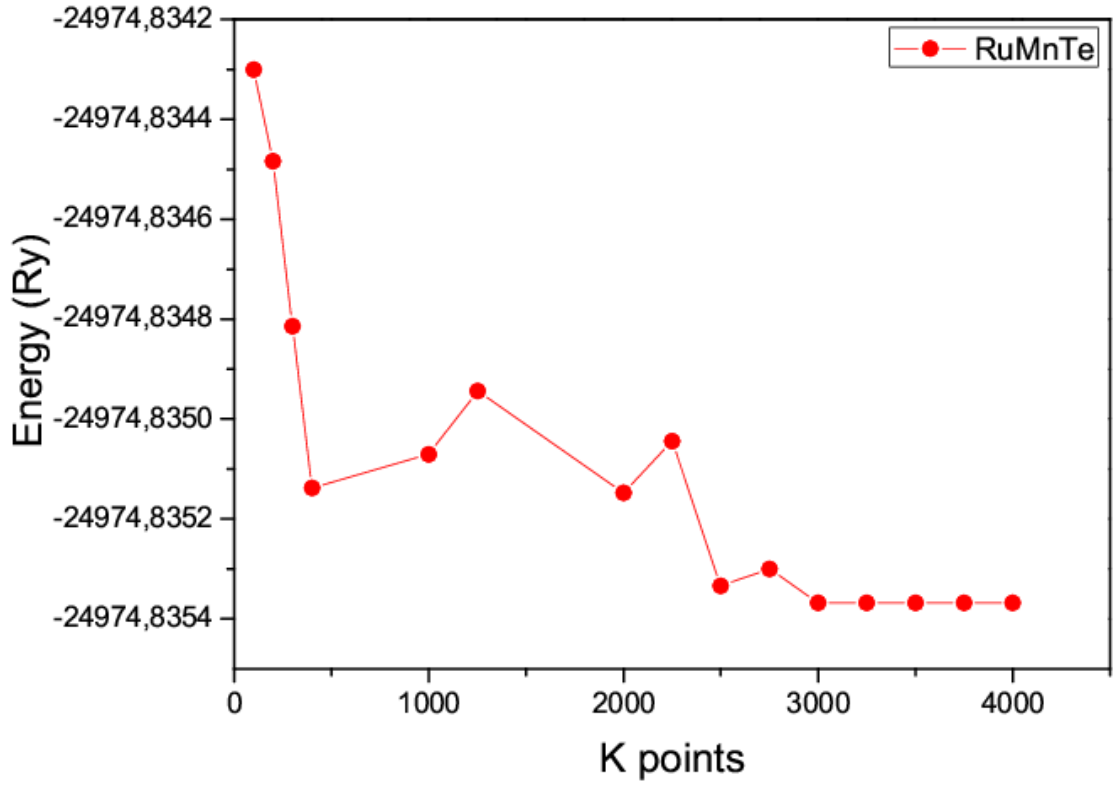

Fig. 4.5: Energy as function of K points for RuMnTe.

By the use of total energy convergence test to obtain the energy precision of 10^5 Ry/formula unit, 3000 k-points are adopted in the first part of Brillouin zone as shown in the figures 4.4 and 4.5.

To study thermal effects, quasi-harmonic Debye model realized in Gibbs program [24] is used. This model is sufficiently flexible in giving all thermo dynamical quantities by incorporating the obtained results of energy and volume. We give, here, a brief description of this model. [24–29] In this model non-equilibrium Gibbs function G*(V; P, T) is described in the following form:

$$G^*(V;P,T) = E(V) + PV + A_{Vib}(\Theta(V);T), \tag{4.1}$$

Where *E (V)* represents total energy/formula unit, *PV* the constant hydrostatic pressure condition, *Θ(V)* the Debye temperature, A_{Vib} the lattice vibration that is expressed as

$$A_{Vib}(\Theta;T) = nk_BT\left[\frac{9\Theta}{8T} + 3\,ln\left(1 - e^{-\Theta/T}\right) - D(\Theta/T)\right]. \tag{4.2}$$

In the equation (2), *n* represents the number of atoms/formula unit, k_B represents the well-known Boltzmann constant, and the last term $D(\Theta/T)$ on the right-hand side represents the Debye integral. Here for anisotropic solid, Θ is expressed by the following expression:

$$\Theta = \frac{\hbar}{K}\left[6\pi^2V^{1/2}n\right]^{1/3} f(\sigma)\sqrt{\frac{B_s}{M}}\ . \tag{4.3}$$

In the equation (3), *M* is the molecular mass, B_S is the adiabatic bulk modulus, which is estimated in terms of static compressibility by using following relation:

$$B_s \cong B(V) = V\frac{d^2E(V)}{dV^2}, \tag{4.4}$$

where *f (ν)* is defined as

$$f(\nu) = \left\{3\left[2\left(\frac{21+\nu}{31-2\nu}\right)^{\frac{3}{2}} + \left(\frac{11+\nu}{31-\nu}\right)^{\frac{3}{2}}\right]^{-1}\right\}^{\frac{1}{3}}, \tag{4.5}$$

and ν is the Poisson ratio in the above relation.

The minimization of the non-equilibrium Gibbs function *G*(V; P, T)* with respect to the volume V at constant pressure and temperature is attained as;

$$\left(\frac{\partial G^*(V;P,T)}{\partial V}\right)_{P,T} = 0\,. \tag{4.6}$$

By solving the equation (6), one can obtain a relation for *V(P,T)* i.e. thermal equation of state (EOS). Using the equation (6) for different thermal properties, i.e., isothermal bulk modulus (BT), specific heat capacity values at constant volume (C_V) and at constant pressure (C_P), and thermal expansion coefficient α can be evaluated using the following formulas:

$$B_T(P,T) = V\left(\frac{\partial^2 G^*(V;P,T)}{\partial V^2}\right)_{P,T}, \tag{4.7}$$

$$C_V = 3nk_B\left[4D(\Theta/T) - \frac{3\,\Theta/T}{e^{\Theta/T}-1}\right], \tag{4.8}$$

$$C_P = C_V(1+\alpha\gamma T), \tag{4.9}$$

$$\alpha = \frac{\gamma C_V}{B_T V}, \tag{4.10}$$

where γ is used to represent the Grüneisen parameter and is calculated from the following expression:

$$\gamma = -\frac{d\, ln\, \Theta\, (V)}{d\, ln\, V} \tag{4.11}$$

4.3 Results and discussion

4.3.1 Total energy and electronic structure

For both Heusler CoMnTe and RuMnTe compounds, first of all, the total energies of for their paramagnetic and ferromagnetic states are calculated in terms of volume per formula unit. It is found that the paramagnetic phase has high energy as compared with the ferromagnetic phase. Our optimized results for volume (V_0), energy (E_0), equilibrium lattice constant (a_0) and bulk modulus (B) calculated for ferromagnetic phase are shown in Table 4.1. These results are obtained for both compounds by fitting data for energy as a function of volume to the Murnaghan equation of state [32] as shown in the figures 4.6 and 4.7. The energy difference (ΔE) between paramagnetic and ferromagnetic states is also calculated and the results are given in Table 4.1. There are no experimental results available to us for these compounds, but our values for CoMnTe are in excellent agreement with those obtained by Selçuk Kervan et al.[30] using the full potential linearized augmented plane wave method.

At equilibrium lattice constants, the calculated spin polarized band structures in ferromagnetic phase, for majority and minority spin electrons, are demonstrated in figures 4.8, 4.10 and 4.9, 4.11 for CoMnTe and RuMnTe compounds respectively.

From the figures 4.8 and 4.9, it is obvious that the majority spin electrons exhibit metallic natures of the compounds and from the figures 4.10 and 4.11, it is evident that the minority spin channels display a band gap of 1.08 eV for CoMnTe and 0.83 eV for RuMnTe around the Fermi level, revealing their semiconducting natures.

However natures of band energy gaps are found to be indirect between Γ point of the highest occupied band (valence band) and X point for the lowest unoccupied band (conduction band). These semiconducting natures of the minority spin electrons and metallic natures of majority spin channel of these compounds are very analogous to those of NiMnSb and FeMnSb [33] and show that these systems are half-metallic ferromagnetic.

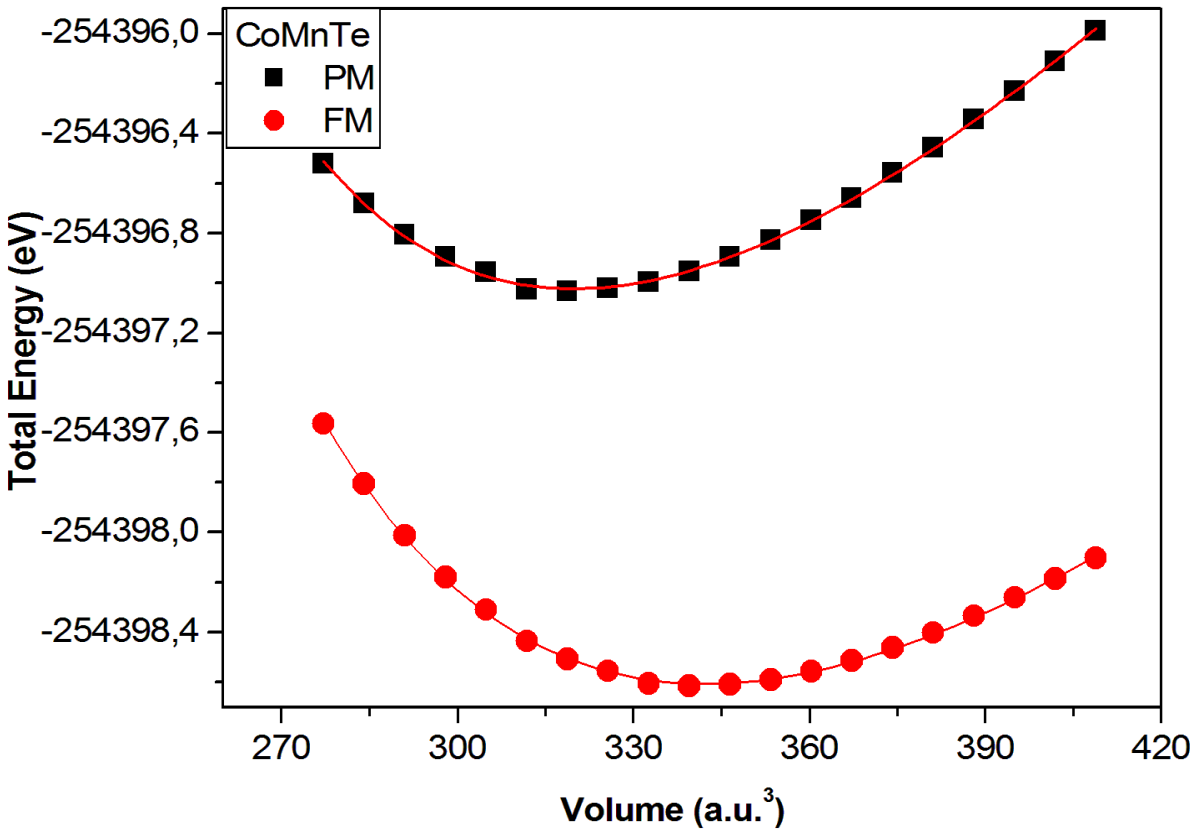

Fig.4.6 : Curves of total energy versus volume per formula unit for the paramagnetic (PM) and ferromagnetic (FM) states of CoMnTe.

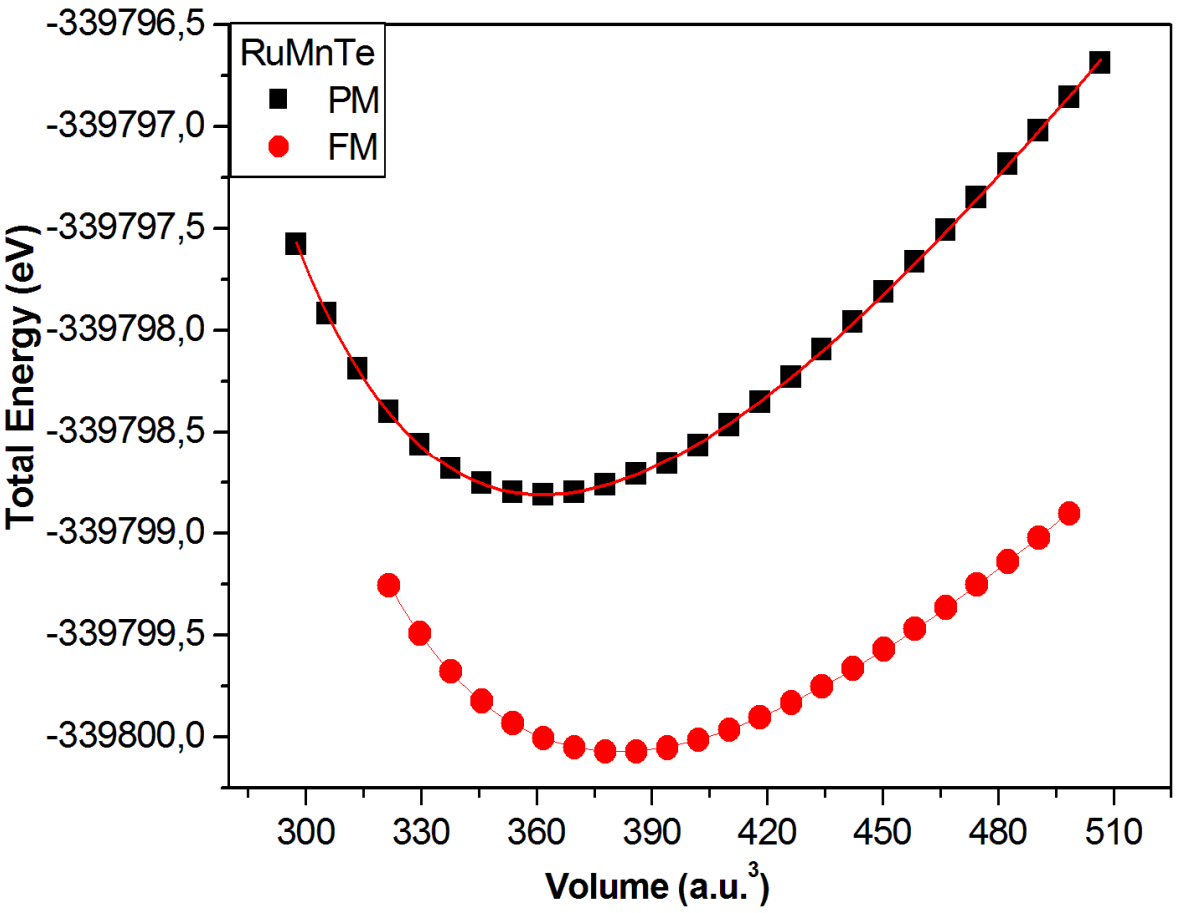

Fig. 4.7 : Curves of total energy versus volume per formula unit for the paramagnetic (PM) and ferromagnetic (FM) states of RuMnTe.

Table 4.1: Predicted values of equilibrium lattice constant a_0, volume V_0, energy E_0 and bulk modulus B for the ferromagnetic phase and ΔE energy difference between paramagnetic states and the ferromagnetic states.

	a_0(Å)	V_0(a.u.^{3})	B(GPa)	B'	E_0 (eV)	ΔE (eV)
CoMnTe	5.876	342.347	118.869	4.832	-254398.605	1.583
	5.86[a]		119.97[a]			1.55[a]
RuMnTe	6.092	381.373	124.485	5.978	-339800.069	1.254

[a] Ref. [30]

To further depict the electronic structures of these compounds, spin-projected total and partial density of states (DOS) are also calculated and are represented in the figures 4.12 and 4.13 for CoMnTe and RuMnTe, respectively. The negative values of total and partial densities of states correspond to the minority-spin electrons. Examinations of the figures 4.12 and 4.13 reveal that the densities of states near the half metallic gap, where the influences of the s and p states are insignificant, are dominated by the d-states of Co, Ru and Mn. It is point to note that the bonding d states are largely contributed from Co and Ru, whereas anti-bonding d states are predominantly belonging to Mn characteristic.

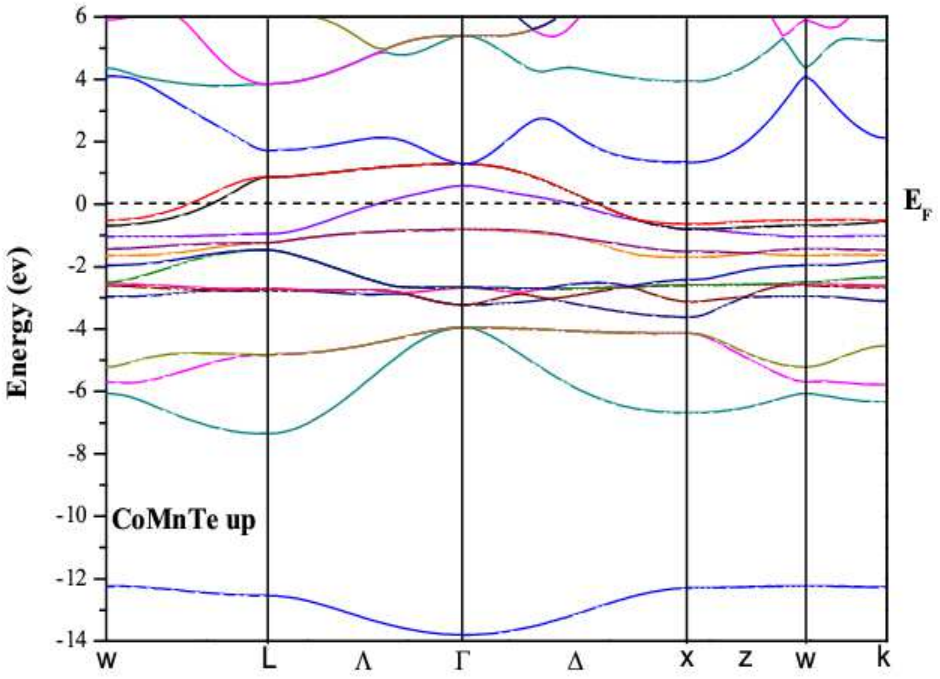

Fig. 4.8: Electronic band structure for majority spin electrons in CoMnTe

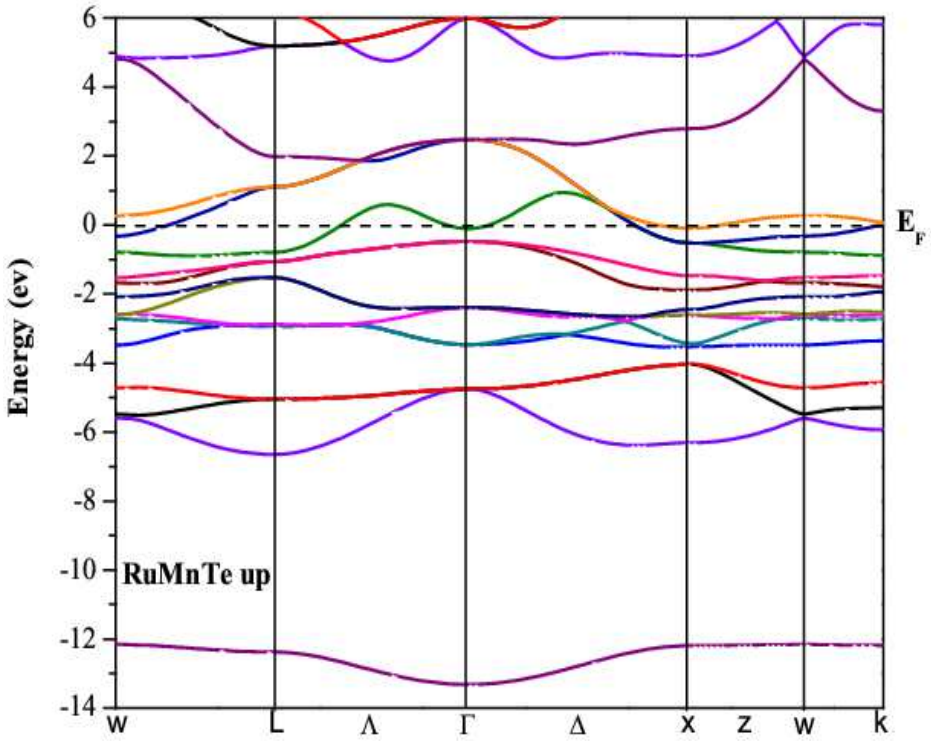

Fig. 4.9: Electronic band structure for majority spin electrons in RuMnTe.

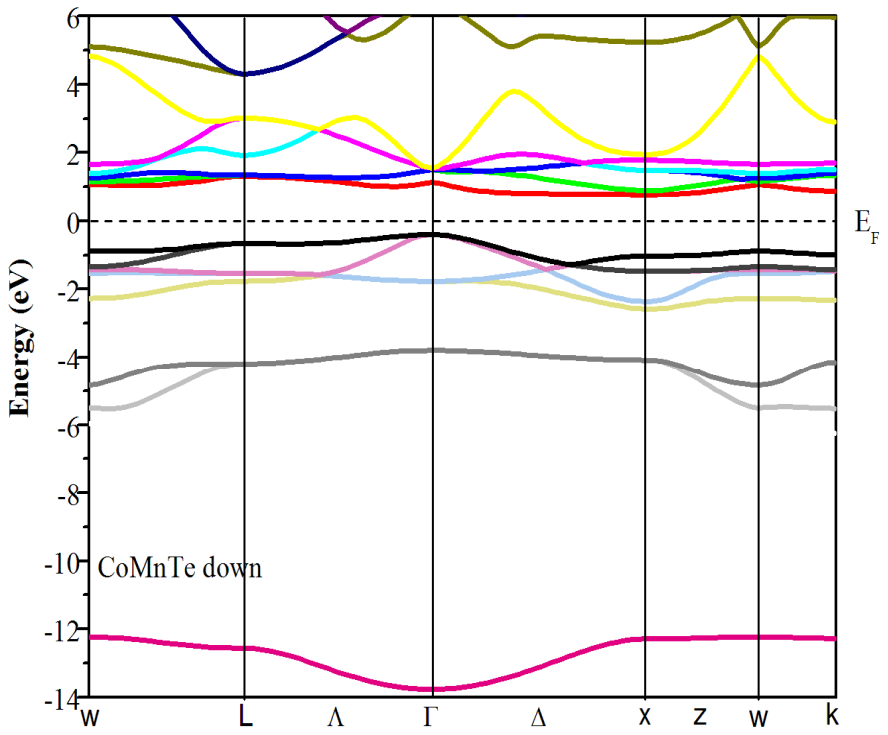

Fig. 4.10: Electronic band structure for minority spin electrons in CoMnTe.

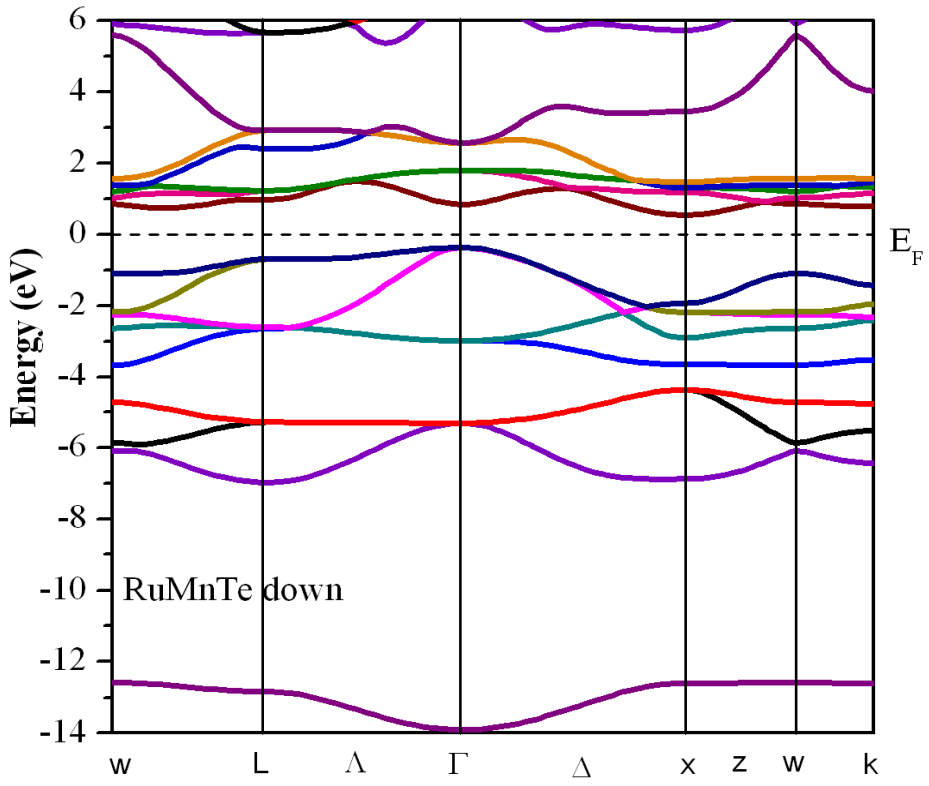

Fig. 4.11: Electronic band structure for minority spin electrons in RuMnTe.

Table 4.2: Values of magnetic moment per formula unit (μ_{tot}), M (M=Co, Ru, Mn and Te) magnetic moment (μ_M), magnetic moment in the interstitial region (μ_{int}), Fermi level E_F and HM gap (E_g).

	μ_{tot} (μ_B)	μ_{Co} (μ_B)	μ_{Ru} (μ_B)	μ_{Mn} (μ_B)	μ_{Te} (μ_B)	μ_{int} (μ_B)	E_F (eV)	HM gaps (eV)
CoMnTe	4.00	0.39	-	3.49	-0.01	0.14	9.13	1.08
	4.00[a]	0.38[a]		3.50[a]	-0.04[a]			1.13[a]
	4.00[b]	0.40[b]		3.48[b]				
RuMnTe	3.00	-	-0.29	3.28	-0.03	0.05	10.50	0.83

[a] Ref. [31]

[b] Ref. [30]

The corresponding d-d band gap near the Fermi level orignates from the strong hybridization between d states of higher valent TM atoms and the d states of lower valent TM atoms. The vertical dashed lines in the DOS presented in the figures 4.12 and 4.13 represent the Fermi level, which is fixed to zero.

For the spin-up states, the Fermi levels of CoMnTe and RuMnTe are located on the tails of the peaks of the partial densities of states (PDOSs) of Co and Ru, which are situated at ≈-0.47 eV for Co and at ≈0.24 eV for Ru; alternatively, the Fermi levels can be considered to be located on the tail of the peak at ≈-0.48 eV of the total density of states (TDOS) for CoMnTe and on the tail of the peak at ≈0.23 eV of the TDOS for RuMnTe. By contrast, the Fermi levels are located at the energy gaps for the spin-down states.

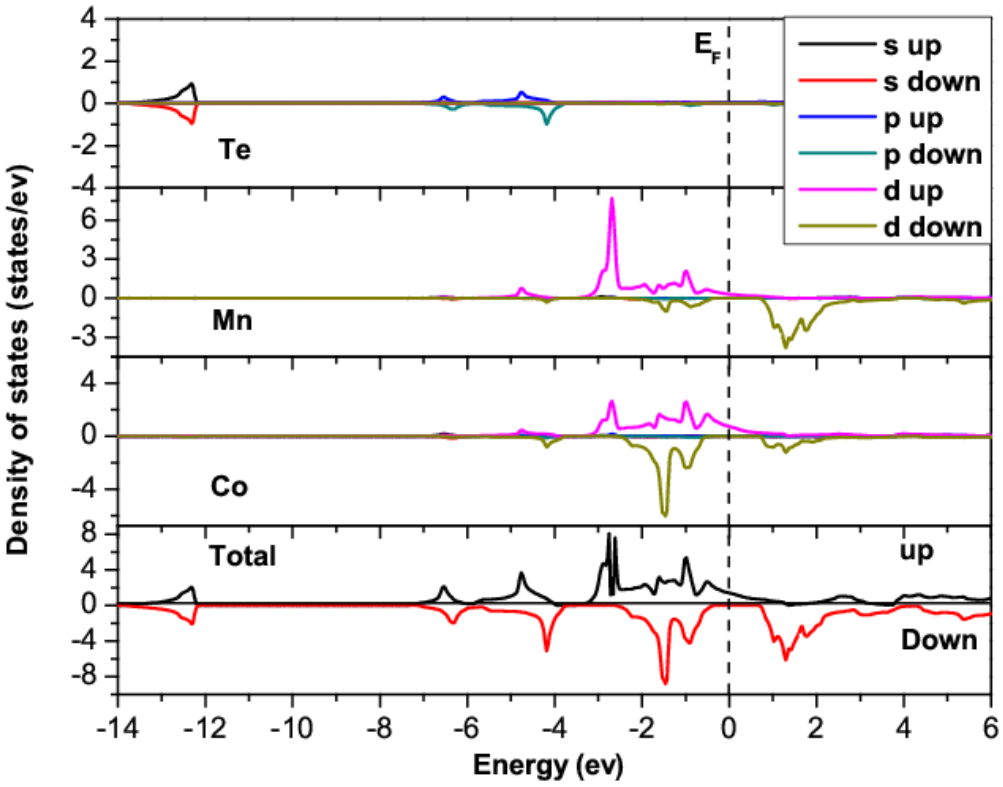

Fig. 4.12 : Calculated spin-projected total and partial DOSs of CoMnTe.

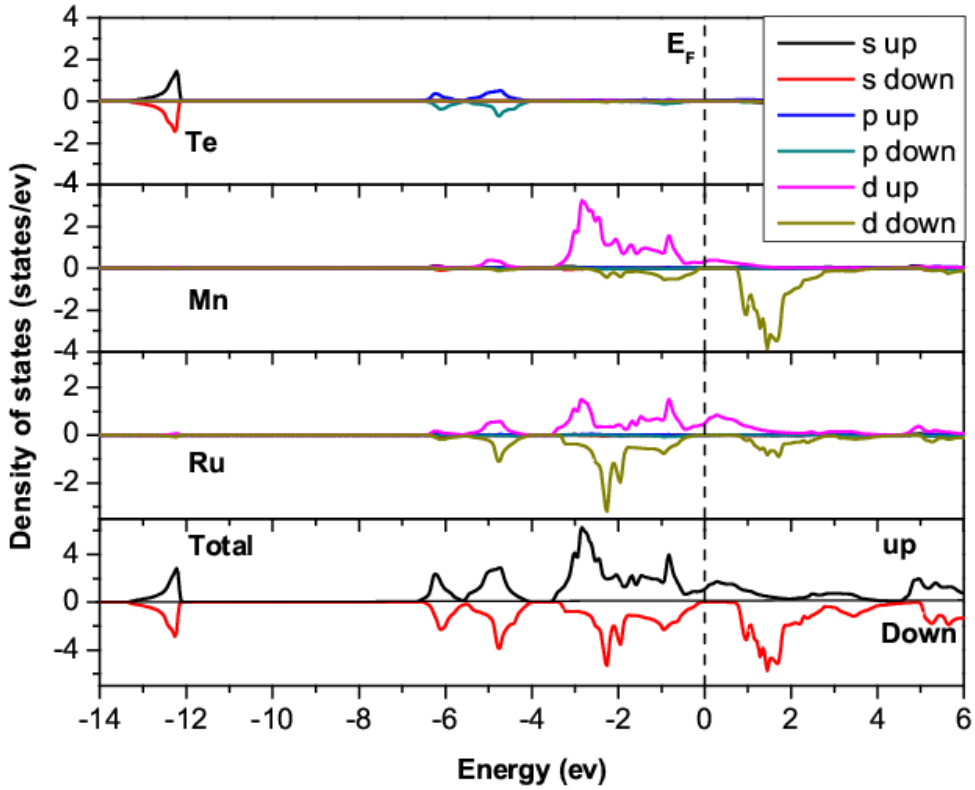

Fig. 4.13 : Calculated spin-projected total and partial DOSs of RuMnTe.

The positions of main Co peaks are located at -1.47 eV for the spin down and at -2.68 eV for the spin up, whereas for the Ru, they are situated at -2.59 eV for the spin down and at -3.04 eV for the spin up. Total densities of states result from the contribution of each partial density of states; it is noticeable that the main peaks remain approximately at the same positions as in the partial densities of states. Similar profiles of the densities of states are noted in both compounds. However, the band gap in the spin down is wider for CoMnTe. From the further analyses of Te-DOS in figures 4.12 and 4.13, it is found that the s and p states of Te reside in the lowest parts of the total densities of states and Te-s states are situated at ≈12.6 eV below E_F.

4.3.2 Origin of the half-metallic gap

The admixture of the several elements is responsible for the peculiarities of half-metallic ferromagnetism of CoMnTe and RuMnTe. Half-metallic behaviors of these compounds are closely related to the symmetry of their $C1_b$ crystal structure, the number of valence electrons, covalent bonding, and the large swap splitting of the Mn-3d electron band states [34]. As described by Galanakis et al. [35,36], the main reason for the creation of bonding and anti-bonding bands is because of strong hybridization between the d states of the lower valent TM (Mn) atoms and the higher valent TM (Co and Ru) atoms. Filled bonding states are located typically at higher valent TM atom site, while unoccupied anti-bonding states are at lower valent TM atom site. Minority occupied d state bonding is largely contributed from Co and Ru whereas anti-bonding d states are predominantly belonging to Mn characteristic. These types of structures are stable when solely the bonding states are occupied. The elements containing sp states are very important for half-Heusler compounds because of their particular role in tuning their several physical properties and structural stabilities of $C1_b$ compounds. Each Mn atom is surrounded by six nearest neighbors Te atoms in the structure under investigation. The strong electrostatic repulsion of the eg states at the Te atoms leads partly to the splitting of 3d states of Mn atoms into low-lying t2g triplet states, this phenomenon is a result of the interaction of Mn with the Te-p states. The development of band gap is a result of the separation of occupied d bonding states from unoccupied d anti-bonding states because of the shifting of Mn-3d states to higher energies in the minority band as schematically shown in figure 4.14, whereas in majority band, by the shifting of Mn-3d states to lower energies, a common 3d band together with Co-3d states is formed. A similar reason can be applied to RuMnTe to explain its band gap origin. Thus, CoMnTe and RuMnTe are half-metal in minority band with a gap at EF and metallic in majority band. Therefore, in the sense of their band gap origin these compounds are comparable to the semiconducting compounds like GaAs as the GaAs is strengthened by hybridizing the higher Ga-s and p states with the lower As-s and p states.

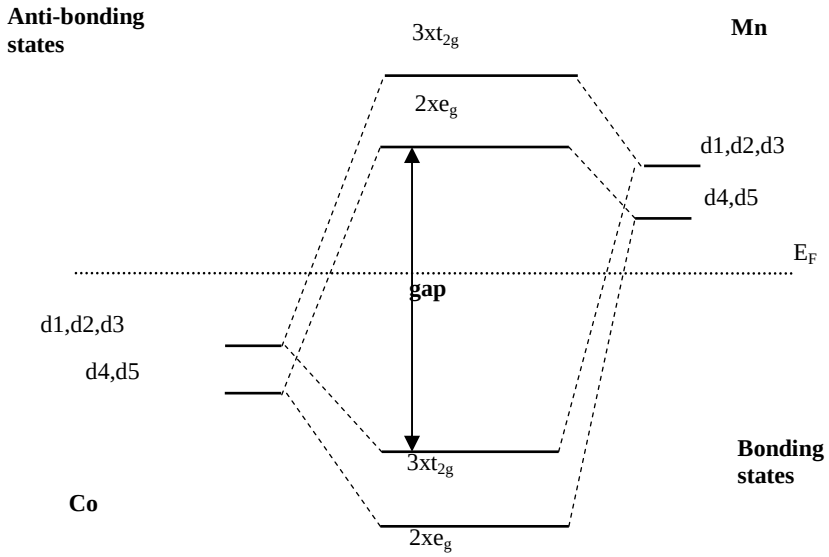

Fig. 4.14: Schematic illustration of the origin of the gap in the minority band in CoMnTe. [36]

The calculated values of total and partial magnetic moment μtot are listed in the table 4.2. The values of μtot are $4\mu_B$ and $3\mu_B$ per unit cell, respectively, for CoMnTe and RuMnTe and most part is contributed from Mn atom. Up to now, there have been no experimental results on magnetic moments available to compare with our values. Our computed magnetic moments for CoMnTe compound are in excellent agreement with FPLAW and Pseudo Potential values obtained by Selçuk Kervan and Nazmiye Kervan [30] and by Lin et al. [31], respectively. Total magnetic moment of the half metallic half-Heusler compound is estimated by applying the rule $\mu_{tot}=Z_t-18$, where $Z_t=N\uparrow+N\downarrow$ and $\mu_{tot}=N\uparrow-N\downarrow$. N↑ represents the number of spin-up electrons, and N↓ is the number of spin-down electrons.

Nine minority bands of half-Heusler compounds are fully occupied, which is in accordance with the straightforward rule of 18 regarding half-metallicity in the $C1_b$ structure [37-42]. CoMnTe has 22 valence electrons per unit cell and RuMnTe has 21. 9 valence electrons are contributed from Co, 8 valence electrons from Ru, 7 valence electrons from Mn and 6 valence electrons from Te. Value of the calculated total magnetic moment nicely follows the above rule, i.e. $\mu_{tot} = Z_t - 18$.

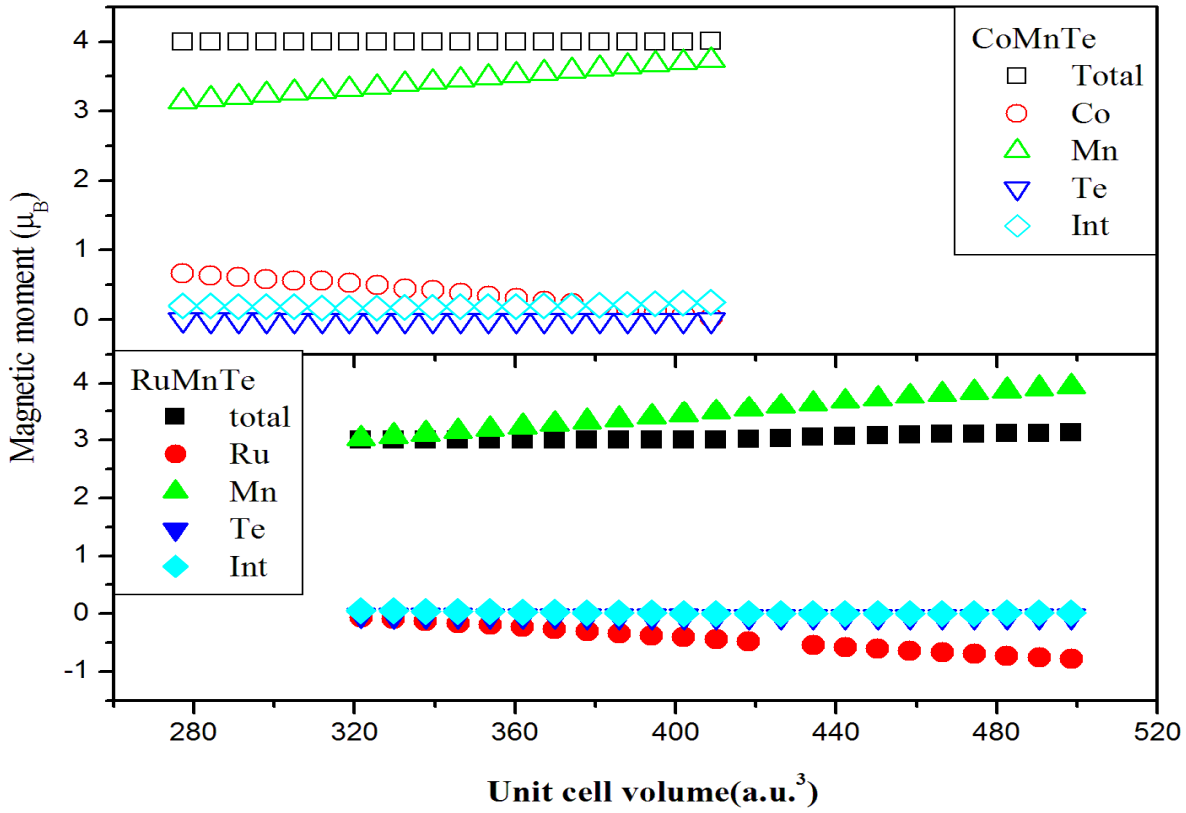

Fig. 4.15: Unit cell volume dependences of the total magnetic moment, and the spin moments of Co, Ru, Mn and Te atoms for CoMnTe and RuMnTe, respectively.

The calculated magnetic moment at the Mn site is 3.28 μ_B in RuMnTe but it is increased if Ru is replaced by Co (≈3.49 μ_B) as shown in the Table 4.2 while, contribution of Te is negative.

The magnetic moment at the Co site is 0.39 μ_B, which is significantly larger than at the Ru site (-0.29 μ_B). Thus, the replacement of Co by Ru modifies the total magnetic moment from 4 μ_B to 3 μ_B. In fact all half Heusler compounds containing Mn each have a large value of total magnetic moment due to the contributions of Mn in the full-Heusler compounds [31].

4.3.3 Effect of the unit cell volume

To see the influences of strains on the magnetic characteristics of the CoMnTe and RuMnTe, we study the variation of the magnetic moment with unit cell volume. Figure 4.15 depicts the variations of total magnetic moment and spin moment of Co, Ru, Mn and Te atoms with cell volume.

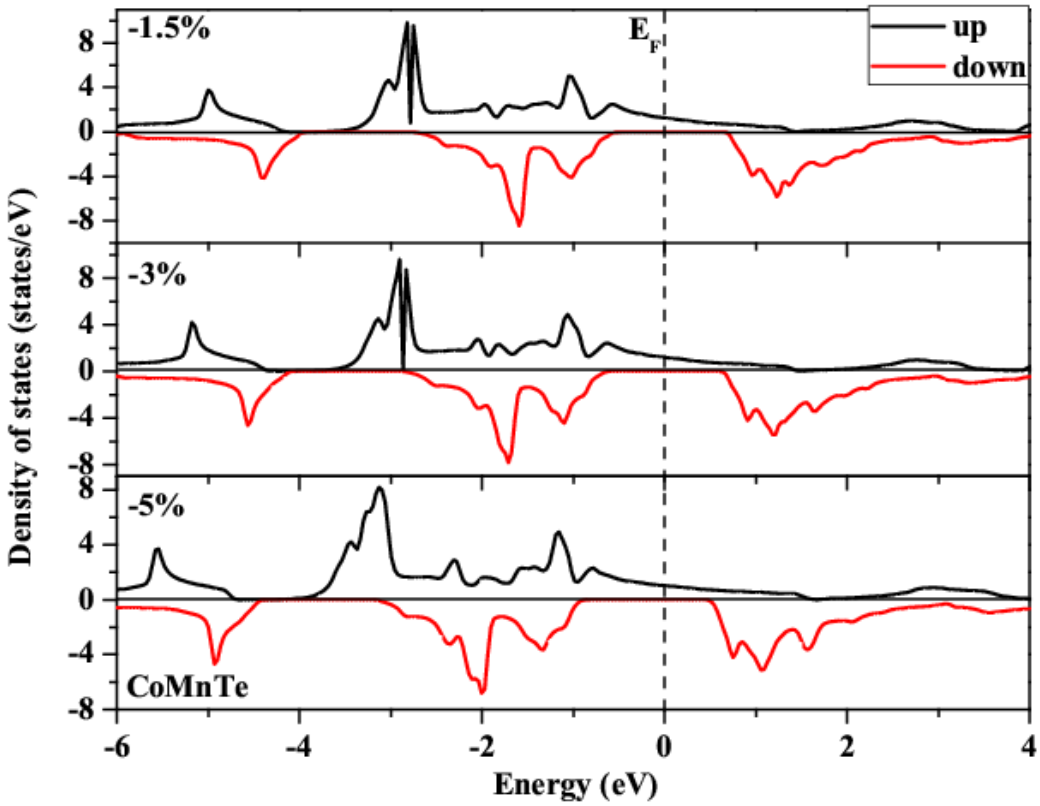

Fig. 4.16: The total densities of states when the unit cell volumes of CoMnTe are contracted (-).

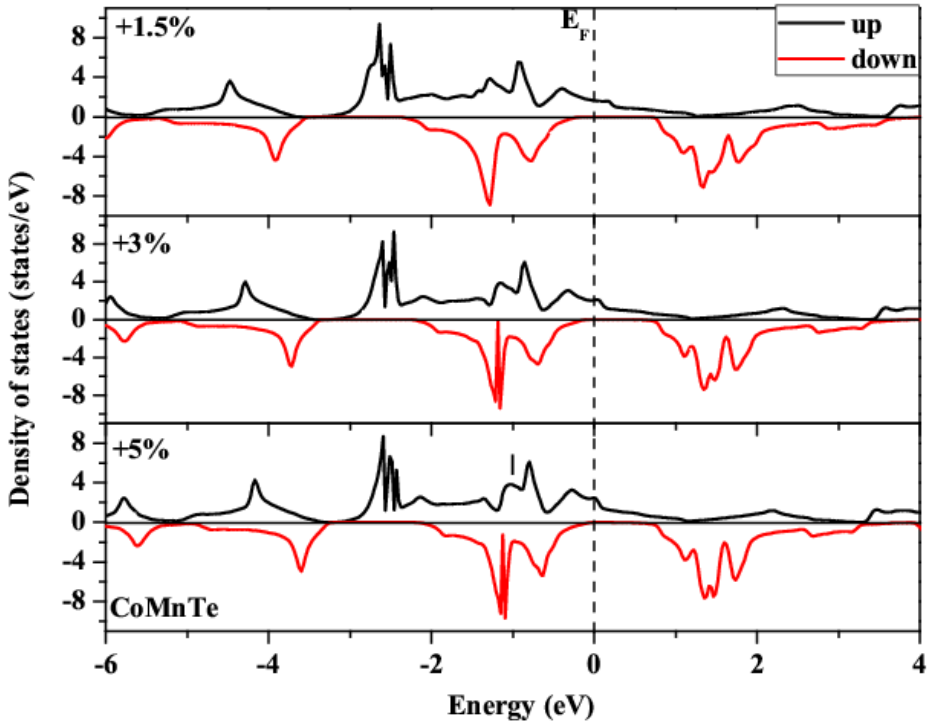

Fig. 4.17: The total densities of states when the unit cell volumes of CoMnTe are expanded (+).

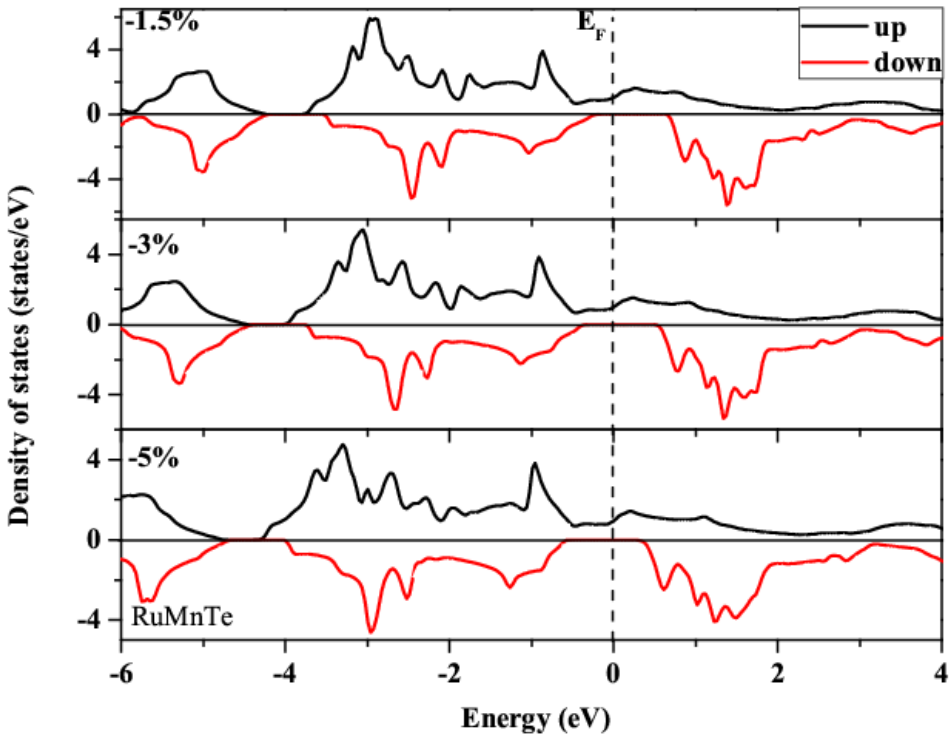

Fig. 4.18: The total densities of states when the unit cell volumes of RuMnTe are contracted (-).

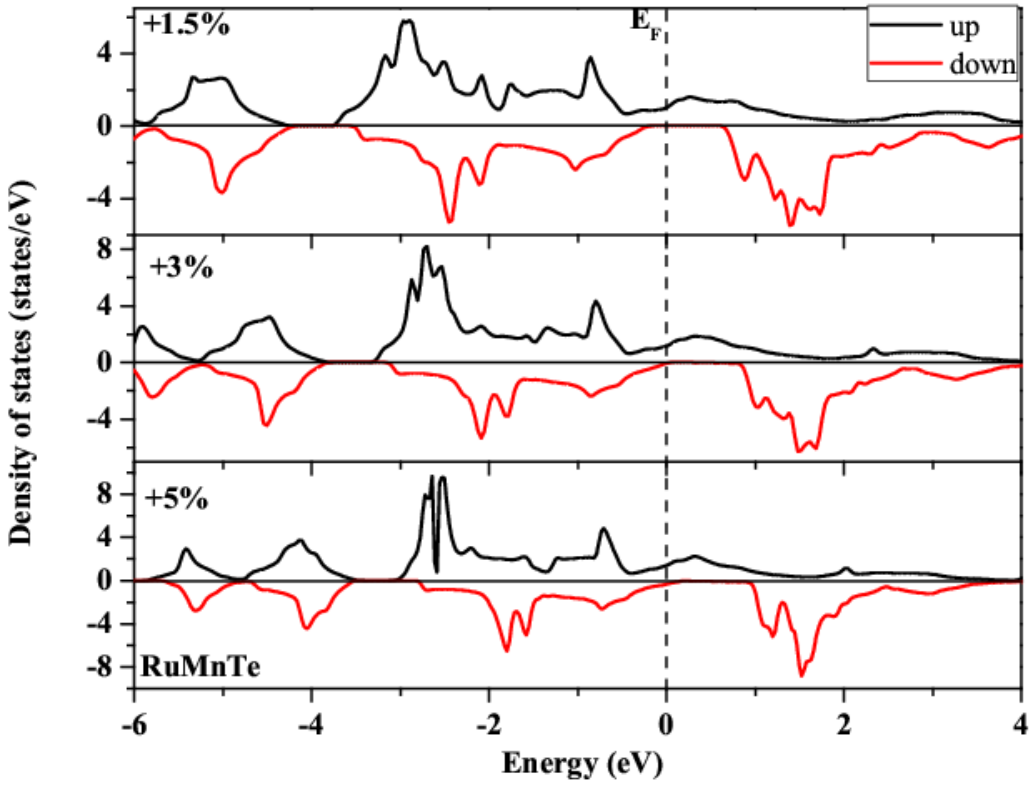

Fig. 4.19: The total densities of states when the unit cell volumes of RuMnTe are expanded (+).

It is clear from the figure 4.15 that when CoMnTe and RuMnTe unit cells are expanded, hybridizations between Co, Ru and Mn decrease, as a result spin moments of the Co and Ru decrease, while the Mn spin moment increases. However total magnetic moments/formula unit almost remain unchanged for both CoMnTe and RuMnTe compounds. The variation in the total moment is found to be less than $0.01\mu_B$ for each compound during contraction and expansion as compared with the predicted equilibrium unit cell volume. It is interesting to note that during the contraction and expansion, the change in the number of occupied minority-spin states is also small. Regarding E_F, contraction shifts it upwards in energy whereas the expansion shifts it downwards [24].

In figures 4.16, 4.17, 4.18 and 4.19 the densities of states are plotted for the contraction and expansion of CoMnTe and RuMnTe. Contraction moves E_F upwards in energy whereas expansion moves it downwards. The half-metallic gaps remain non-zero when unit cell volume is changed from −5% to +5% for CoMnTe and RuMnTe but for NiCrSe, reinforcement of the half-metallicity behavior is reported during expansion, and vice versa [24]. Thus, these results signify the crucial role of unit cell volume in the magnetic properties and half- metallicity.

Table 4.3: Predicted elastic constants Cij (GPa), shear modulus G (GPa) and B/G.

	C11	C12	C44	G	B/G
CoMnTe	208.800	80.229	167.330	98.95	1.244
RuMnTe	181.705	98.745	161.919	94,328	1.3399

The elastic constants of solids supply a relation between dynamical and the mechanical behaviors of crystals, and provide significant information about the character of the forces operating in solids. Especially, they give indication on the stability and rigidity of materials. The elastic constants are calculated via the “stress–strain” method [25] and shown on the table 4.3. the two compounds are mechanically stable.

4.4 Thermodynamic properties

The values of thermodynamic parameters are computed at the level of quasi-harmonic Debye model approach for half-Heusler CoMnTe and RuMnTe compounds. These calculations are done for specific heats at constant volume (C_V) and constant pressure (C_P), Debye temperature (θ), the thermal expansion coefficient (α) and Grüneisen parameter (γ) in a temperature range of 0K-1200K in steps of 100K and at pressure ranging from 0GPa to 45GPa in steps of 5GPa.

Table 4.4 : Calculated values of Debye temperature θ (K) and Grüneisen parameter (γ) of CoMnTe and RuMnTe at various pressures and temperatures.

T (K)		P (GPa)	0	15	30	45
300	RuMnTe	θ	363.91	461.66	525.79	574.97
		γ	2.79	2.14	1.82	1.63
	CoMnTe	θ	365.83	477.93	558.28	622.18
		γ	2.71	2.41	2.20	2.04
600	RuMnTe	θ	347.22	454.15	520.93	571.43
		γ	2.93	2.18	1.84	1.64
	CoMnTe	θ	347.66	466.32	549.94	615.63
		γ	2.76	2.44	2.22	2.06
900	RuMnTe	θ	326.05	445.82	515.80	567.68
		γ	3.12	2.22	1.87	1.65
	CoMnTe	θ	327.58	453.80	540.85	608.51
		γ	2.80	2.48	2.24	2.08
1200	RuMnTe	θ	297.80	436.65	510.09	563.78
		γ	3.39	2.28	1.89	1.67
	CoMnTe	θ	305.63	440.27	531.38	601.06
		γ	2.86	2.51	2.27	2.09

It is seen from figures 4.20 and 4.21 that the isothermal bulk modulus increases at the constant temperature as pressure increases, whereas the isothermal bulk modulus decreases at the constant pressure with the increase of temperature.

In figures 4.22 and 4.23, our calculated results for C_V and C_P each as a function of temperature are illustrated for CoMnTe and RuMnTe compounds.

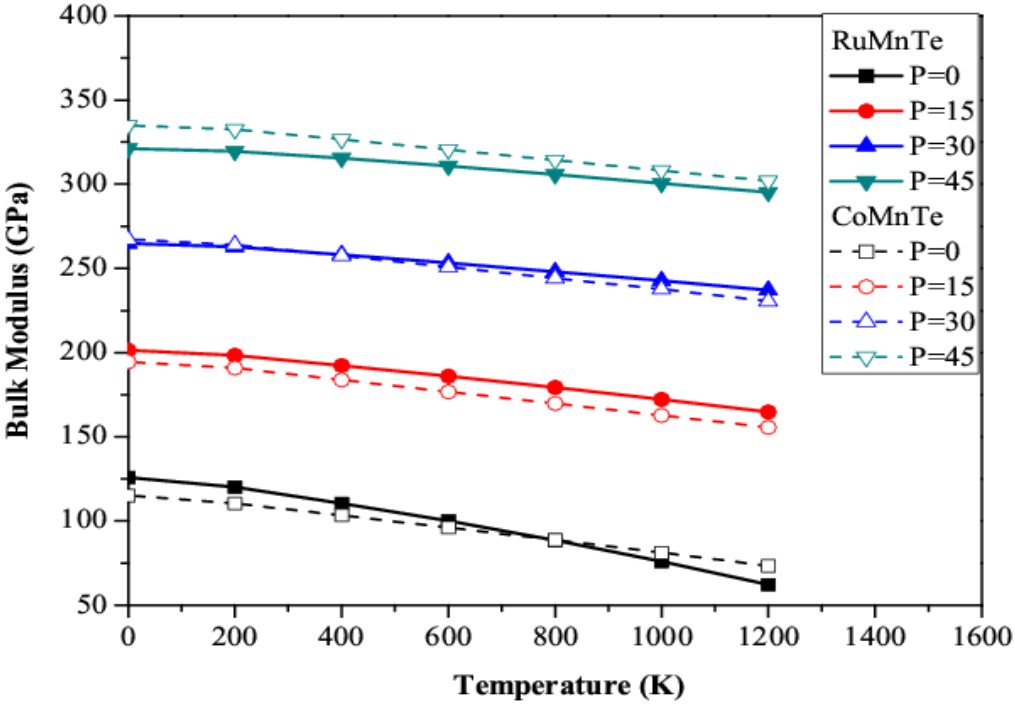

Fig. 4.20: Curves of bulk modulus versus temperature at different pressures for RuMnTe and CoMnTe.

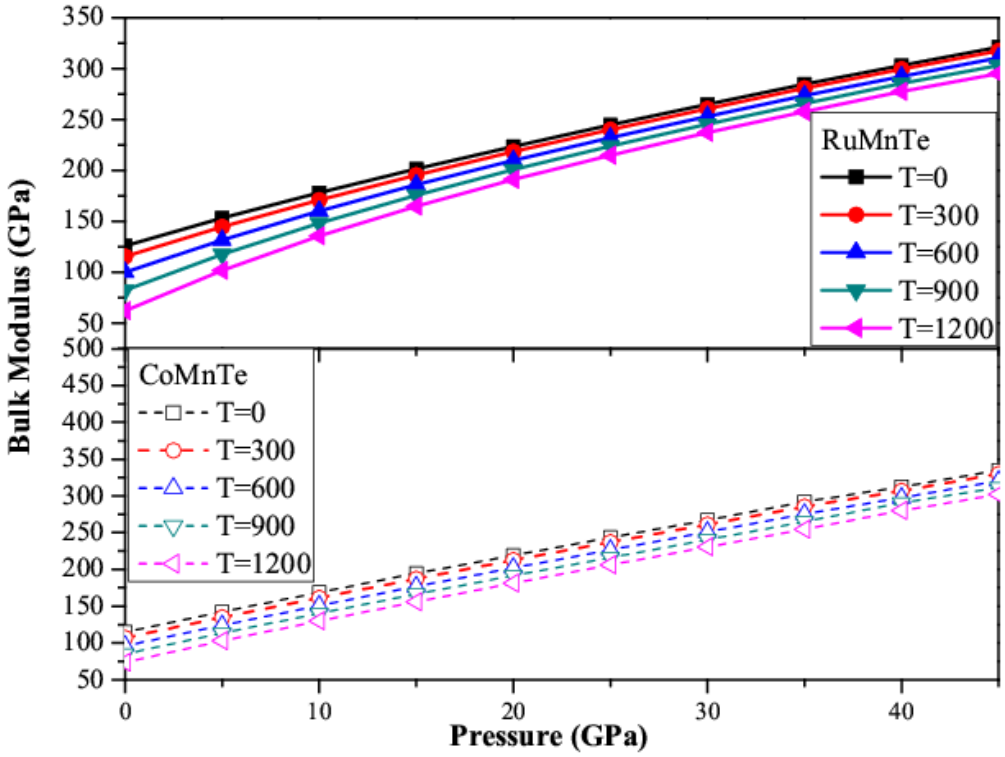

Fig. 4.21: Curves of bulk modulus versus pressure at different temperatures for RuMnTe and CoMnTe.

The specific heat capacity is closely related to the temperature dependence of fundamental thermodynamic functions, and it is the most important parameter for linking thermodynamics with dynamics and microscopic structure.

It is clear that when the temperature is below 650 K, the C_V and C_P variations are very close together exhibiting strong dependent on temperature due to the anharmonic approximation used in this scheme of calculations. While at high temperatures, the C_v approaches to a constant value ($\approx 75\ \mathrm{Jmol^{-1}K^{-1}}$), obeying Dulong and Petit's rule, which is followed by all solids at high temperatures, owing to the suppression of the anharmonic effect [29].

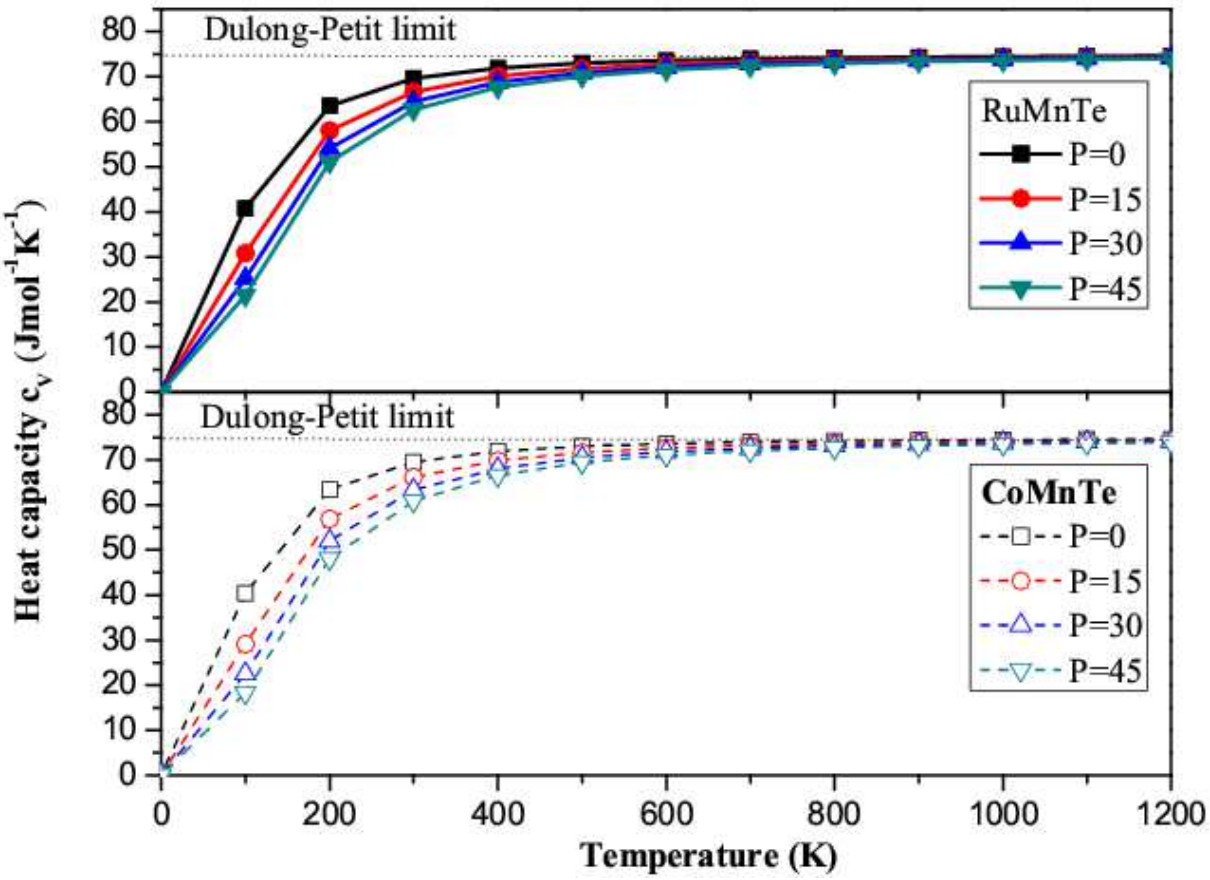

Fig. 4.22: Variations of specific heat capacity C_V with temperature at various pressures for the half-Heusler alloys RuMnTe and CoMnTe.

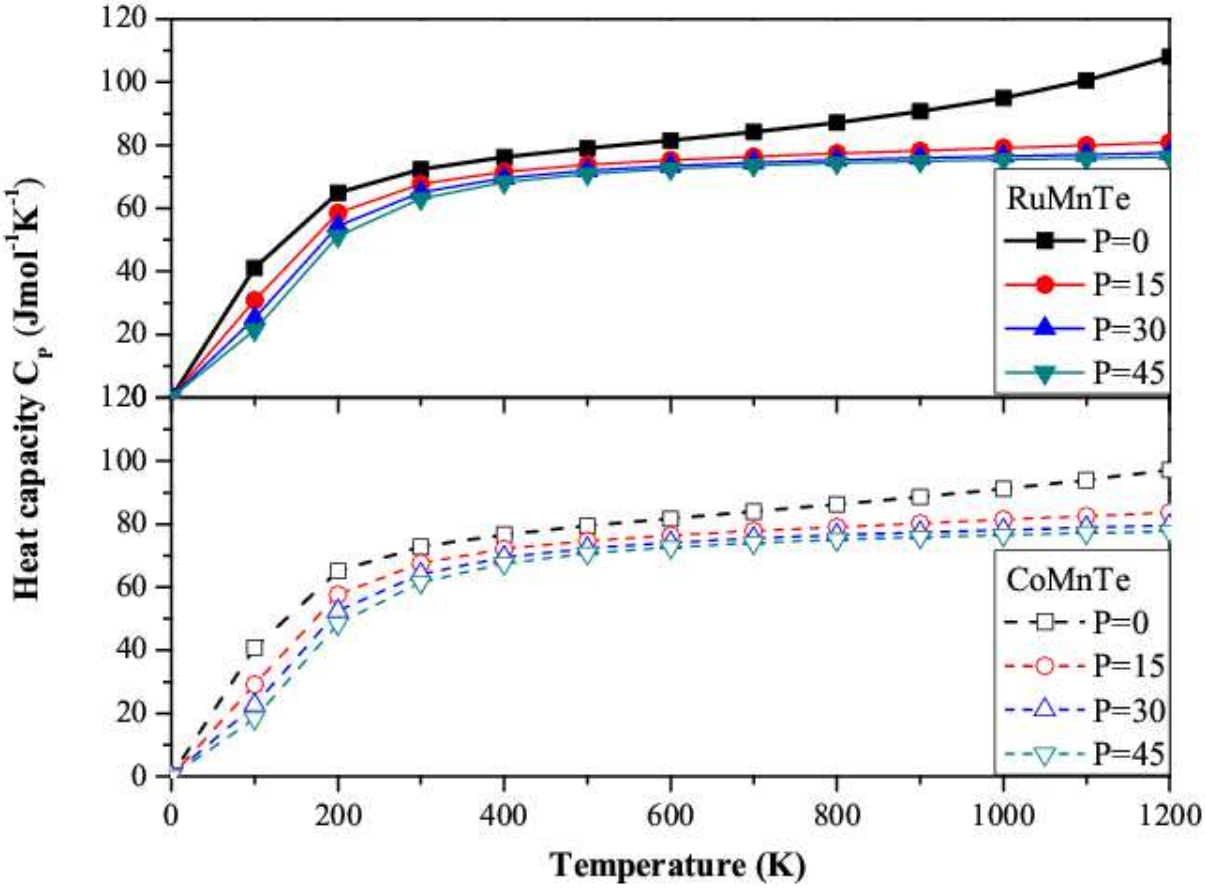

Fig. 4.23: Variations of specific heat capacity C_P with temperature at various pressures for the half-Heusler alloys RuMnTe and CoMnTe.

It is remarkable that the specific heat capacity at constant pressure CP increases monotonically with the increase of the temperature.

Many physical properties of solids are closely related to the Debye temperature (θ) and Grüneisen parameter (γ). The variations of the results of these parameters are shown in Table 4.3. It is found that the Debye temperature increases with increasing pressure whereas the Grüneisen parameter decreases when temperature is kept constant. However, at the constant pressure, the Debye temperature decreases and the Grüneisen parameter increases as temperature increases.

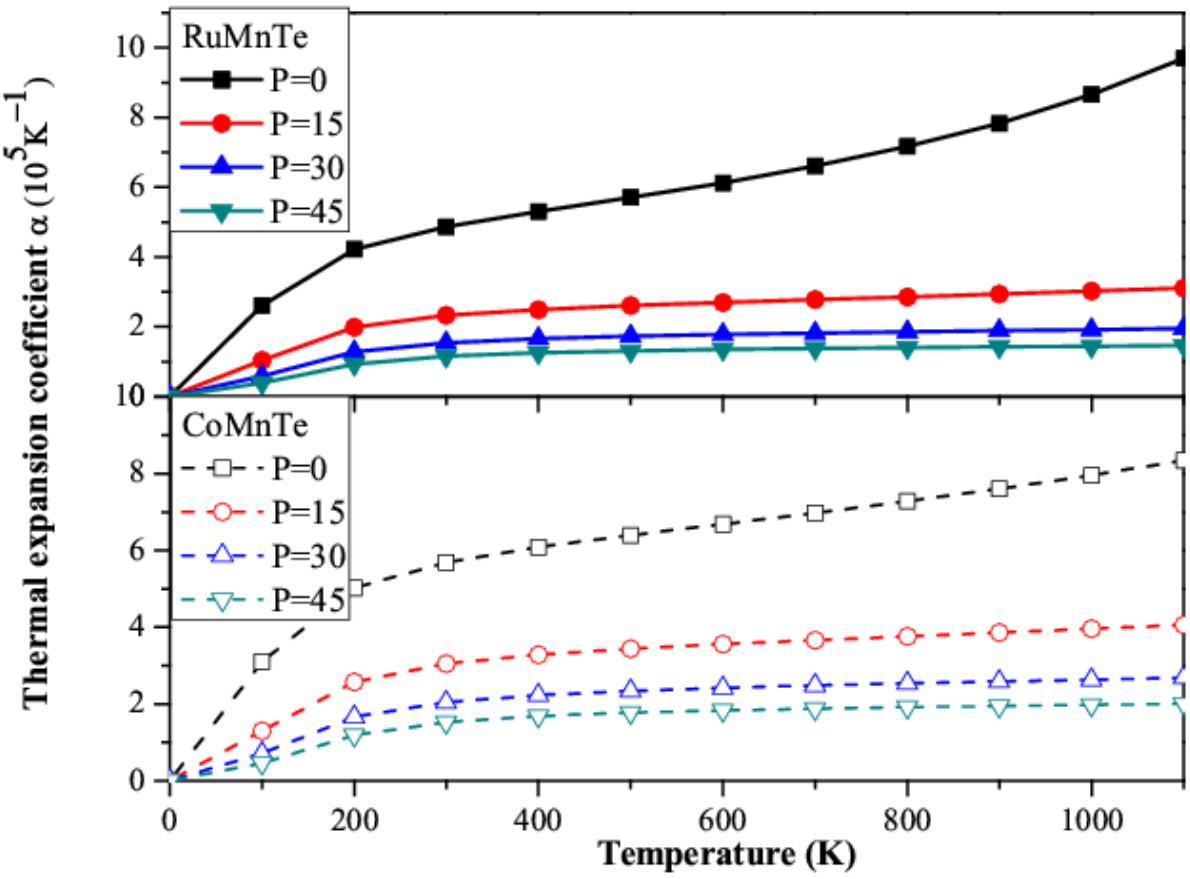

Fig. 4.24: Variations of calculated values of thermal expansion α with temperature at various pressures for half-Heusler alloys RuMnTe and CoMnTe.

The volume thermal expansion coefficient (α) reflects the temperature dependence of volume at constant pressure : $\alpha = \frac{1}{V}\left(\frac{\partial V}{\partial T}\right)_P$. Figure 4.24 shows the variations of the thermal expansion coefficient with temperatures at different pressures. From this figure, we can see that the thermal expansion increases sharply with temperature going up to 300 K then slowly for temperature higher than 300 K, and gradually turns into a linear increase. At a fixed temperature, the higher the pressure, the smaller the thermal expansion coefficient is, indicating that high pressure suppresses thermal expansion. At zero pressure and 300 K, the values of the thermal expansion α for RuMnTe and CoMnTe are 4.89 × 10^{-5} K^{-1} and 5.71× 10^{-5} K^{-1}, respectively.

References

[1] F. Heusler, Verh. Dtsch. Phys. Ges. **5,** (1903) 219

[2] R. A. de Groot, F. M. Mueller, P. G. van Engen and K. H. J. Buschow, Appl. Phys. **55,** (1984) 2151

[3] I . Galanakis and P. H. Dederichs, J. Phys. : *Condens. Matter* **676,** (2005) 1

[4] K. Endo, T. Phayama and R. Kitamura J. Phys. Soc. Jpn. **19,** (1964) 1494

[5] J. Kubler, Physica B **127, (**1984) 257

[6] R. Dunlap, G. Stroink and K. Dini, J. Phys. F. Met. Phys. **16,** (1986) 1083

[7] W. Zukovski, A. Andrejezuk, L. Dobrzyeski, M. J. Cooper, M. A. G. Dixon, S. Gardelis, P. K. Lawson, T. Buslaps, S. Kaprzyk, K. U. Neumann and K. R. Ziebeck, J. Phys.: condens. Matter **9,** (1997) 10993

[8] J. Worgull, E. Petit and J. Trivisonno, Phys. Rev. B **54,** (1996) 15695

[9] S. Plogmann, T. Schlatholter, J. Braun and M. Neumann, Phys. Rev. B **60,** (1999) 6428

[10] S. Ishada, J. Ishada, S. Asano and J. Yamashita, J. Phys. Soc. Jpn. **45,** (1978) 1239

[11] J. Kubler, A. R. Williams and C. B. Sommers, Phys. Rev. B **28,** (1983) 1745

[12] S. Fujii, S. Ishida and S. Asano, J. Phys. Soc. Jpn. **58,** (1989) 3657

[13] P. J. Webster and K. R. A. Ziebeck, J. Phys. Chem. Solids. **34,** (1973) 1647

[14] A. A. Aquela, J. Enkovaara, K. Uliakko and R. E. Nieminen, J. Phys.: Condens. Matter **11,** (1999) 2017

[15] A. Deb and Y. Sakurai, J. Phys.: Condens. Matter **12,** (2000) 2997

[16] K. Kakeshita and K. Ullakko, MRS Bulletin **27,** (2002) 105

[17] R. Mullner, V. A. Chermenko and G. Kostorz, Ser. Mater. **49,** (2003) 129

[18] V. A. Chernenko, V. A. L'vov, R. Mullner, G. Kostorz and T. Takagi, Phys. Rev. B **69,** (2004) 134410

[19] S. E. Kulkova, S. V. Eremeev and S. S. Kulkov, Solid State commun. **130,** (2004) 793

[20] S. E. Kulkova, S. V. Eremeev, T. Kakeshita, S. S. Kulkov and G. E. Rudenski, Materials Transactions **47,** (2006) 599

[21] R. A. de Groot, A. M. van der Kraan and K. H. J. Buschow, J. Magn. Magn. Mater. **61,** (1986) 330

[22] P. Blaha, K. Schwarz, P. Sorantin and S. B. Trickey, comput. Phys. Commun. **59,** (1990) 399

[23] J. P. Perdew, K. Burke and M. Ernzerhof, Phys. Rev. Lett. **77,** (1996) 3865

[24] M. A. Blonco, E. Francisco and V. Luaña, Comput. Phys. Commun. **158,** (2004) 57

[25] M. A. Blonco, A. M. Pendás, E. Francisco, J. M. Recio and R. Franco, J. Mol. Struct.Theochem. **368,** (1996)245

[26] E. Francisco, M. A. Blonco and G. Sanjurjo, Phys. Rev. B **63,** (2001) 049107

[27] O. Merabiha, T. Seddik, R. Khenata, G. Murtaza, A. Bouhemadou, Y. Takagiwa, S. Bin Omran and D. Rached, Journal of Alloys and Compounds **586,** (2014) 529

[28] A. Bouhemadou, R Khenata and B. Amrani, Physica B **404,** (2009) 3534

[29] F. Peng, H. Fu and X. Yang, Physica B **403,** (2008) 2851

[30] K. Selçuk and K. Nazmiye, Intermetallics **46,** (2014) 45

[31] S. Y. Lin, X. B. Yang and Y. J. Zhao, J. Magn. Magn. Mater. **350,** (2014) 119

[32] F. D. Murnaghan, Proc. Natl. Acad. Sci. U.S.A. **30,** (1944) 244

[33] M. J. Otto, R. A. M. van Woerden, P. J. van der Valk, J. Wijngaard, C. F. van Bruggen, C. Haas and K. H. J. Buschow, *J. Phys.: Condens. Matter* **1,** (1989) 2341

[34] R. A. de Groot, F. M. Mueller, P. G. van Engen and K. H. J. Buschow, Phys. Rev. Lett. **50,** (1983) 2024

[35] I. Galanakis, P. H. Dederichs and N. Papanikolaou, Phys. Rev. B **66** (2002) 134428

[36] I. Galanakis, P. H. Dederichs and N. Papanikolaou, Phys. Rev. B **66,** (2002) 174429

[37] S. Ishida, S, Fujii, S. Kashiwagi and S. Asano, J. Phys. Soc. Japan **64,** (1995) 2152

[38] S. Fujii, S. Ishida and S. Asano, J. Phys. Soc. Japan **64,** (1995) 185

[39] M. Zhang, Z. H. Liu, H. N. Hu, G. D. Liu, Y. T. Cui, G. H. Wu, R. Brek, F. R. de Boer and Y. X. Li, J. Appl. Phys. **95,** (2004) 7219

[40] B. R. K. Nanda and I. Dasgupta, J. Phys.: Condens. Matter **15,** (2003) 7307

[41] D. Jung, H. J. Koo and M. J. Whangbo, J. Mol. Struct. Theochem. **527,** (2000) 113

[42] M. Zhang, X. Dai, H. Hu, G. Lui, Y. Cui, J. Chen, J. Wang and G. Wu, J. Phys.: Condens. Matter **15,** (2003) 7891

5 Conclusions

Within the framework of this thesis, The First-principles DFT studies related to CoMnTe and RuMnTe compounds are performed. The calculations are accomplished within the state of the art full-potential (FP) linearized (L) augmented plane wave (APW) computational approach. Generalized gradient approximation (GGA) parameterized by Perdew, Burke and Ernzerhof (PBE) is implemented as an exchange correlation functional as a part of total energy calculation. The structural, electronic, magnetic and thermodynamics characteristics are carried out. For both Heusler CoMnTe and RuMnTe compounds, first of all, the total energies of their paramagnetic and ferromagnetic states are calculated in terms of volume per formula unit. It is found that the paramagnetic phase has high energy as compared with the ferromagnetic phase. volume (V_0), energy (E_0), equilibrium lattice constant (a_0) and bulk modulus (B) are calculated for ferromagnetic phase. These results are obtained for both compounds by fitting data for energy as a function of volume to the Murnaghan equation of state. The energy difference (ΔE) between paramagnetic and ferromagnetic states is also calculated. There are no experimental results available to us for these compounds, but our values for CoMnTe are in excellent agreement with those obtained by Selçuk Kervan using the full potential linearized augmented plane wave method.

However natures of band energy gaps are found to be indirect between Γ point of the highest occupied band (valence band) and X point for the lowest unoccupied band (conduction band). The densities of states near the half metallic gap, where the influences of the s and p states are insignificant, are dominated by the d-states of Co, Ru and Mn. It is point to note that the bonding d states are largely contributed from Co and Ru, whereas anti-bonding d states are predominantly belonging to Mn characteristic.

Our studies of the calculated electronic bands structures, the densities of states and the magnetic moments of ground state confirm that CoMnTe and RuMnTe compounds are half-metallic ferromagnetic materials. It is found that these materials behave as metals for the majority spin bands and exhibit semiconducting characteristics for minority spin bands. Total densities of states result from the contribution of each partial density of states; it is noticeable that the main peaks remain approximately at the same positions as in the partial densities of states.

Origin of the band gap is traced out in the strong hybridization between the d states of higher valent TM atoms and lower valent TM atoms. The role of the elements containing sp states is crucial in tuning several physical properties of half Heusler compounds and structural stability of $C1_b$ compounds. Our calculated values of total magnetic moment μ_{tot} are $4\mu B$ and $3\mu B$ per unit cell for CoMnTe and RuMnTe, respectively, and most of the part is contributed from Mn atom. The total spin moment scale is accurately in agreement with total number of valence electrons contained by the atoms of these compounds. The calculated value of μ_{tot} is in the line with the rule of μ_{tot} = Zt -18.

The effect of the unit cell volume is found to be decisive for the magnetic properties and the half-metallicity characteristics. When CoMnTe and RuMnTe unit cells are expanded, hybridizations between Co, Ru and Mn decrease, as a result spin moments of the Co and Ru decrease, while the Mn spin moment increases. However total magnetic moments/formula unit almost remain unchanged for both CoMnTe and RuMnTe compounds. The variation in the total moment is found to be less than $0.01\mu_B$ for each compound during contraction and expansion as compared with the predicted equilibrium unit cell volume. It is interesting to note that during the contraction and expansion, the change in the number of occupied minority-spin states is also small.

Contraction moves E_F upwards in energy whereas expansion moves it downwards. The half-metallic gaps remain non-zero when unit cell volume is changed from −5% to +5% for CoMnTe and RuMnTe but for NiCrSe, reinforcement of the half-metallicity behavior is reported during expansion, and vice versa. Thus, these results signify the crucial role of unit cell volume in the magnetic properties and half-metallicity.

Finally thermodynamic properties including the isothermal bulk modulus, heat capacity, Debye temperature, and the thermal expansion coefficients of the half-Heusler CoMnTe and RuMnTe compounds are investigated using the quasi-harmonic Debye model. The observed variations accord well with the results of the Debye theory which is regularly applied to several materials.